

IDENTIFICATION OF NEW PORPHYRY POTENTIAL UNDER COVER IN BRITISH COLUMBIA

Geoscience BC Central Interior Copper-Gold Research Project

Mitchinson, D.E., Fournier, D., Hart, C.J.R., Astic, T., Cowan, D.C., and Lee, R.G.

Geoscience BC Report 2022-07

MDRU Publication 457



IDENTIFICATION OF NEW PORPHYRY POTENTIAL UNDER COVER IN BRITISH COLUMBIA

Geoscience BC Central Interior Copper-Gold Research Project

Mitchinson, D.E., Fournier, D., Hart, C.J.R., Astic, T., Cowan, D.C., and Lee, R.G

Geoscience BC* Report 2022-07

MDRU Publication 457

Suggested Citation:

Mitchinson, D.E., Fournier, D., Hart, C.J.R., Astic, T., Cowan, D.C., and Lee, R.G. (2022). Identification of New Porphyry Potential Under Cover in British Columbia. Geoscience BC Report 2022-07, MDRU Publication 457, 97 p.

Report prepared by MDRU[†]

©2022 MDRU—Mineral Deposit Research Unit

Dept. Earth, Ocean and Atmospheric Sciences, The University of British Columbia

Vancouver, BC V6T 1Z4, Canada

Tel: +1-604-822-6136

Email: mdru@eoas.ubc.ca

Includes bibliographic references.

Electronic monograph issued in PDF format.

ISBN 978-0-88865-479-3

*Geoscience BC is an independent, non-profit organization that generates earth science in collaboration with First Nations, local communities, government, academia and the resource sector. Our independent earth science enables informed resource management decisions and attracts investment and jobs. Geoscience BC gratefully acknowledges the financial support of the Province of British Columbia.

[†]MDRU—Mineral Deposit Research Unit is an internationally-recognized collaborative venture between the mining industry and Earth, Ocean and Atmospheric Sciences Department at The University of British Columbia (UBC), established with assistance from the Natural Sciences and Engineering Research Council of Canada (NSERC), and devoted to solving mineral exploration-related problems.

Cover image: Perspective view of 3-D high magnetic susceptibility bodies with potential to be porphyry copper-gold deposit host intrusions, central Quesnel terrane, British Columbia. Image generated using Geoscience Analyst.

CONTENTS

ABSTRACT	1
1. INTRODUCTION	2
2. BACKGROUND	2
2.1 Alkalic porphyry deposits in British Columbia	2
2.2 Geophysical data available in the project area	7
2.3 Previous work using geophysical data in the Quesnel terrane	7
3. INITIAL PORPHYRY TARGET IDENTIFICATION	7
3.1 Geophysical footprints of known alkalic porphyry deposits in British Columbia	7
3.2 Physical properties of alkalic porphyry deposit host rocks	9
3.2.1 Physical property data	9
3.2.2 Magnetic susceptibility and density trends of Quesnel terrane rocks	9
3.3 Target selection based on regional geophysical trends and physical properties	16
4. OVERBURDEN MODELLING	16
4.1 Constraining data	16
4.1.1 Water wells	16
4.1.2 ARIS mineral exploration drilling logs	18
4.1.3 Outcrop location data	18
4.1.4 Bedrock depth from electromagnetic data interpretations	18
4.2 Method	20
4.3 Results	20
5. 3-D INVERSION MODELLING OF TARGETS	24
5.1 Magnetic inversions	24
5.1.1 Data and Methods	24
5.1.2 Results	25
5.2 Gravity inversions	25
5.2.1 Data and Methods	25
5.2.2 Results	25
6. SUMMARY OF INVERSION-DERIVED PETROPHYSICS OF CENTRAL QUESNEL TERRANE TARGETS	25
6.1 Targets in the Fort St. James area (“FSJ” targets)	25
6.2 Targets in the northern Prince George area (“PG” targets 1–10)	30
6.3 Targets in the southern Prince George area (“PG” targets 11–18)	30
6.4 Targets in the Quesnel area (“Q” targets)	30
7. TARGET PRIORITIZATION AND EXPLORATION IMPLICATIONS	34
8. SUMMARY	36
9. LIST OF PROJECT DELIVERABLES	36
10. ACKNOWLEDGEMENTS	37
11. REFERENCES	37
LIST OF APPENDICES	41
APPENDIX 1: SUPPLEMENTAL PETROGRAPHY REPORT	42
APPENDIX 2: MAGNETIC INVERSION METHODOLOGY	68
APPENDIX 3: GRAVITY INVERSION METHODOLOGY	82

ABSTRACT

There is high prospectivity for gold-rich alkalic porphyry deposits through the central Quesnel terrane of British Columbia, based on geology and mineralization trends within this volcano-magmatic arc. Hindering exploration is a blanket of mostly glacially-derived sediment that obscures bedrock. Geophysical surveys, which remotely collect information about the near to deep subsurface, allow mineral explorers to interpret bedrock geology through this surficial cover material. Recognizing the potential of geophysical data to enhance exploration efforts, Geoscience BC funded regional scale magnetic, electromagnetic, and gravity surveys of the central Quesnel terrane. These surveys have shed new light on the geological understanding of this region, with several follow-up studies interpreting geology and structure under cover. This project takes advantage of these public datasets to model overburden thickness and to evaluate the mineral potential of a suite of magnetic targets, chosen based on their similarities to magnetic signatures of known porphyry deposit host rocks in the northern and southern Quesnel terrane. Electromagnetic inversions, completed as part of an earlier Geoscience BC initiative, identify conductive cover material. Interpretations of overburden–bedrock contacts from these inversions, combined with groundwater well, exploration drilling, and outcrop data, provide constraints for a revised overburden thickness model for the central Quesnel terrane. Three dimensional magnetic and gravity inversion models were then generated; these provided estimates of magnetic susceptibility and density values for each target that were compared to physical property ranges of known porphyry deposit host, or source, intrusions. Targets were prioritized based on petrophysical similarities to known Quesnel terrane porphyry host rocks, the overburden thickness, and additional cultural and geographic factors. Three dimensional magnetic susceptibility and density models generated by inversion can be used by porphyry explorers to predict the physical size and shape of the interpreted subsurface intrusions, to direct claim-staking, and to plan follow-up exploration.

1. INTRODUCTION

Demand for copper is growing with global movements to electrify the economy (Schipper et al., 2018), however, discoveries of mineable copper resources have slowed significantly over the last decade (e.g., Schodde, 2019). Future mineral discoveries are likely to be made in places that have been underexplored or difficult to access. British Columbia is well known for having geology favorable for porphyry copper-gold deposits. As of 2021, the province has six operating porphyry copper mines: Gibraltar (MINFILE 093B 012), Copper Mountain (MINFILE 092HSE001), New Afton (MINFILE 092INE023), Highland Valley (MINFILE 092ISW012), Mount Milligan (MINFILE 093N 194), and Red Chris (MINFILE 104H 005). For these deposits, there is greater than 11 million tonnes of measured and indicated contained copper (British Columbia Geological Survey, 2015). In addition, British Columbia has a large number of developed porphyry deposit properties, occurrences, and prospects. However, some regions are clearly underexplored due to extensive (primarily glacially-derived) surficial deposits. One such region is an approximately 250 km x 100 km area within the central Quesnel terrane. Very few copper-gold porphyry occurrences are recorded within this region, yet hundreds of porphyry occurrences are identified north and south of it, and the Mount Milligan and Mount Polley (MINFILE 093A 008) mines bookend the area (Figure 1). Geologic mapping and geophysical interpretation suggest continuity of Quesnel terrane arc geology between Mount Polley and Mount Milligan (Sanchez et al., 2015), and consequently potential for porphyry deposits is thought to be high. However, relatively little exploration has occurred compared to other areas in British Columbia, likely due to the perceived thickness and extent of cover material. Geophysical data collected over the last decade and a half provide an excellent means for both understanding overburden distribution in the central Quesnel terrane and identifying exploration targets under cover.

Magnetic and gravity surveys over the central Quesnel terrane have been utilized in past studies to interpret geology and structure under the surficial material, and to develop mineral potential models for the region (Mira Geoscience, 2009; Granek, 2016; Sanchez et al., 2015; Montsion et al., 2019). This project further interprets the data from magnetic, gravity and electromagnetic surveys to: 1) model the thickness of the overburden; and 2) assess prospectivity of a suite of geophysical targets resembling known copper-gold alkalic porphyry deposit host rocks, considering the estimated overburden thickness. The goal is to generate regional-scale porphyry exploration targets in the central Quesnel terrane that may be evaluated with more detailed exploration work, such as mapping, sampling, or local geophysical surveys. The revised overburden model will enable explorers to plan their field sampling programs with consideration for the overburden thickness, and 3-D geophysical inversions of targets will provide information on the expected sizes and shapes of the sources of the targeted anomalies.

2. BACKGROUND

2.1 Alkalic porphyry deposits in British Columbia

British Columbia is Canada's largest copper producer, contributing 54.4% of Canada's copper in 2019 (Natural Resources Canada, 2021). British Columbia produces ~175,000 – 360,000 t of copper a year (Government of British Columbia, 2021), with much of this coming from the mining of British Columbia's porphyry copper deposits including Highland Valley, Gibraltar, Red Chris, Copper Mountain, and Mount Milligan.

Porphyry deposits form in volcanic arc settings at subductions zones (Sillitoe, 1972). Partial melting of the crust in the overriding plate forms magma chambers, from which magma escapes and travels to the near-surface. Magmas, under specific compositional and pressure-temperature conditions, evolve to produce hydrothermal fluids concentrated in metals. Copper, gold, molybdenum, and base metals are deposited from these fluids in fractures, veins, breccias, and other open spaces at the edges and apices of the evolved porphyritic intrusions. The deposits are typically associated with large (often 1–5 km) hydrothermal footprints. Magmatic-hydrothermal fluids travel through and modify host rock mineralogy, resulting in alteration zones surrounding the deposit where alteration mineral assemblages reflect the composition of the source magmatic-hydrothermal fluid and the temperature of the fluid (Sillitoe, 2010).

British Columbia has two predominant types of porphyry deposits, calc-alkalic and alkalic (Barr et al., 1976). These designations are based on the lithogeochemical character of the deposit's host or source intrusive rocks, where calc-alkalic hosts are more enriched in silica relative to alkali elements, and alkalic hosts are depleted in silica relative to alkali elements (Lang et al., 1995a). Calc-alkalic porphyry deposits are common throughout the world in volcano-magmatic arcs, whereas alkalic porphyry deposits are known to occur only in a few locations globally—New South Wales, Australia; in the Philippines; and in Greece—in addition to British Columbia (Jensen and Barton, 2000; Sillitoe, 2000). The limited global distribution of alkalic porphyry deposits is attributed to the unique subduction settings in which they form, with lithogeochemical signatures reflective of a more primitive magmatic source derived from the mantle (possibly explained by subduction slab tears or windows (e.g., Mihalynuk and Logan 2010; Logan and Mihalynuk, 2014)). Alkalic porphyry deposits are typically lucrative in that, in addition to being a copper resource, they have elevated gold and platinum group elements (Jensen and Barton, 2000; Thompson et al., 2001; Hanley et al., 2020).

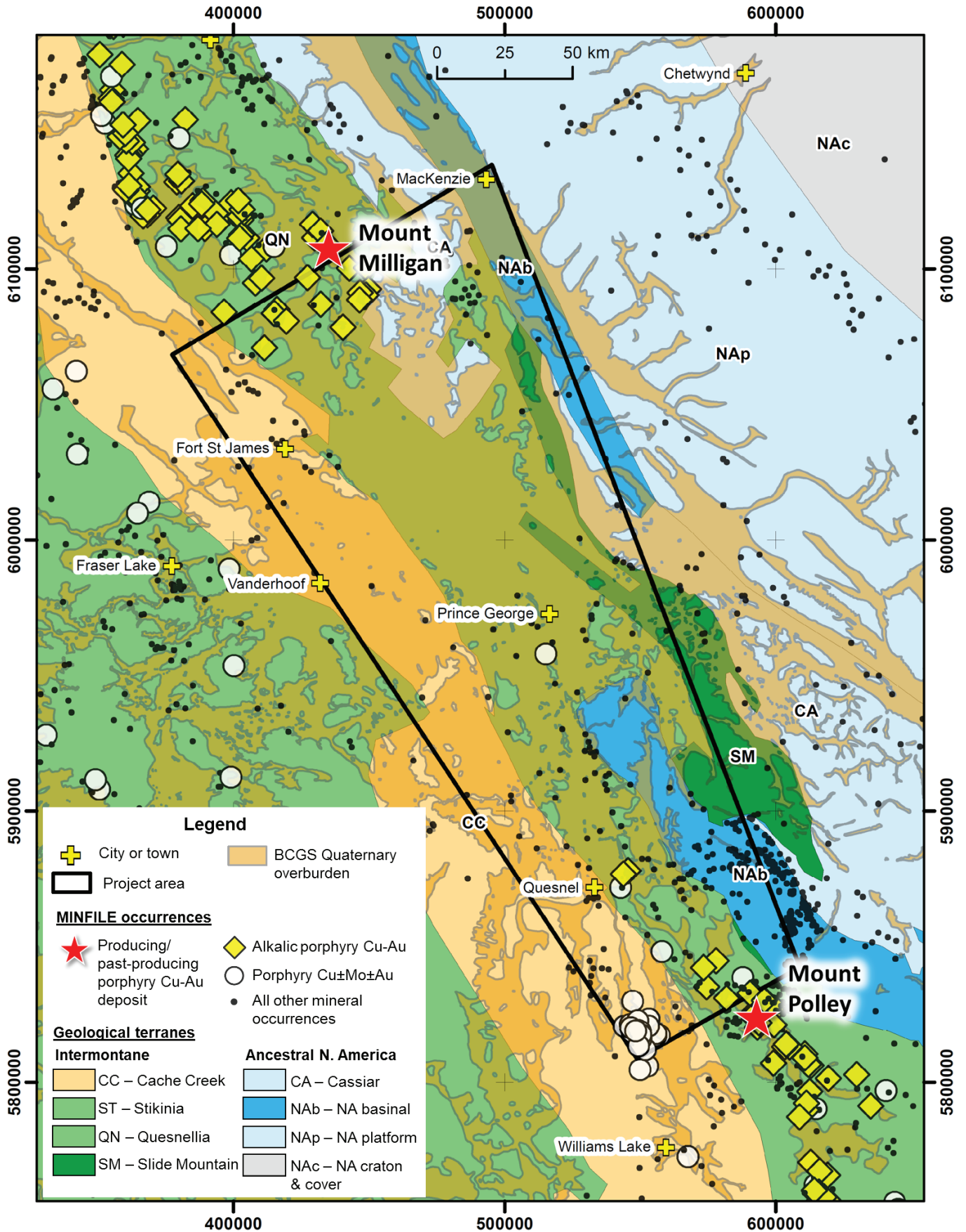


Figure 1: Project area overlain on the northern Cordilleran geological terrane map (Colpron and Nelson, 2011). Surficial geology indicating Quaternary overburden distribution through the region shown in pale transparent yellow (Cui et al., 2017). Locations of mineral occurrences: yellow diamonds are alkalic-porphyry Cu-Au occurrences, white circles are porphyry Cu-Mo-Au occurrences, black points are all other occurrences (MINFILE BC, BC Geological Survey, 2020). Project area outlined in black. Map coordinates in UTM zone 10, NAD 83.

Over the last 20 years there has been an increasing focus on identifying the similarities and differences between alkalic and calc-alkalic porphyry deposits, in an effort to improve exploration strategies. Aside from the intrinsic differing lithogeochemical compositions of host rocks, alkalic porphyry deposits are distinguished by their deposit size, alteration mineral assemblages (Figure 2), size of their magmatic-hydrothermal footprint, and their spatial distributions (Lang et al., 1995c; Chamberlain et al., 2007; Cooke et al., 2007; Bissig and Cooke, 2014). Alkalic porphyry deposits are found within the Quesnel and Stikine terranes of British Columbia. Currently, three alkalic porphyry deposits are mined in British Columbia: the New Afton, Copper Mountain, and Mount Milligan mines (Figure 3). The formerly active Mount Polley mine suspended operations in 2019.

Four magmatic belts can be traced in the southern Quesnel terrane, representing four intrusive events ranging from Late Triassic to Early Jurassic in age (Logan and Mihalynuk, 2014; Logan and Schiarizza, 2011). All are associated with porphyry deposits and occurrences (Figure 4). The belts are aligned northwest-southeast, parallel to the terrane boundaries, and young from west to east. The oldest magmatic belt, with intrusive rocks dated between 229–206 Ma, is associated with calc-alkaline magmas. The Highland Valley and the Gibraltar copper porphyry deposits are hosted by intrusions of this belt. From 207–198.6 Ma, an alkalic magmatic event occurred. Several alkalic porphyry copper-gold deposits were formed during this event, including the Mount Polley, New Afton, and Copper Mountain deposits. Another calc-alkalic magmatic event occurred between 202–192.7 Ma and intrusions associated with this arc host the past-producing Brenda Mine (MINFILE 092HNE047), and the Woodjam porphyry deposit (MINFILE 093A 078). The youngest magmatic belt in the southern Quesnel terrane is dated 197–185 Ma and has an alkalic affinity. Several small skarns and porphyry showings are related to this youngest event. The dates above were compiled and summarized by Ledoux and Hart (2021) and Logan and Schiarizza (2011).

Mount Polley and Mount Milligan occur at the southern and northern ends of the study area (Figure 3), respectively. Both are alkalic porphyry deposits. Host intrusions to the Mount Polley deposit formed during the Late Triassic 207–198.6 Ma alkalic event and Mount Milligan is hosted by intrusions that are Early Jurassic in age (~182–189 Ma; Mortensen et al., 1995). Due to the surficial cover in the expanse between the two deposits, it has not been possible to trace the known magmatic belts north of Mount Polley to Mount Milligan. The existence of the two deposits of distinct age at the boundaries of the covered area, and the semi-continuous southeast-northwest strike of arc stratigraphy (Sánchez et al., 2015) between them, indicates that alkalic porphyry intrusions of either age may be discoverable within the central Quesnel terrane.

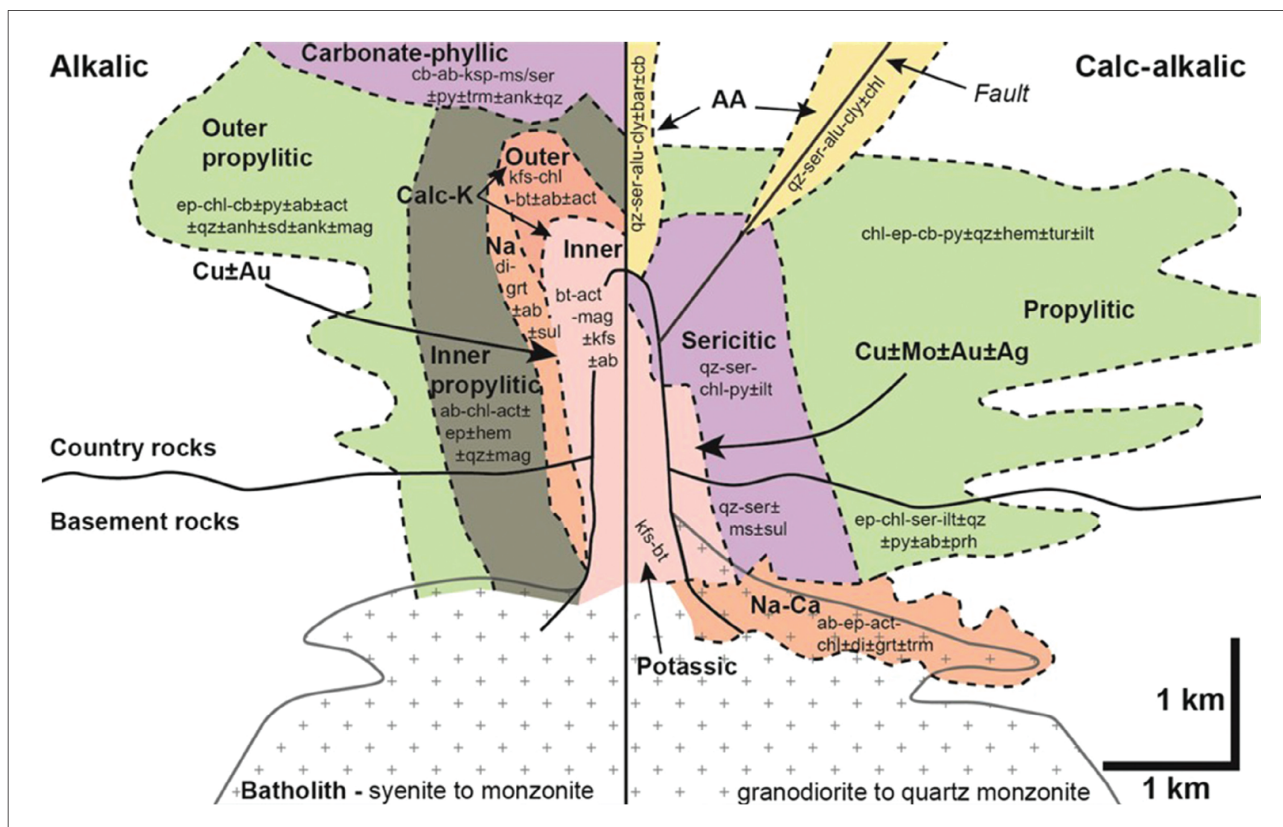


Figure 2: A schematic comparison between source rocks and alteration zoning associated with calc-alkalic and alkalic porphyry deposits (Figure 7 from Lee et al. (2020), p. 80. Reprinted with permission of the Canadian Institute of Mining, Metallurgy and Petroleum). Abbreviations: AA, advanced argillic; ab, albite; act, actinolite; alu, alunite; anh, anhydrite; ank, ankerite; bar, barite; bt, biotite; cb, carbonate; chl, chlorite; cly, undifferentiated clay; di, dickite; ep, epidote; grt, garnet; hem, hematite; ilt, illite; kfs, K-feldspar; mag, magnetite; ms, muscovite; prh, prehnite; py, pyrite; trm/tur, tourmaline; qz, quartz; ser, sericite; sd, siderite; sul, sulfides.

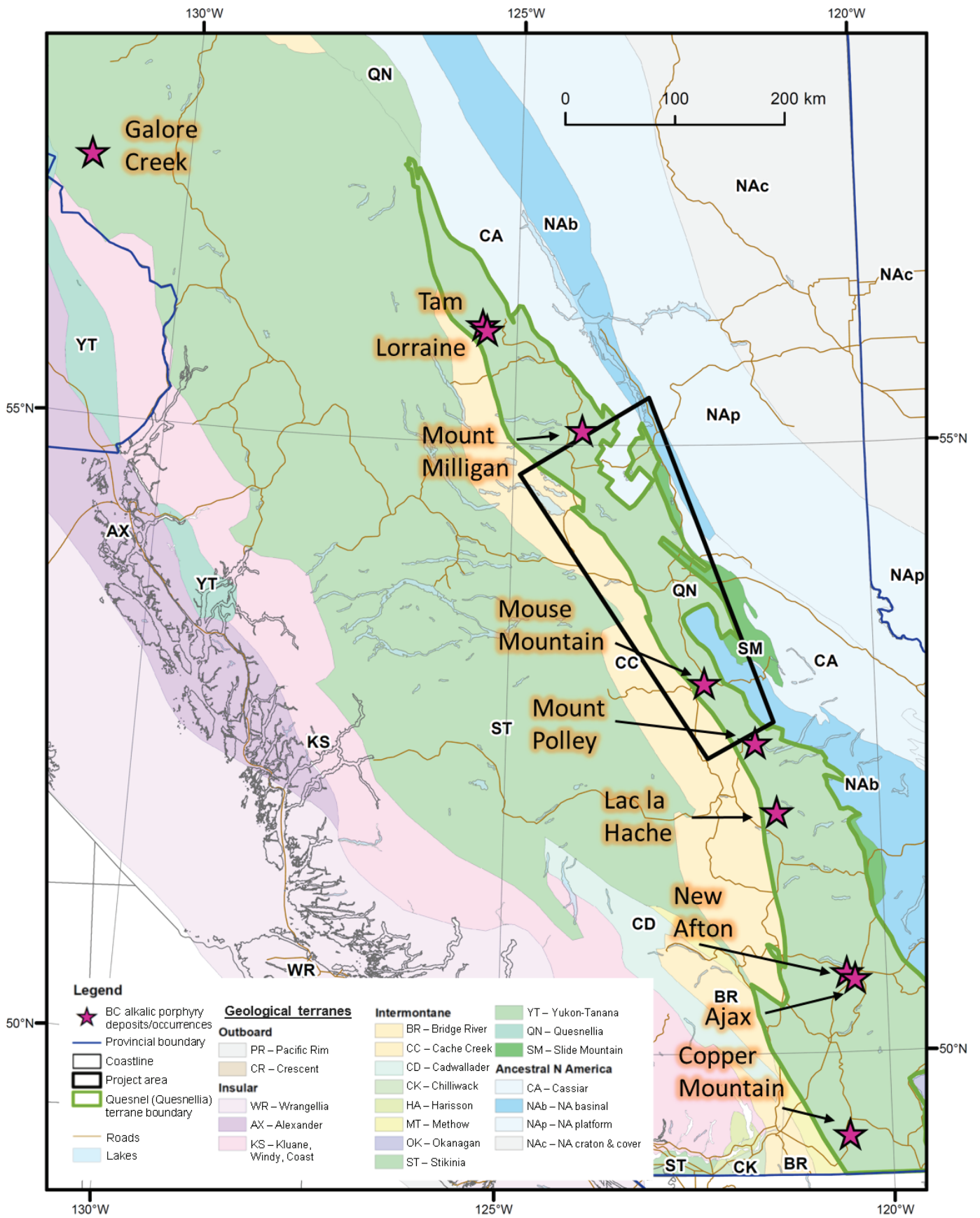


Figure 3: Distribution of alkalic porphyry Cu-Au deposits and mineralized centers in British Columbia. Cordilleran geological terrane map from Colpron and Nelson (2011).

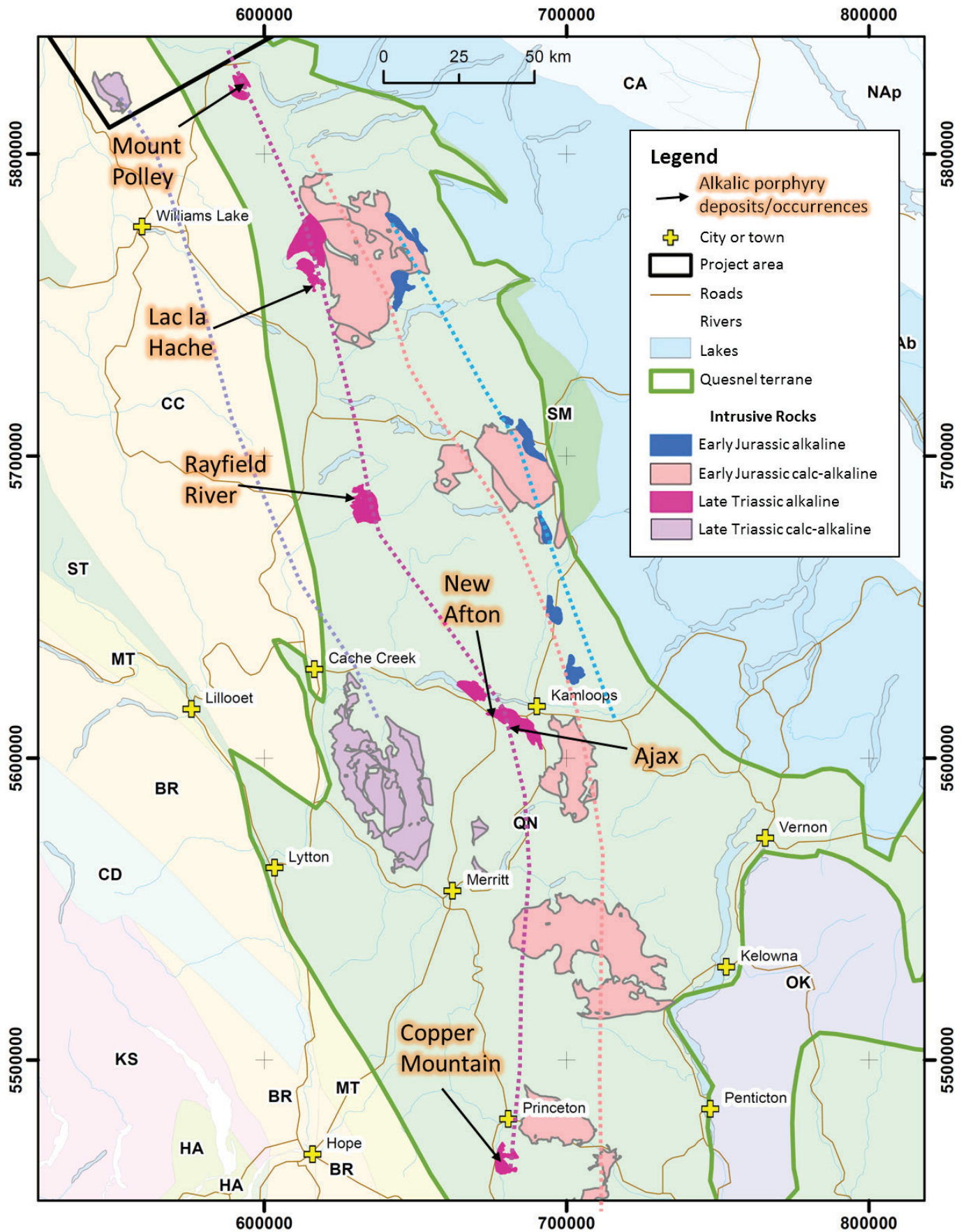


Figure 4: Four magmatic belts (shown as dotted lines) and associated intrusions in the southern Quesnel terrane (Logan and Schiarizza, 2011), with Late Triassic alkalic porphyry deposits indicated. Terrane abbreviations: ST, Stikine; MT, Methow; BR, Bridge River; CC, Cache Creek; CD - Cadwallader; HA - Harrison; KS - Kluane; NAp, North American platform; OK, Okanagan; QN, Quesnel; SM, Slide Mountain. Intrusions from B.C. Geological Survey bedrock geology map (Cui et al., 2017) and northern Cordilleran geological terrane map (Colpron and Nelson, 2011). Map coordinates in UTM zone 10, NAD 83.

2.2 Geophysical data available in the project area

Geophysical data is an essential exploration resource where bedrock exposure is limited, or mineral deposits are sitting deeper in the crust. The implied mineral prospectivity of the central Quesnel terrane has spurred multiple efforts to add to and enhance geophysical data to understand the bedrock geology under surficial cover. Geoscience BC has played an important role in creation of data and advancement of geological understanding for explorers looking for mineral deposits in prospective, yet underexplored, areas of British Columbia.

In 2007, Geoscience BC funded the collection of electromagnetic, magnetic, and gravity data (Geotech Ltd., 2008; Sander Geophysics, 2008) across the central Quesnel terrane as part of the QUEST project. In 2009, another gravity survey (Sander Geophysics, 2010) was flown in the southern Quesnel terrane, as part of the QUEST South project. This gravity survey characterized the porphyry deposits in southern Quesnel terrane and provided geophysical signatures to guide targeting in the project area.

Magnetic data collected and compiled by Natural Resources Canada (NRCan) covers Canada, including most of British Columbia (Natural Resources Canada, 2020). This dataset has a resolution that is well-suited for examining the regional magnetic responses of intrusive rocks hosting British Columbia porphyry deposits, and it is the principle magnetic dataset for regional targeting and modelling in this work. Local modelling is conducted using historic magnetic data collected in 1961, which was digitized and is available from the Canadian Airborne Geophysical Database as a geodatabase (.gdb) file (Series Issue ID: British Columbia - 61-1, Natural Resources Canada, 1962).

2.3 Previous work using geophysical data in the Quesnel terrane

Interpretation of the QUEST and QUEST South geophysical datasets was initiated and supported by a number of Geoscience BC research projects. Mira Geoscience Ltd. (2009) completed regional scale 3-D modelling of the datasets. They inverted the gravity, magnetic, and electromagnetic data, to yield density contrast, magnetic susceptibility, and conductivity models. Mira Geoscience's stitched 1-D inversions of EM data were used in this work to interpret overburden thickness. Sanchez et al. (2015) interpreted structure and geologic domains from NRCan magnetic and QUEST gravity data. This work investigated geological continuity between the southern Quesnel terrane and the central Quesnel terrane, such that prospective structures and lithologies might be traced from south to north. Thomas et al. (2011) and Thomas (2019) interpreted southern Quesnel terrane bedrock geology from magnetic and gravity data, looking in detail at data collected over the Iron Mask Batholith, host to the New Afton porphyry deposit. This work provides guidance in interpretation of geologic features from geophysical data in the central Quesnel terrane. Granek (2016) and Montsion et al. (2019) completed mineral potential modelling exercises using data from the QUEST projects, and from follow-up interpretations. The results of these regional mineral potential assessments are of interest for comparison to the outcomes from this project.

3. INITIAL PORPHYRY TARGET IDENTIFICATION

3.1 Geophysical footprints of known alkalic porphyry deposits in British Columbia

Initial target selection was based on magnetic data and an understanding of the common regional-scale geophysical signatures of alkalic porphyry-related intrusions in British Columbia. High amplitude positive magnetic anomalies, approximately 4-8 km wide, occur over intrusions hosting the Mount Polley and Mount Milligan deposits. The Mount Milligan deposit (Figure 5a) is situated within plagioclase-porphyrific monzonite stocks that are mapped 6 km southeast of a large composite monzonite-diorite-granite pluton referred to as the Mount Milligan Pluton (Nelson and Bellefontaine, 1996). Both the larger pluton to the north and the smaller mineralized stocks are encompassed within a regional magnetic high, suggesting that the Mount Milligan pluton continues southward but possibly at depth (Figure 5b), and appears to be the terminus of a magnetic trend related to the Hogem intrusive suite (Nelson and Bellefontaine, 1996). Geoscience BC QUEST gravity data indicates that the large Mount Milligan Pluton is dense relative to surrounding rocks, with a large positive gravity anomaly (Figure 5c). The coarseness of the gravity data does not provide adequate information on the gravity response of the smaller stocks hosting the Mount Milligan deposit to the south. While the Mount Milligan Pluton has yielded age dates pre- and post-dating the Mount Milligan deposit host rocks and a genetic relationship is not explicit, the proximity of alkalic porphyry mineralization to larger magnetic plutons, like the relationship seen at Mount Milligan, is a consistent trend further detailed in this section.

Several mineralized centers occur at Mount Polley (Figure 5d), most of which are hosted within brecciated zones of the dioritic to monzonitic Mount Polley Intrusive Complex (Logan and Mihalyuk, 2005; Rees et al., 2014). The rocks of the Mount Polley Intrusive Complex are associated with a positive magnetic response (Figure 5e). In contrast to the Mount Milligan area intrusive rocks, the Mount Polley Intrusive Complex is associated with a gravity low (Figure 5e). The lower gravity response at Mount Polley is possibly related to the influence of a large syenitic intrusion south of the deposit, which may have lower abundances of dense mafic minerals than the bulk rock compositions of intrusions at Mount Milligan.

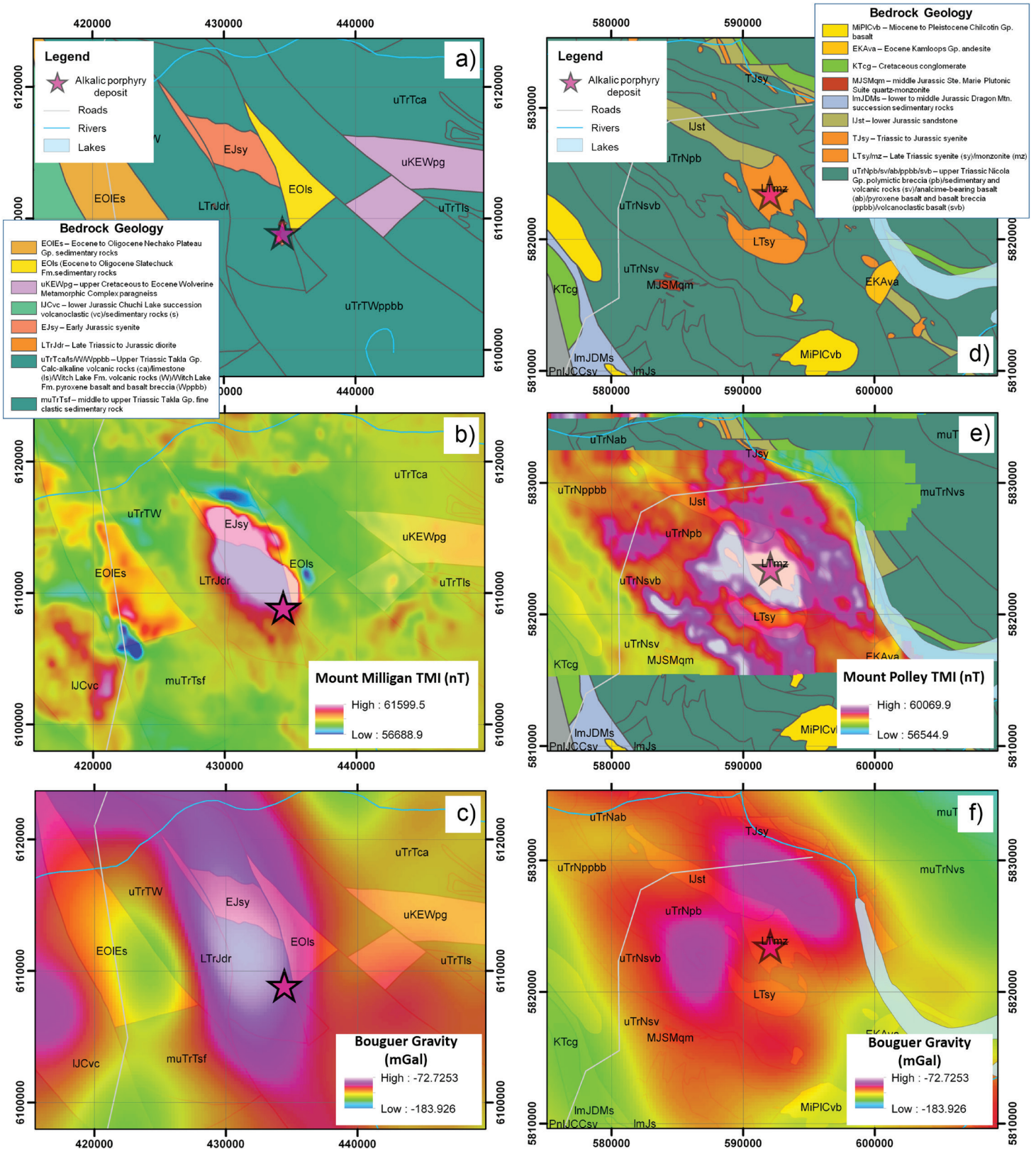


Figure 5: Geology (Cui et al., 2017), total magnetic intensity (TMI) data (Natural Resources Canada 1992 and 2004, Canadian Airborne Geophysical Database), and QUEST Bouguer gravity data (Sander Geophysics Ltd., 2008) over the Mount Milligan (5a, b, and c) and Mount Polley (5d, e, and f) deposit areas. See Figure 2 for location of Mount Milligan and Mount Polley deposits within the Quesnel terrane.

At Mount Milligan and Mount Polley, alteration assemblages proximal to mineralization contain secondary magnetite that may amplify the magnetic response at more local scales. In both camps, magnetic data has been useful for exploration of magnetite-bearing alteration zones (Fitzgerald et al., 2020; Brown et al., 2016).

Geophysical data from other known alkalic porphyry deposits in southern Quesnel terrane give similar insight to the character of the typical British Columbia alkalic porphyry deposit geophysical 'footprint'. The Copper Mountain and New Afton deposits, as well as prospects within the Lac la Hache camp (MINFILE 092P 153), are hosted by—often notably at the margins of—magnetic (magnetite-bearing) intrusions (Figure 6). The gravity data, though coarser, indicate that most of these alkalic intrusions (except for the Rayfield River pluton), are associated with positive gravity anomalies (Figure 7). The gravity highs associated with alkalic intrusions contrast with gravity lows related to Late Triassic and Early Jurassic calc-alkalic plutons.

3.2 Physical properties of alkalic porphyry deposit host rocks

Geophysical surveys respond to a rock unit's physical properties, its contrast with neighboring rocks, and the relative distribution of the rocks in the Earth's crust. To evaluate geophysical responses within the project area, and to help identify prospective domains using inversion models, it is important to investigate the physical properties of rocks that are common to the project area (and especially those of typical porphyry host rocks). Targets can be chosen that are consistent with the profile of alkalic porphyry deposit host rocks, and anomalies not meeting the petrophysical criteria of porphyry host rocks can be filtered out. The following sections describe existing and newly acquired physical property data from the central Quesnel terrane, highlighting the ranges of rock property values typical of some known porphyry deposit-hosting intrusions in this region.

3.2.1 Physical property data

Existing physical property data were sourced from the Canadian Rock Physical Property Database (Enkin, 2018). From nearly 20,000 database samples, approximately thirteen hundred samples occur within the Quesnel terrane. For evaluation, 161 Quesnel terrane samples were excluded as being rock types less relevant to this study (e.g. breccia, mineralized samples). Magnetic susceptibility and density data were available for most of the samples. The data were derived from many sources and work spanning decades. Some of the data were generated at the Geological Survey of Canada (GSC)-Pacific Paleomagnetism and Petrophysics Laboratory, and other historical data collected using similar tools and methodologies.

Thirty-two rock samples were collected as part of this project. The rock samples were collected across the project area capturing a broad representation of various intrusive and volcanic rocks within the central Quesnel terrane (Figure 8). Petrography and Terraspec measurements were completed on the rocks to confirm rock type and identify alteration minerals. Details are provided in Appendix 1. Rock property measurements for these samples were made at the GSC-Pacific Paleomagnetism and Petrophysics Laboratory (Digital Appendix 1). Physical property samples were prepared by drilling 2.5 cm diameter by approximately 2.2 cm long cores from rock samples. The magnetic susceptibility of each sample was measured using a Sapphire Instruments SI2B susceptibility meter, and magnetic remanence measured using an Agico JR5-A spinner magnetometer. Density was calculated using sample volumes and masses, derived from weighing samples in air and submerged in water. Resistivity and chargeability data were calculated from impedance spectra that were collected using the Solartron 1260 Frequency Response Analyzer. Complete details on petrophysical measurement methodologies are found in Enkin et al. (2012).

3.2.2 Magnetic susceptibility and density trends of Quesnel terrane rocks

Magnetic susceptibility values for all compiled samples from the Quesnel terrane range from 0.01×10^{-3} SI to 1330×10^{-3} SI (Table 1). For statistical analysis, samples were subdivided into 4 categories: ultramafic/gabbroic samples; volcanic rock samples; felsic to intermediate intrusive rock samples; and volcano-sedimentary/sedimentary rock samples. All sample suites span nearly the full range of magnetic susceptibilities seen in the Quesnel terrane (Figure 9), and all exhibit two magnetic susceptibility populations, which is common to large heterogeneous sample sets (Henkel, 1991; Enkin, 2018). These populations comprise the paramagnetic and magnetic populations within the sample suites. Rocks with low magnetic susceptibilities typically have only minor contributions of susceptibility from Fe-Mg silicate minerals (paramagnetic population), and do not contain significant magnetite, or have had magnetite destroyed through secondary hydrothermal processes. The high magnetic susceptibility rocks (magnetic population) are those which contain magnetite (either primary or secondary).

Ultramafic rocks and gabbro samples from the central Quesnel terrane have relatively high median magnetic susceptibilities (~ 12 to 78×10^{-3} SI). Intermediate to mafic volcanic rocks and greenschist (assumed to be largely meta-volcanic) rocks have low to moderate median magnetic susceptibility values (~ 0.2 to 10×10^{-3} SI). Felsic to intermediate intrusive rock samples have low to high median magnetic susceptibility values (0.7 to 60×10^{-3} SI). Sedimentary rocks have low magnetic susceptibility median values (0.3 to 0.7×10^{-3} SI).

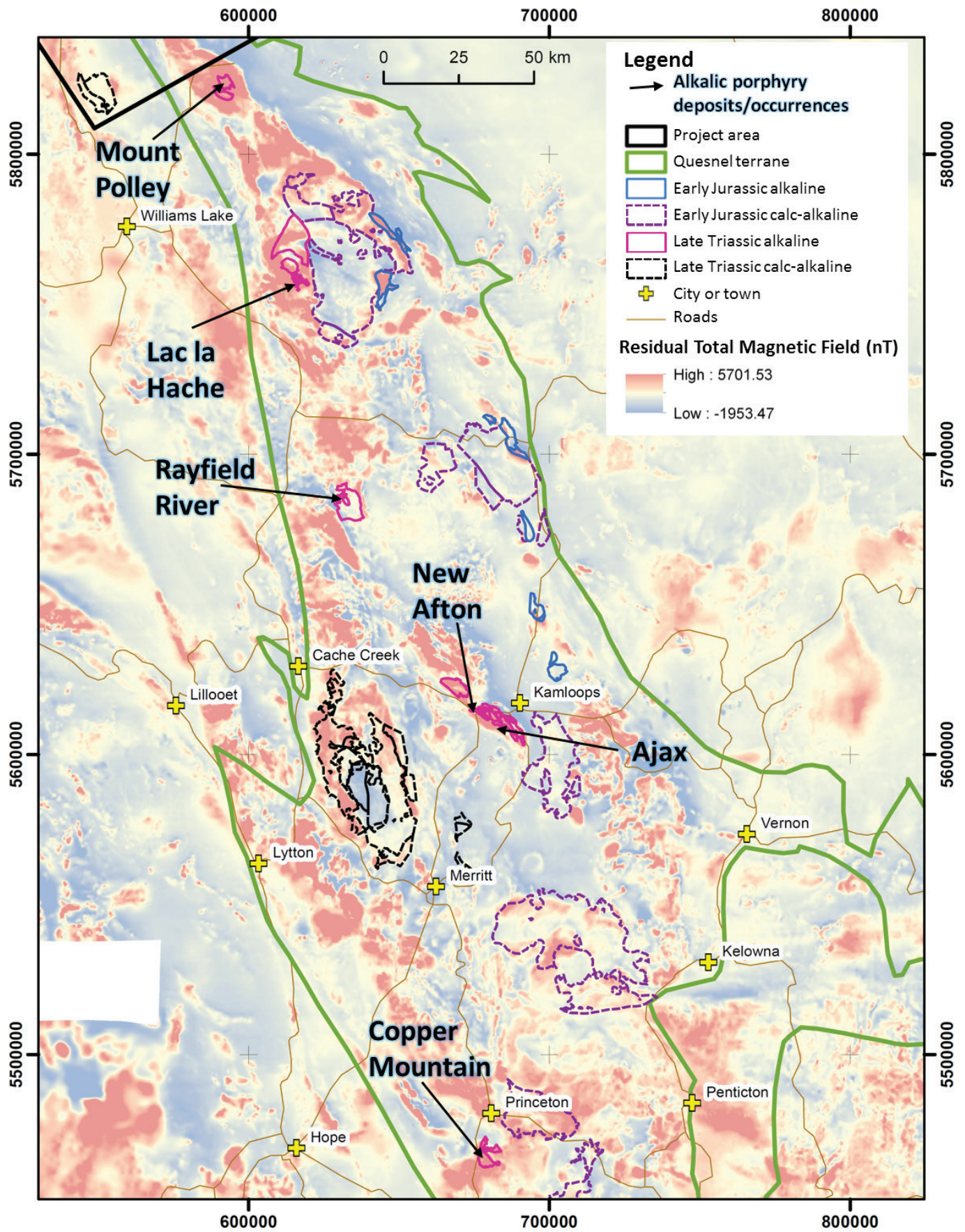


Figure 6: Residual total field (RTF) magnetic data (Natural Resources Canada, 2020) over the southern Quesnel terrane. Intrusions related to the four magmatic belts of Logan and Schiarizza (2011) are indicated, with alkalic porphyry deposits associated with the Late Triassic alkaline belt noted. Map coordinates in UTM Zone 10, NAD 83.

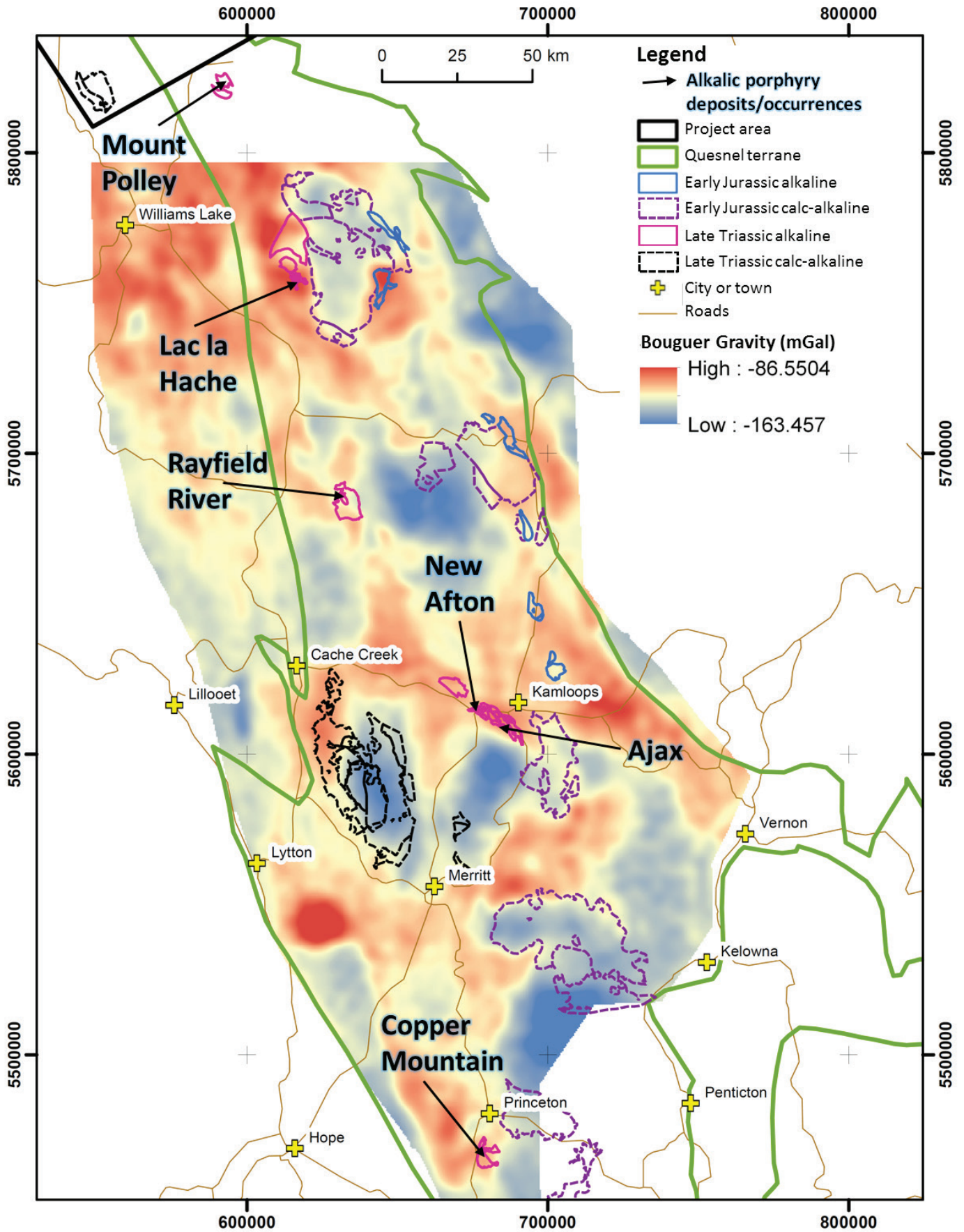


Figure 7: Bouguer gravity data (Sander Geophysics Ltd., 2010) over the southern Quesnel terrane. Intrusions related to the four magmatic belts of Logan and Schiarizza (2011) are indicated, with alkalic porphyry deposits associated with the Late Triassic alkalic belt noted. Map coordinates in UTM zone 10, NAD 83.

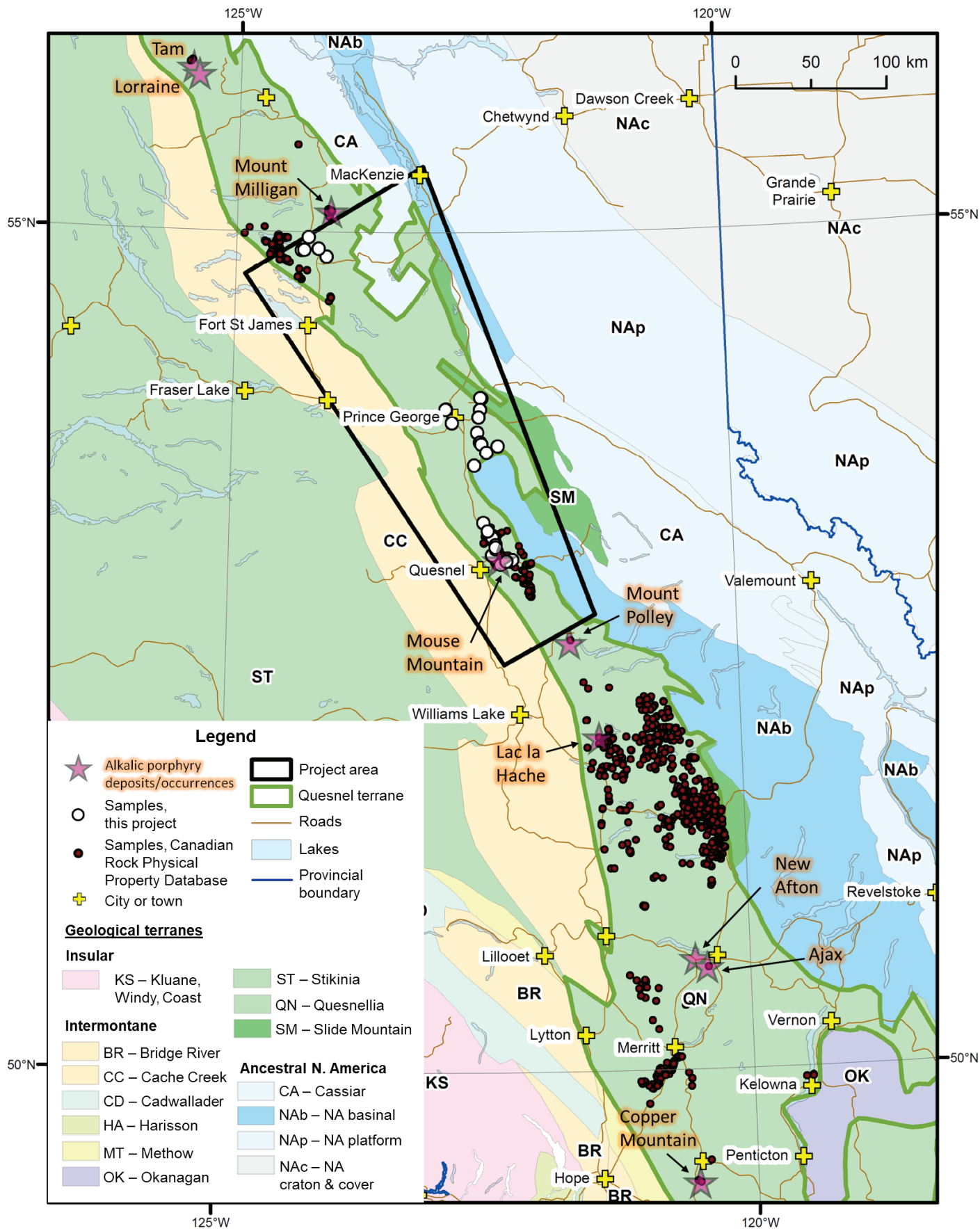


Figure 8: Map showing samples collected as part of this project, and Quesnel terrane samples from the Canadian Rock Physical Property Database (Enkin, 2018). Northern Cordilleran geological terrane map from Colpron and Nelson (2011).

Table 1: Summary of rock properties from the Quesnel terrane (Canadian Rock Physical Property Database; Enkin, 2018), and from this study (“NPP” – Geoscience BC New Porphyry Potential project). Uncolored rows are not used in statistics or plots. Values are rounded to two decimal places.

Lithology	Magnetic Susceptibility ($\times 10^{-3}$ SI)				Density (g/cm^3)			
	Count	Med	Min	Max	Count	Med	Min	Max
<i>All samples</i>	1162	2.05	0.01	1330.00	856	2.78	2.24	3.72
Ultramafic	37	77.50	0.27	1330.00	27	3.00	2.58	3.43
Gabbro	35	12.60	0.18	136.00	27	2.95	2.77	3.23
Gabbro (NPP)	3	18.59	0.67	49.36	3	2.94	2.91	3.10
Basalt	249	2.11	0.01	539.00	205	2.84	2.24	3.72
Basalt (NPP)	6	0.48	0.17	100.70	6	2.85	2.62	3.00
Greenschist	1	0.25	0.25	0.25	1	2.75	2.75	2.75
Greenschist (NPP)	1	0.48	0.48	0.48	2	2.80	2.76	2.84
Volcanic rock	30	1.77	0.12	77.70	4	2.75	2.66	2.82
Andesite	36	9.90	0.23	122.00	29	2.75	2.57	2.90
Andesite (NPP)	1	0.26	0.26	0.26	1	2.65	2.65	2.65
Dacite	13	0.96	0.10	47.10	9	2.60	2.49	2.95
Rhyolite	11	0.93	0.02	10.70	0			
Diorite	127	8.00	0.05	180.00	67	2.86	2.55	3.37
Diorite (NPP)	2	60.32	35.38	85.25	2	2.86	2.78	2.93
Monzodiorite	60	11.15	0.24	128.00	24	2.80	2.60	2.97
Monzodiorite (NPP)	2	0.73	0.27	1.19	2	2.72	2.70	2.75
Qtz-monzodiorite (NPP)	1	34.95	34.95	34.95	1	2.71	2.71	2.71
Granodiorite	48	16.45	0.23	60.45	27	2.67	2.59	3.00
Monzonite	36	7.71	0.05	276.00	28	2.68	2.55	2.84
Monzonite (NPP)	1	9.10	9.10	9.10	1	2.67	2.67	2.67
Monzogranite (NPP)	1	6.68	6.68	6.68	1	2.67	2.67	2.67
Syenite	21	8.39	0.03	45.90	19	2.66	2.48	2.87
Granite	20	1.08	0.12	88.10	4	2.77	2.65	2.86
Plutonic rock	19	50.52	0.08	662.00	5	2.93	2.71	3.44
Porphyritic rock	22	1.19	0.06	131.00	19	2.86	2.65	3.00
Volcanic sediment	202	0.70	0.02	200.00	184	2.76	2.43	3.09
Volcanic sediment (NPP)	7	0.33	0.03	0.54	8	2.72	2.60	2.79
Sedimentary rock	146	0.45	0.01	325.00	123	2.74	2.36	3.05
Sedimentary rock (NPP)	2	0.29	0.23	0.35	2	2.70	2.63	2.76
Limestone	22	0.11	0.01	1.55	25	2.71	2.65	2.84

Binary plots of magnetic susceptibility versus density show the relationship between the two rock properties for the major rock types of the Quesnel terrane (Figure 10). Felsic to intermediate intrusive rocks (Figure 10a) are clustered predominantly in the higher magnetic susceptibility ranges and have low to moderate densities. Dioritic rocks have the highest densities of all the felsic to intermediate intrusive rocks. Samples derived from known porphyry deposit-associated intrusions plot as part of the high magnetic susceptibility population (Figure 10a). Details of these samples, such as their proximity to mineralization or degree of alteration are not available, with the exception of a suite of monzonitic samples from Mount Milligan (Mitchinson et al., 2013). The suite of Mount Milligan samples comes from the core of the Mount Milligan deposit and exhibit a range of magnetic susceptibilities that reflects their degree of alteration from low magnetic susceptibility sodic-calcic-altered monzonite samples to high magnetic susceptibility secondary magnetite-bearing potassic-altered monzonite samples. Very few unaltered rocks are represented in this suite. The average magnetic susceptibility of all Mount Milligan samples in the database is 40×10^{-3} SI Units.

Ultramafic rocks, gabbros, and mafic volcanic rocks (Figure 10b and 10c) can attain high magnetic susceptibility values like felsic to intermediate intrusive rocks but are generally distinguished by their higher densities. Volcanic sedimentary rocks (Figure 10d and 10e), rocks classified as sedimentary (not specified as volcanic sedimentary in the database, and assumed to be clastic sedimentary), and limestones, are largely distinguished from felsic to intermediate intrusive rocks by their lower average magnetic susceptibility ranges.

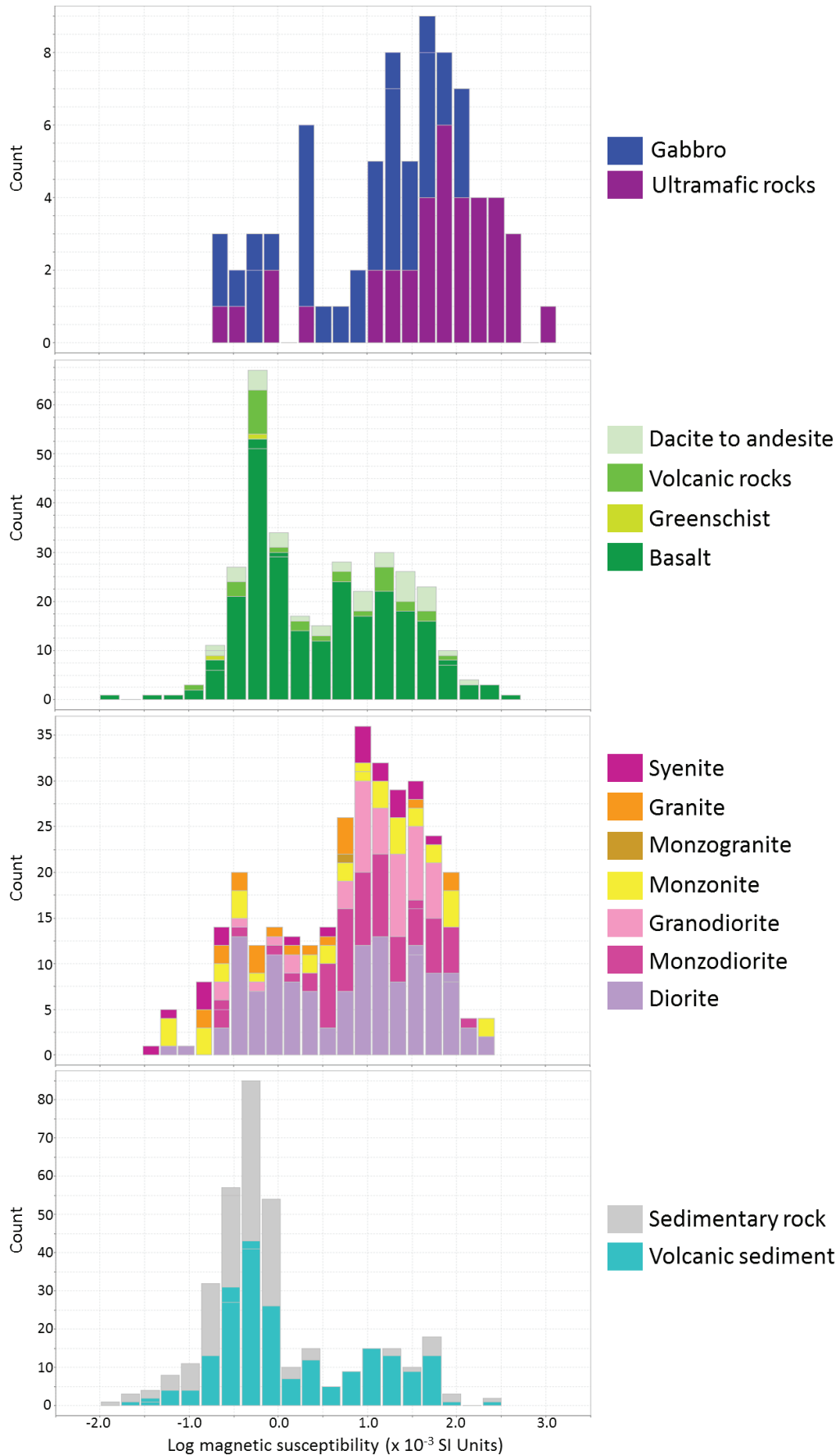


Figure 9: Log magnetic susceptibility data for samples from major rock groups in the Quesnel terrane of British Columbia.

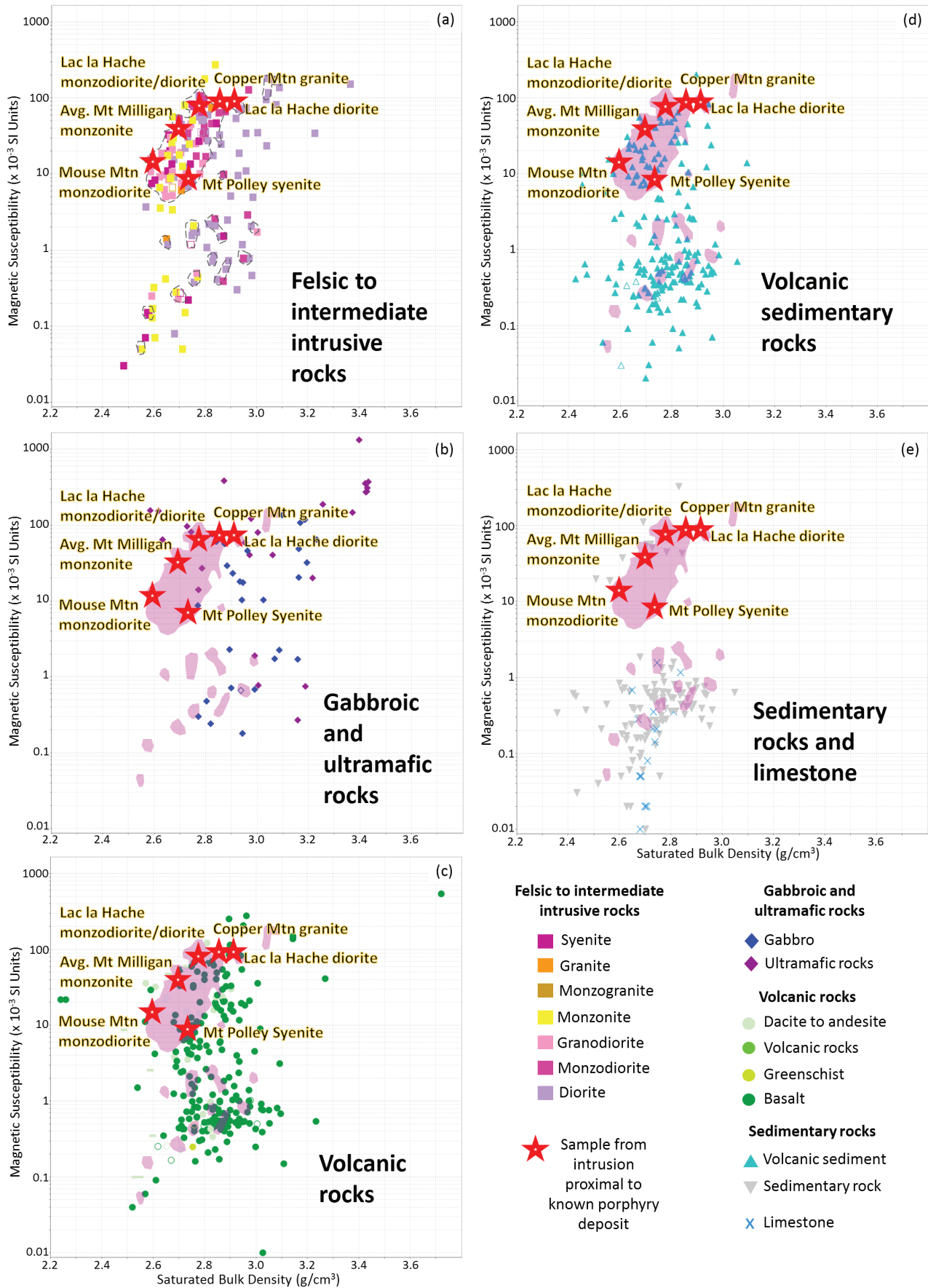


Figure 10: Saturated bulk density versus magnetic susceptibility plots for major rock types within the Quesnel terrane. The dashed and pink regions represent greatest sample density for felsic to intermediate intrusive rocks for comparison to other rock types. Red stars represent samples from known porphyry host rocks. Open symbols are samples from this project, and closed symbols are samples from the Canadian Rock Physical Property Database (Enkin, 2018).

Intrusive rocks that have an affiliation with alkalic porphyry deposits in the Quesnel terrane are not entirely petrophysically unique, but do have high magnetic susceptibilities, as suggested from initial reviews of magnetic data from the southern Quesnel terrane, and low to moderate densities relative to mafic and ultramafic rocks. Felsic to intermediate intrusive rocks should be distinguishable from volcanic sedimentary and clastic sedimentary rocks by their overall higher magnetic susceptibility values.

The limited number of samples from known porphyry hosts and the incomplete information about their alteration state precludes deductions about the typical petrophysical character of intrusive rocks at specific porphyry deposit sites. That said, a trend from lower density more felsic mineral-abundant porphyry deposit hosts (monzonites, syenites) to higher density dioritic porphyry hosts may be surmised.

3.3 Target selection based on regional geophysical trends and physical properties

Based on geophysical and petrophysical trends indicating that gold-rich alkalic porphyry deposits in British Columbia are commonly hosted by magnetic (magnetite-bearing) intrusive rocks, a suite of magnetic anomalies within the project area was selected using the Natural Resources Canada 200 m grid magnetic data (Natural Resources Canada, 2020). The data were reduced to pole, and derivative maps of the magnetic data were produced to help distinguish and best locate anomalies.

Targets were chosen visually based on several criteria: having 1) a positive magnetic anomaly; 2) a size similar to known intrusive hosts or intrusive source rocks for porphyry deposits in central British Columbia; 3) a rounded shape consistent with a plutonic body; and 4) cross-cutting relationship(s) with surrounding rocks or stratigraphy. Some of the Nicola and Takla group volcanic stratigraphy, as well as ultramafic units of various ages, are magnetically anomalous. Positive magnetic anomalies clearly attributed to mapped mafic to ultramafic rock types were avoided in target selection. The final suite of 57 targets (Figure 11) thus have shapes, sizes, and magnetic characteristics similar to known porphyry host and source rocks situated north and south of the project area.

The magnetic anomalies chosen range in size from approximately 2–50 km² (Figure 11). Some are coincident with intrusive rocks that are mapped at the surface, whereas others do not have an obvious link to mapped or interpreted bedrock geology and may therefore represent a deeper, or under cover, magnetic body. The magnetic targets can be subdivided roughly into four clusters: 1) east and north of Quesnel, where the majority of anomalies are aligned with the regional northwest geological strike; 2) south of Prince George, where anomalies occur along an east-west trend; 3) north of Prince George, where a north-northeast trend is apparent; and 4) east of Fort St. James, where the cluster of anomalies strikes northwest again.

4. OVERBURDEN MODELLING

Following target selection, a revised model of the overburden thickness across the project area was developed. This model allowed us to effectively assess cover thickness over the chosen targets, as well as account for (constrain) this layer when inverting the geophysical data.

4.1 Constraining data

There exists a significant amount of information with which to constrain a 3-D model of the overburden thickness of the central Quesnel terrane. Previous work used data from water wells and mapping to interpolate overburden thickness (Andrews and Russell, 2008; Maynard et al., 2010). Helicopter-borne Versatile Time-Domain Electromagnetic (VTEM™) data inversion models provide an additional source of information for constraining overburden thickness, with overburden clearly indicated as a near-surface, flat-lying conductor. Combining all the available observed data with the base of overburden interpreted from VTEM inversion models provides nearly full coverage of the project area from which overburden thickness can be estimated. Details on constraining data sets are outlined in the following sections. Refer to Table 2 for details on constraints derived from each data source.

4.1.1 Water wells

Groundwater well data were sourced from the British Columbia Ministry of Environment and Climate Change Strategy (2020). In most cases, for each groundwater well, a geology log, bedrock depth, and water depth, among other hydrogeological data, are recorded in the public database. In some instances, it was found that there were discrepancies between the bedrock depths recorded in the database, and those recorded in the original water well record which is archived for each well. The original records for each hole where bedrock was intercepted were thus carefully reviewed and the bedrock depths were updated within the project database to match those noted in the records. Over 1100 wells intercepted bedrock, and approximately 100 of these well records were updated. There were discrepancies up to 500 ft difference in the bedrock depth recorded in the database and that recorded in the original log. For the remaining wells where bedrock was not intercepted, a random spot-check was completed on the original records to confirm that

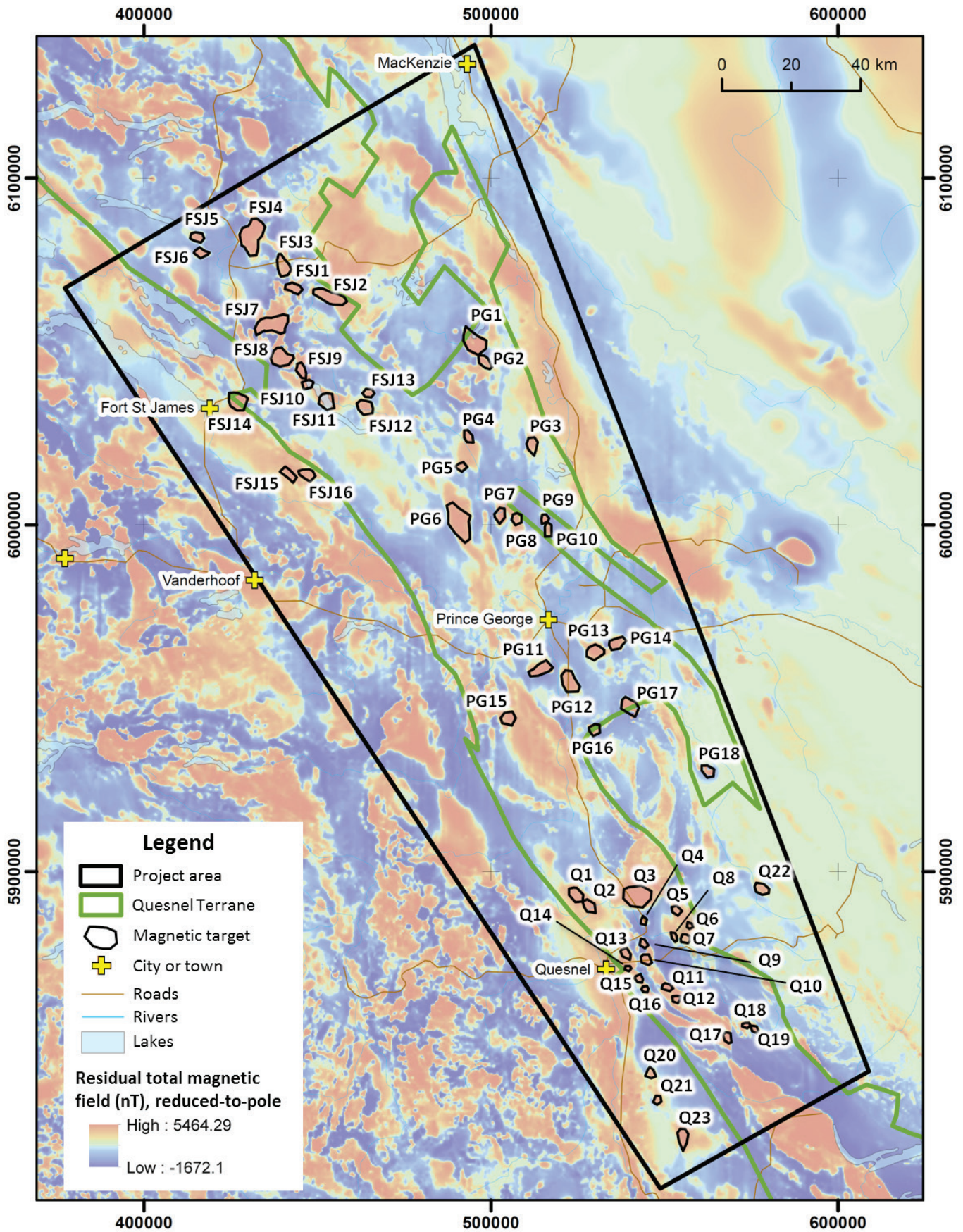


Figure 11: Magnetic targets selected within the project area. Natural Resources Canada (2020) magnetic data. Map coordinates in UTM Zone 10, NAD 83.

Table 2: Types and numbers of data constraints used for overburden thickness modelling in this project.

Constraining Data	Number of Data	Source
<u>Ground water wells</u>		Ministry of Environment and Climate Change Strategy (2020)
<i>Bedrock interface</i>	1169	
<i>Minimum thickness where bedrock not recorded</i>	5924	
<u>Exploration drill hole data from BCGS assessment reports</u>		BC Ministry of Energy, Mines and Petroleum Resources (2020)
<i>Bedrock interface</i>	198	
<i>Minimum thickness where bedrock not recorded</i>	30	
<u>Outcrop location</u>		Logan et al. (2010), Maynard et al. (2010)
<i>BC Geological Survey QUEST Compilation</i>	1225	
<i>Maynard et al. (2010) surficial mapping project</i>	95	
<u>QUEST program VTEM model interpretations</u>		This study
<i>Points digitized from base of overburden interpretations</i>	25965	
<i>Points digitized from areas of no apparent overburden</i>	1047	

bedrock was not hit. About 160 wells were checked and 15 inconsistencies were found, suggesting there might be regular discrepancies. It should be noted that the authors are not fluent in working with water well logs or data and there is a possibility of misinterpretation of the logs. A digital appendix (Digital Appendix 2) is provided containing the water well data extracted for this project, and noting the updated bedrock depth records. A confidence is assigned to the data record based on whether the original water well record was checked. The bedrock depth or final depth of well (essentially minimum overburden thickness) were the only two variables that were applied as constraints for modelling overburden thickness.

4.1.2 ARIS mineral exploration drilling logs

Publicly available mineral exploration drillhole logs are another source of bedrock depth data. Exploration drill log data were accessed from the mineral exploration assessment report indexing system (ARIS) database maintained by the British Columbia (BC) Ministry of Energy, Mines and Petroleum Resources. Extracting the relevant data was labour-intensive as most filed exploration drilling reports in British Columbia do not include a digital database. It was necessary to manually copy the lithological data from the reports into a database that could be fed into SKUA-GOCAD™, ArcGIS® or other GIS software used by this project for mapping and modelling. The compiled data are made available in a digital appendix accompanying this report (Digital Appendix 3). Drill collar location, survey details, and a simplified lithology assigned by the authors is included. The drilling data are derived from drill reports that were available up to 2020 and was not exhaustive. New drilling data presumably has become available since this time.

4.1.3 Outcrop location data

Outcrop locations were sourced from the British Columbia Geological Survey (Logan et al., 2010), with additional outcrop that was identified by Maynard et al. (2010). The BCGS outcrop data is simply location data, with no information regarding bedrock lithology. Where outcrop exists, bedrock depth is recorded as 0 m for the purposes of overburden thickness modelling.

4.1.4 Bedrock depth from electromagnetic data interpretations

Interpretations from VTEM data inversions help to fill gaps in observed bedrock data. VTEM data collected as part of the QUEST project were noted in early evaluations to be capable of identifying overburden (Kowalczyk et al., 2010), with overburden acting as a conductor, likely due to its water content and high porosity relative to underlying bedrock. The inversion models used for interpretation of overburden thickness are those from Mira Geoscience Ltd. (2009).

VTEM line inversions were compared with information from water wells, exploration drillholes and outcrop databases at localities where these data co-occur to confirm independently whether VTEM models could resolve overburden. Consistently, thin, flat-lying conductors near surface in the inversion models were found to regularly match the base of overburden and minimum thickness depths (end of hole) recorded in water well and exploration drill logs. This gave confidence that overburden is a consistent conductor and can be mapped, as well its thickness estimated, from VTEM inversion results. The upper conductive layer is minimal to absent in areas of known outcrop, which supports this interpretation. Figure 12 illustrates examples of correlation between various constraining data and VTEM conductivity horizons interpreted to represent overburden.

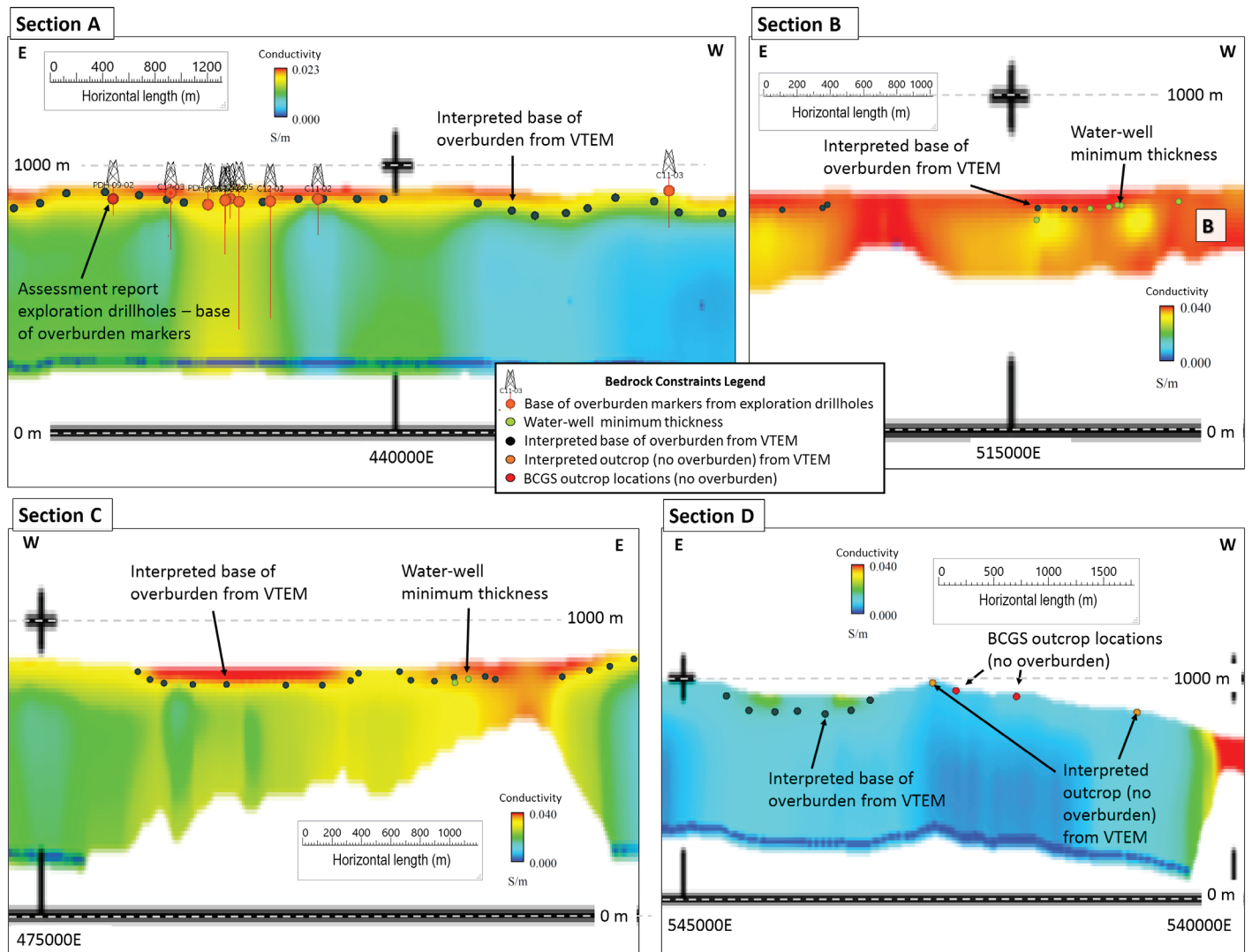


Figure 12: Vertical cross-sections through VTEM 1-D conductivity inversions showing correlation between high-conductivity layers resolved near surface and the presence of overburden as indicated in exploration-drilling, water well, and outcrop data. Vertical scale is elevation with 2x exaggeration. Grid is represented by black lines and crosses. Section locations A–D are shown in Figure 14. Abbreviation: S/m, siemens/meter.

Two types of overburden-thickness constraints were extracted from VTEM inversions: 1) base of conductive overburden, and 2) locations of no apparent overburden. Interpretations of the apparent base of the overburden were manually digitized line by line. For each line that was interpreted, only those conductors that were most obviously related to overburden were marked. Other conductivity anomalies that had several possible geological, geographic or cultural causes, or were ambiguous, were ignored.

To estimate error of interpreted depth of overburden based on VTEM models, the depth of the base of overburden interpreted from VTEM was compared to the depth of overburden from groundwater wells. For this we include all water wells, those intercepting bedrock and those that do not, and assume minimum thickness depths (where bedrock was not intercepted) is the base of overburden. This provides more data points for analysis, and also allows us to determine whether minimum depth markers are reliable to use as an estimate of overburden depth. A 2-D grid with 500 m cells was created and depths from the interpreted base of overburden and groundwater wells were transferred to the grid. Anywhere there is a groundwater well co-located with a VTEM line interpretation it is possible to compare the overburden depths. Figure 13a shows a correlation coefficient between interpreted and observed data of 0.88. Figure 13b shows the difference calculated for all the sites where groundwater wells occur. Using the 10th and 90th percentile, differences between VTEM-interpreted and observed overburden depth can be up to +/- 50-60 m.

Once interpretations were complete, all constraints (Figure 14) were converted to a 3-D pointset in Paradigm’s SKUA-GOCAD 3-D modelling software to model overburden thickness.

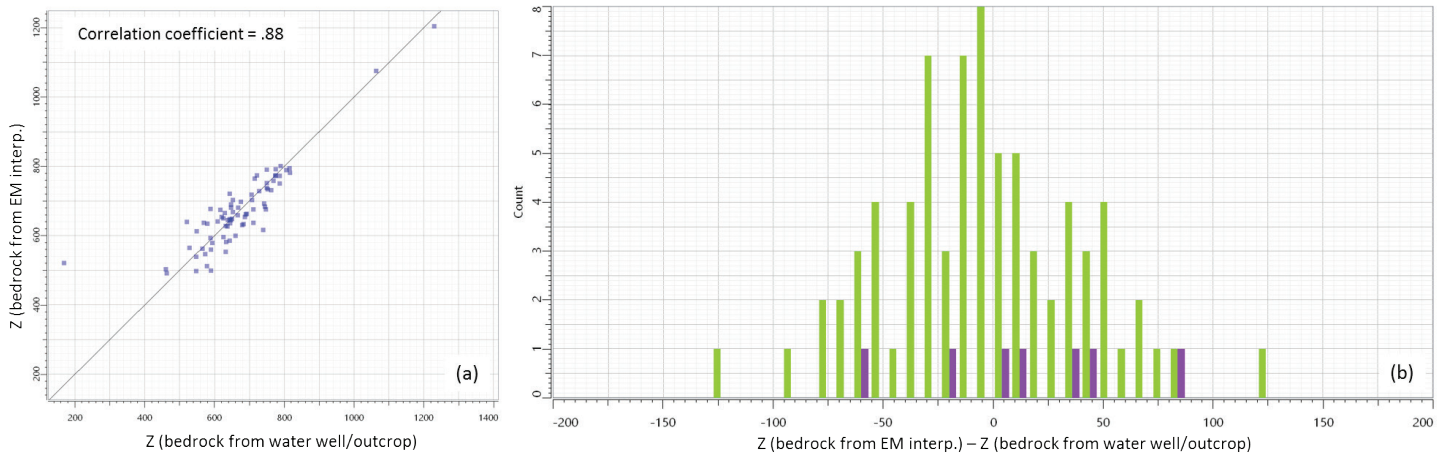


Figure 13: (a) Correlation between depth to base of overburden/top of bedrock interpreted from VTEM models and observed from groundwater well/outcrop; (b) Difference between interpreted and observed depths of overburden at sites where the data co-occur spatially (green - groundwater well, purple - mapped outcrop location).

4.2 Method

SKUA-GOCAD was used to interpolate depth to bedrock across the project area. All constraining data were given equal weight during modelling.

The modelling steps are outlined below.

1. A surface (plane) was generated that sits at the average elevation of all the observed data points.
2. The surface was split equally until the mesh triangles were approximately 500 m resolution (the approximate resolution of the topographic data used for this project).
3. The surface was warped to fit the observed data points using the discrete smooth interpolation algorithm (DSI).
4. The surface mesh was split again to create a slightly higher resolution mesh ($\sim 250 \text{ m}^2$) for refined interpolation steps (step 5).
5. The slightly higher resolution surface was pushed below topography in places where it was interpolated above.

Because of the high resolution of constraining data along EM inversion lines, a smoothing was completed to reduce the effects created by localized concentrations of data.

6. The elevation property from the warped base of overburden/top of bedrock surface was copied onto a 2-D grid.
7. A smoothing was completed on the grid using a median window filter process, which finds the median value of a defined cluster of cells and applies that median value to the central cell.
8. The smoothed data were reverted to a pointset, and the initial top of bedrock surface was smoothed slightly by fitting to these smoothed data.
9. The final top of bedrock surface was once again pushed below topography.

The final top of bedrock surface was then reviewed in 3-D against original observed data to ensure that bedrock constraints continued to be honored. Figure 15 shows the difference between the elevation from the final interpolated top of bedrock surface and the elevation of the bedrock from constraining data. Using the 10th and 90th percentile, differences between bedrock elevations from constraining data and from the interpolated top of bedrock surface range from -32 m to +26 m, respectively, with a mean difference of -2.5 m. The largest differences are mostly seen in areas of greater topographic relief, where a smooth model cannot capture the more high frequency changes in the bedrock and overburden interface (northwest, northeast, and southeast project areas). Some larger discrepancies also occur where there are numerous types of constraining data and there are conflicts between them (e.g., a cluster of water well data immediately south of Prince George in the center of the project area).

4.3 Results

The overburden thickness model (Figure 16) is a regional-scale estimate of depth to bedrock within the project area. The smoothing interpolation grid was 500 m^2 ; as such, lateral information at a higher resolution was not captured. The accuracy of the result depends

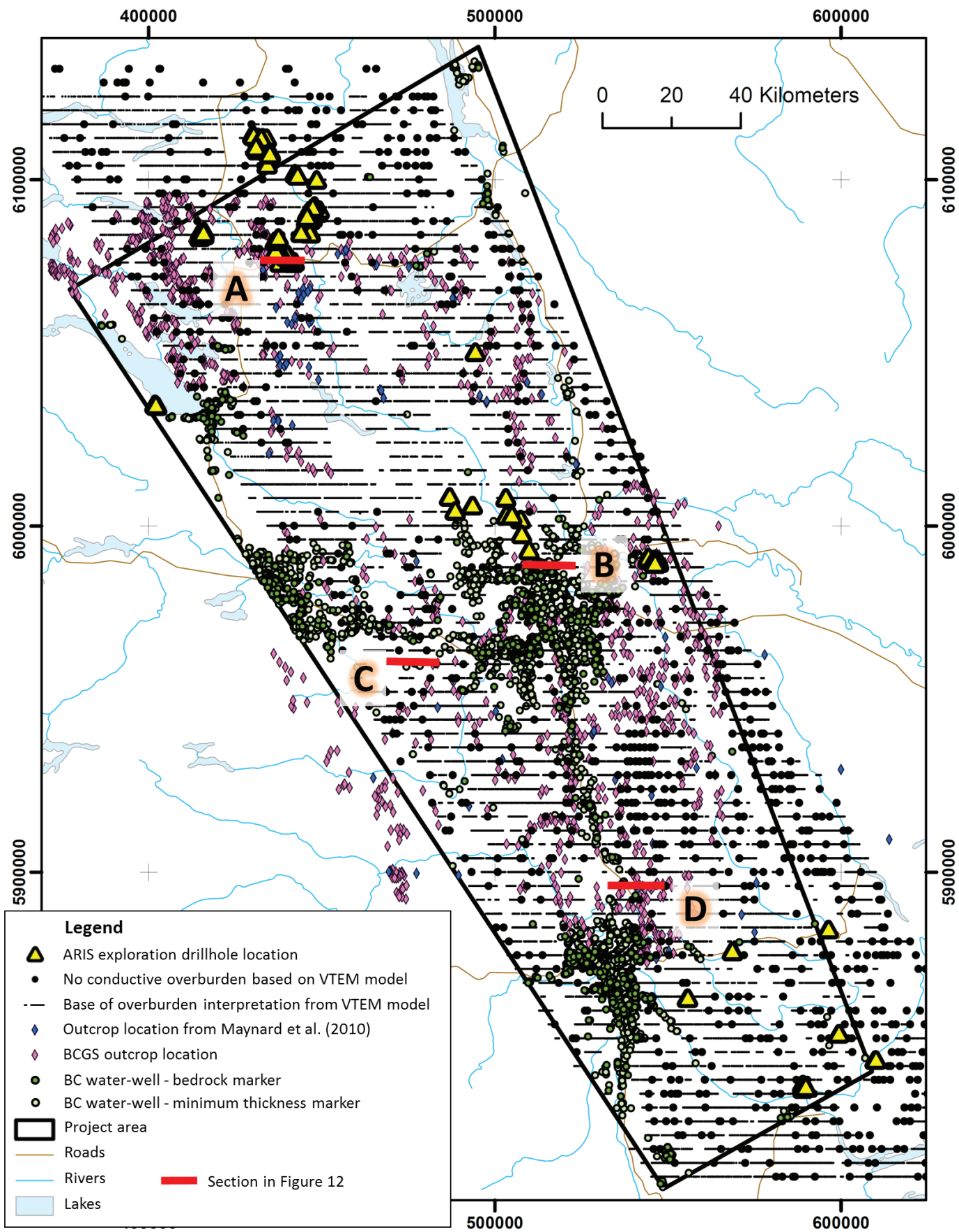


Figure 14: Constraining data in overburden-thickness modelling. Constraining data from VTEM inversion models are derived from interpretations digitized along east-west VTEM lines spaced 4 km apart. Project area lies within the black quadrilateral. Abbreviations: PG, Prince George; FSJ, Fort St. James; Q, Quesnel. Map coordinates in UTM Zone 10, NAD 83.

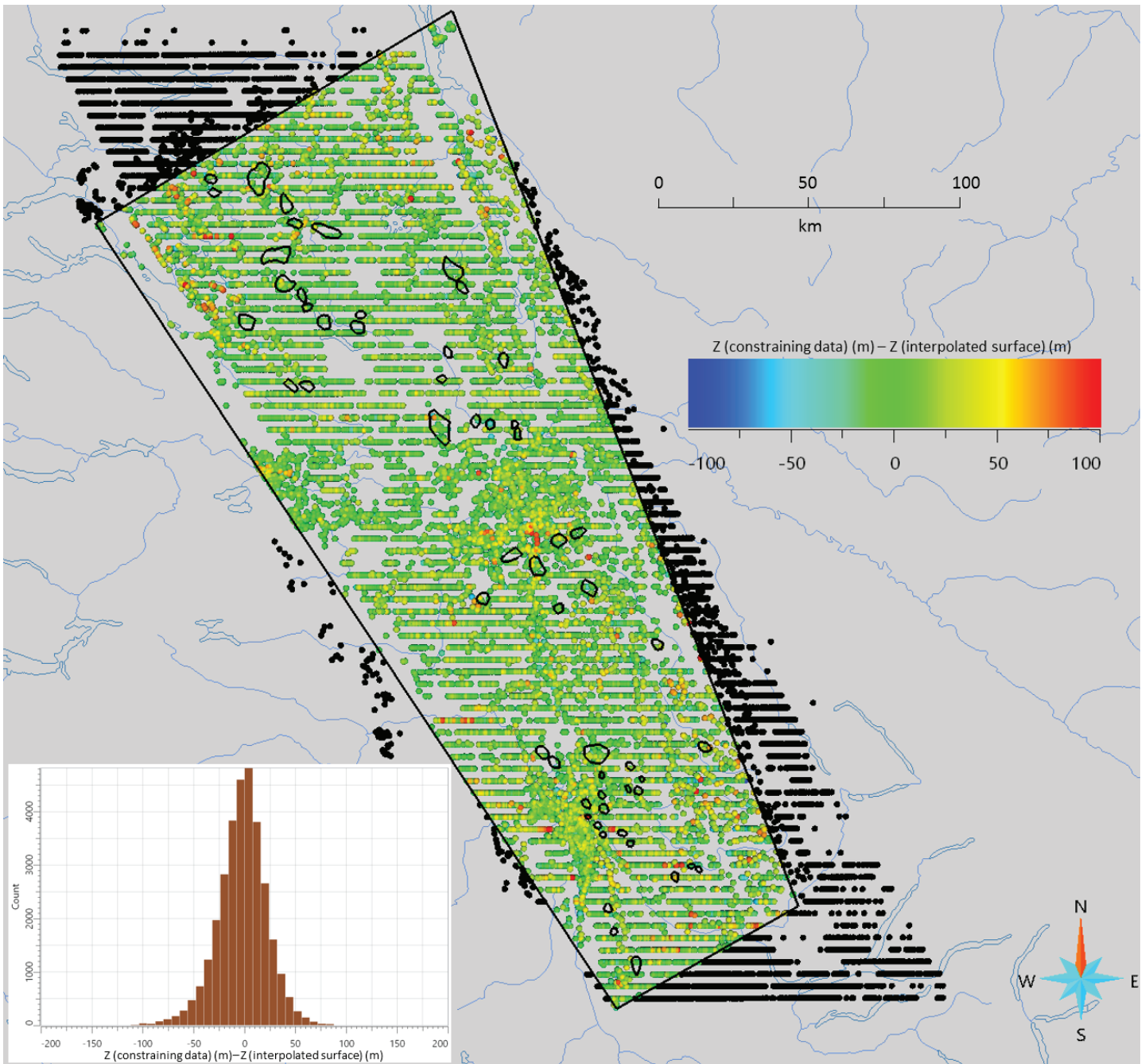


Figure 15: Difference between the bedrock elevations derived from the constraining data and from the interpolated top of bedrock surface. Difference is painted onto the constraining points. Black constraining data points are outside the project area. Magnetic targets are outlined by small black polygons. Inset shows the range of differences in bedrock elevations between the interpolated surface and the constraints.

on the amount and accuracy of the observed data at each location. Bedrock depths from groundwater well and drill logs, as well as spatial coordinates obtained from drill logs and the outcrop location database, could be inaccurate in places. Overburden thickness from VTEM models was manually interpreted and subjective.

There is a good spatial correlation between the regional Quaternary geology map (Cui et al., 2017) and areas of thicker cover material modelled for this project (Figure 16). The addition of detailed constraints from VTEM interpretations results in more detail about overburden thickness in areas that are difficult to access for mapping, and gives a sense of the significant variability in thickness through the region. The model indicates that there are likely additional ‘windows’ of thin to no overburden to those indicated on regional Quaternary geology maps, especially in areas with limited constraining data (red diamonds on Figure 16, areas between Fort St. James and Prince George, and ~50 km southwest of Prince George). These areas of thinner cover present new opportunities to access bedrock for mapping and exploration purposes.

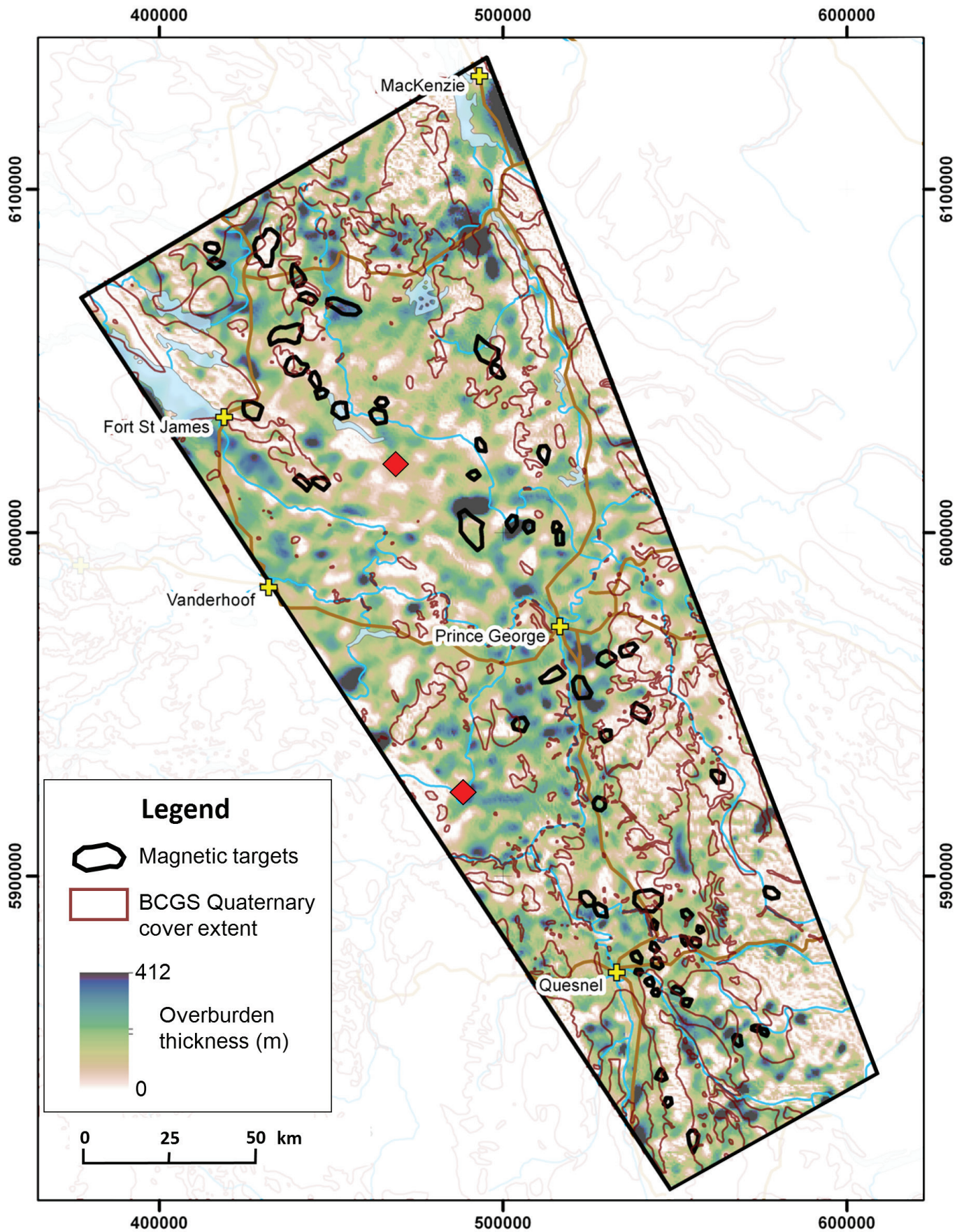


Figure 16: Overburden-thickness model for the project area. Quaternary cover extents from Cui et al. (2017). Red diamonds indicate areas where knowledge about overburden thickness was previously limited but has been enhanced by VTEM interpretations. Refer to Figure 11 for map symbols not in legend. Map coordinates in UTM Zone 10, NAD 83.

In our model, the overburden thickness ranges from 0 to 412 m and averages 40 m. Most of the magnetic targets occur beneath <50 m of interpreted overburden. The thickest overburden, with >100 m modelled thickness, occurs south of Prince George, about 40 km northwest of Prince George, and in the northernmost project area, about 45 km south of Mackenzie.

It is important to recognize that in areas where there are fewer or no constraints, the modelled overburden thickness is unreliable. One such area is in the northeast project area, about 45 km south of Mackenzie (Figure 16), where the model reports thick overburden but is supported by very few constraints.

5. 3-D INVERSION MODELLING OF TARGETS

Geophysical inversions were completed to produce physical property models of each target. This allowed the petrophysical characteristics of each target to be compared against known porphyry deposit hosts or source intrusions. First, for each selected target, magnetic data were inverted to produce 3-D magnetic susceptibility models that estimate the volume of magnetite-bearing rock causing the magnetic anomaly. Next, regional scale density models were generated from gravity data so that density could be assessed for each target. Details on inversion methodology and resulting models are outlined briefly in the following sections, and in more detail in Appendices 2 and 3.

5.1 Magnetic inversions

5.1.1 Data and Methods

Two datasets were used for magnetic inversion modelling. The first is the NRCan 200 m magnetic data grid (Natural Resources Canada, 2020), a dataset covering most of Canada, compiled from individual historic magnetic surveys. This is a gridded product, with cell sizes of ~200 m over British Columbia. The second dataset is one of the original datasets used to create the NRCan magnetic grid. It is a magnetic dataset that was collected in 1961 over the central Quesnel terrane, referred to as the British Columbia 61-1 magnetic dataset (Natural Resources Canada, 1962). Line spacing is approximately 800 m and flight height was 305 m.

An initial step in the inversion of magnetic data was completed to remove or lessen the impact of regional magnetic sources on the response from the localized magnetic bodies that were chosen as targets. The NRCan 200 m magnetic grid was used for regional response removal. The NRCan gridded data were upward continued to 8000 m to minimize the effect of local anomalies. The upward continued data was then inverted to yield a coarse magnetic susceptibility model that estimates the regional background magnetic susceptibility through the project area.

Target-scale inversion modelling, which produced models for each of the chosen magnetic targets, used the British Columbia - 61-1 data, down sampled along-line to 200 m. The regional magnetic susceptibility inversion model was applied two ways. First, the predicted data from the regional magnetic susceptibility model were subtracted from the observed magnetic data at each local site to leave only the signal derived from local material. Second, the regional magnetic susceptibility model acted as a reference model for the local inversions. This means that the local scale inversion model is guided by the regional magnetic susceptibility reference model.

Geophysical inversion is an underdetermined problem, there are more unknowns than there are data. This means there are many possible models that can predict the observed data. To limit the number of solutions, some basic constraints are applied to modelling. Typically, parameters are set to require the model be smoothly varying in all directions, to fit within the limit of defined model values, and to fit the observed data to within a specified error. Within these constraints, there are still many model solutions, and it is important to explore the range of results. One of the parameters that affects the structure and smoothness of the resulting model is the regularization chosen. During modelling for this project, several regularizations were tested, and resulting models evaluated based on known or expected geological features and magnetic susceptibility ranges. Models generated using an L1 norm regularization ultimately were chosen as the final representative models as they exhibit compact magnetic susceptibility bodies with shape, size, depth, and magnetic susceptibility values consistent with available geological and physical property information.

Appendix 2 describes the process in more detail, and outlines each of the model regularizations tested.

A magnetic susceptibility threshold of 0.02 SI (20×10^{-3} SI units) was used to extract a high magnetic susceptibility volume from the local magnetic inversions. This value is consistent with the lower range of magnetic susceptibilities of known porphyry deposit-related intrusions that have been sampled for rock properties. In a few cases, a higher magnetic susceptibility cut-off was used to extract the volume, typically when it seemed as if the modelled source rock was very high magnetic susceptibility, and its core mass better represented by a higher cut-off value. The true magnetic source may be larger or smaller than what is represented here since the choice of magnetic susceptibility threshold to generate a 'geologic' volume will change the apparent size of the body. For example, if a cut off of 0.01 SI (10×10^{-3} SI units) was used, a larger body would be produced than for the 0.02 SI cut off. The volume extracted via the cut-off

value represents an estimation of the extent of magnetite-bearing rock. If any part of the source rock has been extensively altered or is intermingled with other rock phases that do not contain magnetite, those parts of the rock will not be magnetically susceptible and thus not accounted for by the volume.

5.1.2 Results

Fifty-six inversions were completed. One site could not be modelled due to lack of overlapping magnetic data (Q22). All inversions acceptably predicted the observed data. Figure 17 shows a broad view of all the magnetic inversion models within the project area.

5.2 Gravity inversions

5.2.1 Data and Methods

For gravity inversions, the Geoscience BC QUEST project gravity data (Sander Geophysics Ltd., 2008) were used. These data are lower resolution than the magnetic data used for magnetic inversions, with survey lines spaced 2 km apart. However, the resolution is much higher than that of publicly available national gravity datasets, which average 10 km data spacing. Flight height was 300 m on average.

The resolution of the gravity data does not permit targets to be resolved with the same detail as from magnetic data inversion (Appendix 3). Instead of inverting at the target-scale, four intermediate-scale blocks of gravity data were inverted. This seemed to be a more appropriate scale-match for extracting the lithological boundaries and contacts captured in this data. As with the magnetic inversions, a range of regularizations affecting the models smoothness and smallness (closeness to a defined reference value) were used to explore the model space (Appendix 3). Intermediate inversions were run using the 2000 m downsampled data. The smallest inversion cell sizes were 500 m x 500 m x 100 m. Cells increase in size stepwise with depth. The smoothest model was prioritized, and both L1 and L2 norms were applied to yield two results for each inversion. Ultimately density contrast models generated using L1 norms were chosen to derive average density values per target.

5.2.2 Results

Each of the four intermediate-scale density-contrast models acceptably predicted the observed data. The models are shown in plan view in Figure 18.

6. SUMMARY OF INVERSION-DERIVED PETROPHYSICS OF CENTRAL QUESNEL TERRANE TARGETS

Each magnetic target, chosen based on similarities in size, shape, and magnetic character, to known porphyry deposit host or source intrusions in the Quesnel terrane, was further characterized based on their density values. Density values help determine whether targets are geophysically similar to more felsic or more intermediate intrusions typical of those hosting porphyry deposits in British Columbia, or if they are a different lithology entirely (which also happens to be magnetic). Following prioritization based on petrophysical character, the targets were assessed based on overburden thickness.

To compare the petrophysical properties of each of the targets to known porphyry deposit-related intrusions, an average magnetic susceptibility (from the magnetic inversions) and an average density (from the gravity inversions) was retrieved using the high magnetic susceptibility volumes generated from local magnetic inversion modelling. These average values are shown in Table 3.

The average magnetic susceptibility of the targets as derived from magnetic inversion is 67×10^{-3} SI. This is higher than the average magnetic susceptibility values measured from felsic to intermediate intrusive rock samples in the central Quesnel terrane (14×10^{-3} SI). This makes sense because only the highest magnetic susceptibility values greater than 20×10^{-3} SI (the volume threshold) are contributing to this average, and non-magnetic portions of the rock are not included. The average density of the targets from inversion is 2.7 g/cm³. This is actually very similar to the average density of felsic to intermediate intrusive rock samples from the central Quesnel terrane (2.66 g/cm³). But this is also similar to the 2.67 g/cm³ average crustal density value used for standard corrections of gravity data for this inversion. It is not clear whether the inverted density values are accurately estimated, or if they simply reflect the average density of the full inversion result, thus the recovered target densities are subdivided into four density classes: low (<2.65 g/cm³), moderate (2.65-2.7 g/cm³), high (2.7-2.75 g/cm³), and very high (>2.75 g/cm³) density for further evaluation and discussion.

The high magnetic susceptibility targets are shown on Figures 19-22 and colored by density class.

6.1 Targets in the Fort St. James area (“FSJ” targets)

The 16 targets in the Fort St. James area have a range of densities (Table 3, Figure 19). Low density magnetic targets have the petrophysical characteristics of magnetic intrusive rocks with low mafic mineral abundance, such as syenite or monzonite, whereas high

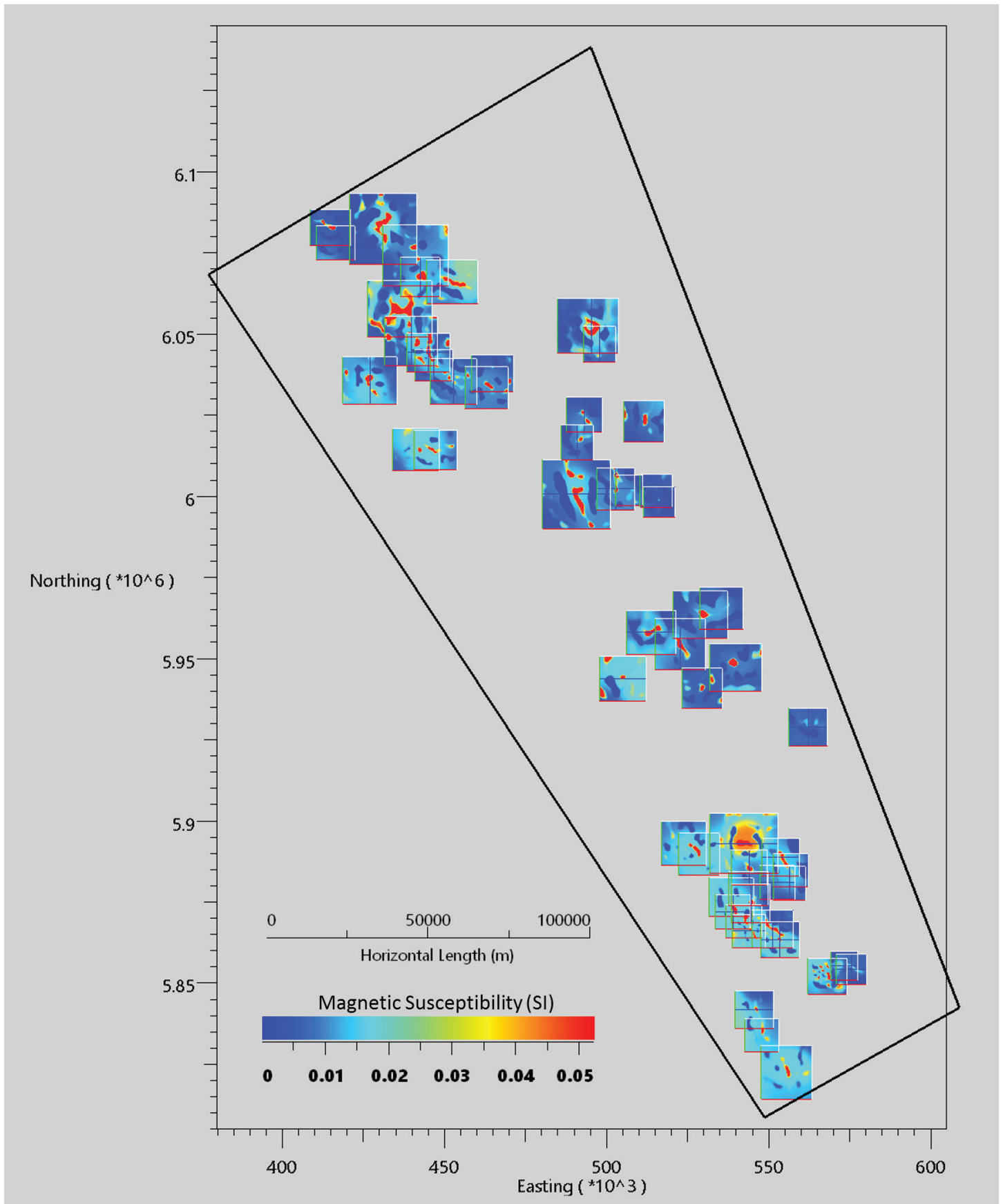


Figure 17: Horizontal slices through magnetic inversion models. Map coordinates in UTM Zone 10, NAD 83.

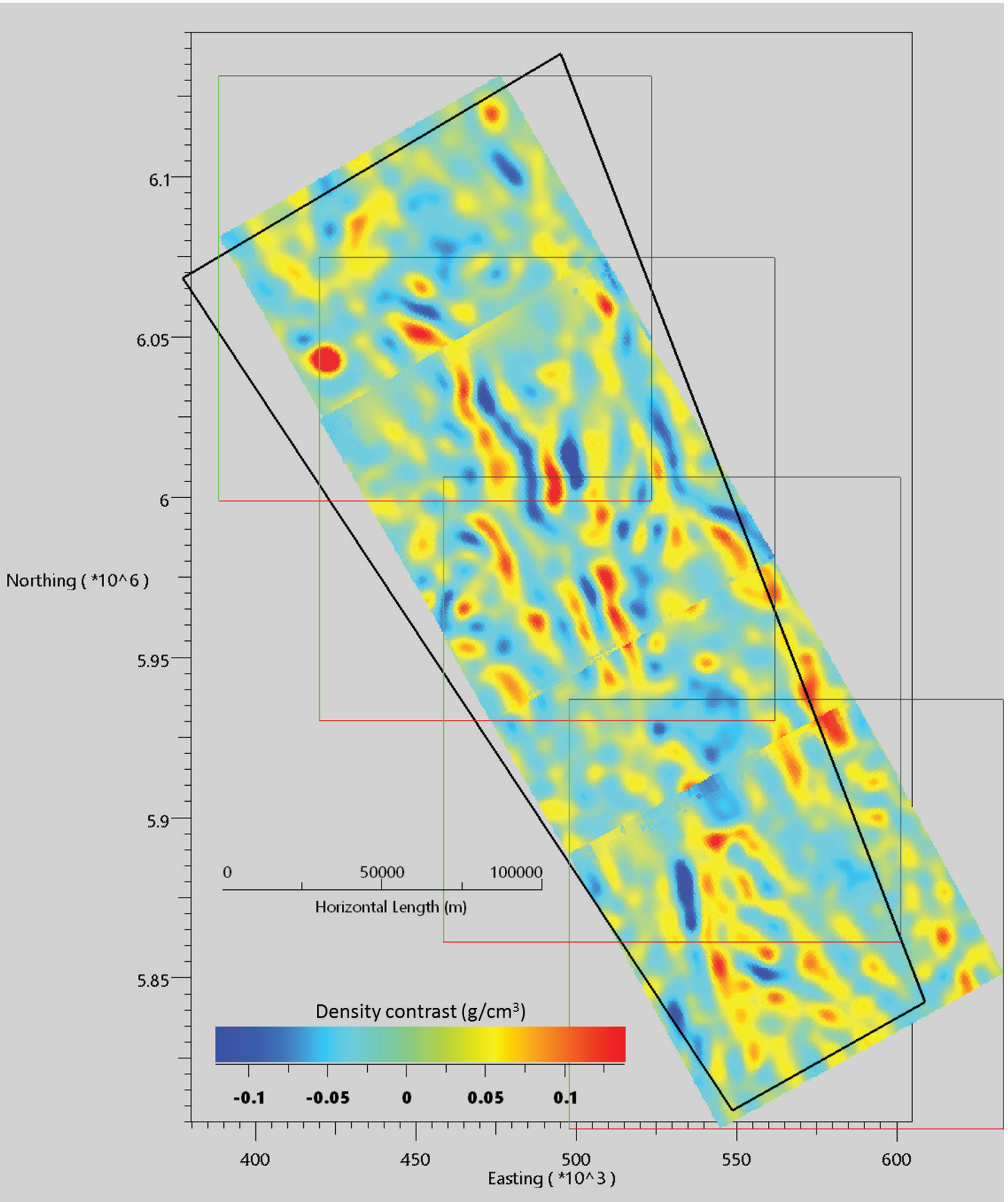


Figure 18: Gravity inversions, horizontal slices at approximately -250 m elevation. Map coordinates in UTM Zone 10, NAD 83.

Table 3: Summary of average magnetic susceptibilities and densities derived from magnetic and gravity inversions for each target. Rows are colored based on density “class” (low-blue, medium-yellow, high-pale orange, or very high density-orange). Also noted are rock types sampled or drilled in proximity to the target.

Target ID	Magnetic susceptibility (10 ⁻³ SI)	Density (g/cm ³)	Density class	Spatially correlated geology BCGS bedrock map	Rock types intersected by nearby drilling	Rock types sampled nearby
FSJ1	43.03	2.64	low	miPICvb/uTtTWppbb		
FSJ2	46.68	2.72	high	TrJTvb		
FSJ3	54.29	2.69	med	miPICvb	diorite, monzodiorite, monzonite, andesite	
FSJ4	67.59	2.75	v high	TrJdr		Q13A, Q13B (basaltic andesite, syenite)
FSJ5	38.81	2.71	high	TrJsy	diorite, andesite, volcanic sediment	Q11A, Q11B, and Q12 (monzonite, monzodiorite, gabbro/amphibolite)
FSJ6	42.30	2.69	med	uTrTI		
FSJ7	77.13	2.65	med	miPICvb		
FSJ8	75.75	2.62	low	miPICvb/muTrTsf/LTrJum		
FSJ9	77.22	2.62	low	miPICvb		
FSJ10	42.39	2.64	low	miPICvb		
FSJ11	37.86	2.71	high	miPICvb		
FSJ12	37.77	2.75	high	muTrTsf		
FSJ13	54.64	2.79	v high	muTrTsf		
FSJ14	76.55	2.63	low	uTrTWppbb/PTrCTum		
FSJ15	31.09	2.68	med	PnTrClm		
FSJ16	29.23	2.69	med	PnTrClm		
PG1	64.13	2.69	med	TrJTvb/Ekgd	overburden	
PG2	33.16	2.69	med	TrJTvb		
PG3	38.05	2.67	med	TrJTvb		
PG4	41.83	2.69	med	uTrTWppbb		
PG5	31.77	2.73	high	muTrTsf		
PG6	46.66	2.74	high	muTrTsf	overburden	
PG7	48.78	2.67	med	muTrTsf	pyroxenite (intersects model)	
PG8	45.38	2.73	high	muTrTsf	diorite	
PG9	44.62	2.69	med	MPA		
PG10	33.22	2.68	med	MPA		
PG11	41.56	2.85	v high	uTrTWppbb		
PG12	49.16	2.68	med	muTrTsf		
PG13	46.37	2.73	high	uTrNsvpb		Q1A, Q1B (basalt, greenschist/volcanic sediment)
PG14	46.57	2.75	v high	uTrNsvpb		
PG15	29.05	2.63	low	miPICvb		
PG16	34.46	2.70	med	uPrPzS		Q6A, Q6B (gneiss, schist)
PG17	61.19	2.74	high	MJSMqm		Q5 (volcanic metasediment)
PG18	36.96	2.74	high	uTrNsvb		
Q1	41.33	2.67	med	uTrTWppbb		
Q2	34.21	2.66	med	uTrNppbb		
Q3	100.21	2.79	v high	Ejmu		CRPPD (diorite, monzonite, monzodiorite, basalt)
Q4	36.13	2.72	high	uTrTWppbb		Q15A, Q15D (volcanic sedimentary rock, monzonite) RPDS (basalt, volcanic sedimentary rock, sedimentary rock)
Q5	33.47	2.69	med	uTrNsvpb		
Q6	24.22	2.65	low	uTrNsvpb		
Q7	29.69	2.65	med	uTrNsvpb		
Q8	35.19	2.71	high	uTrNsv		
Q9	56.49	2.71	high	uTrNpb	diorite, monzonite	CRPPD (volcanic rock, volcanic sedimentary rock)
Q10	41.76	2.74	high	uTrNpb/Ejmu	diorite, monzonite	Q16 (monzonite); CRPPD (diorite, monzonite, volcanic sediment)
Q11	55.45	2.70	high	uTrNpb		
Q12	53.84	2.73	high	uTrNpb/Ejmu		
Q13	50.60	2.70	med	uTrNppbb		
Q14	37.82	2.69	med	uTrNppbb		
Q15	24.16	2.73	high	uTrNppbb/LTrJgd		
Q16	26.40	2.70	med	uTrNppbb		
Q17	30.96	2.64	low	uTrNpb		
Q18	35.99	2.77	v high	uTrNppbb		
Q19	53.77	2.74	high	uTrNsv		
Q20	30.22	2.72	high	ImJDMs		
Q21	50.29	2.70	high	uTrNsv		
Q22	ND	ND	med?	uTrNsvb		
Q23	48.92	2.73	high	uTrNsv/LTrBCqd		

Abbreviations: Ejmu, Early Jurassic mafic to ultramafic intrusive rocks; Ekgd, Early Cretaceous granodiorite; ImJDMs, Lower to Middle Jurassic Dragon Mountain Succession sedimentary rocks; LTrBCqd, Late Triassic Guichon Suite Burgess Creek stock; LTrJgd, Late Triassic to Early Jurassic granodiorite; LTrJum, Late Triassic to Jurassic ultramafic rocks; MiPICvb, Miocene to Pleistocene Chilcotin Gr. basalt; MJSMqm, Middle Jurassic Ste. Marie Plutonic Suite quartz-monzonite/granodiorite/granite; MPA, Mississippian to Permian Slide Mountain Complex basalt; muTrTsf, Middle to Upper Triassic Takla Gr. clastic sedimentary rocks; PnTrClm, Pennsylvanian to Triassic Cache Creek Complex sedimentary rocks; PTrCTum, Early Permian to late Triassic ultramafic rocks; TrJdr, Triassic to Jurassic diorite; TrJsy, Triassic to Jurassic syenite to monzonite; TrJTvb, Triassic to Jurassic Takla Gr. basalt; uPrPzS, Proterozoic to Paleozoic Snowshoe Gr. quartzite/schist; uTrNpb, Upper Triassic Nicola Gr. volcanic breccia; uTrNppbb, Upper Triassic Nicola Gr. basalt; uTrNsv, Upper Triassic Nicola Gr. sedimentary rocks; uTrNsvb, Upper Triassic Nicola Gr. basalt breccia; uTrNsvpb, Upper Triassic Nicola Gr. basalt; uTrTI, Upper Triassic Takla Gr. volcanic sedimentary rocks; uTrTWppbb, Upper Triassic Takla Gr. basalt

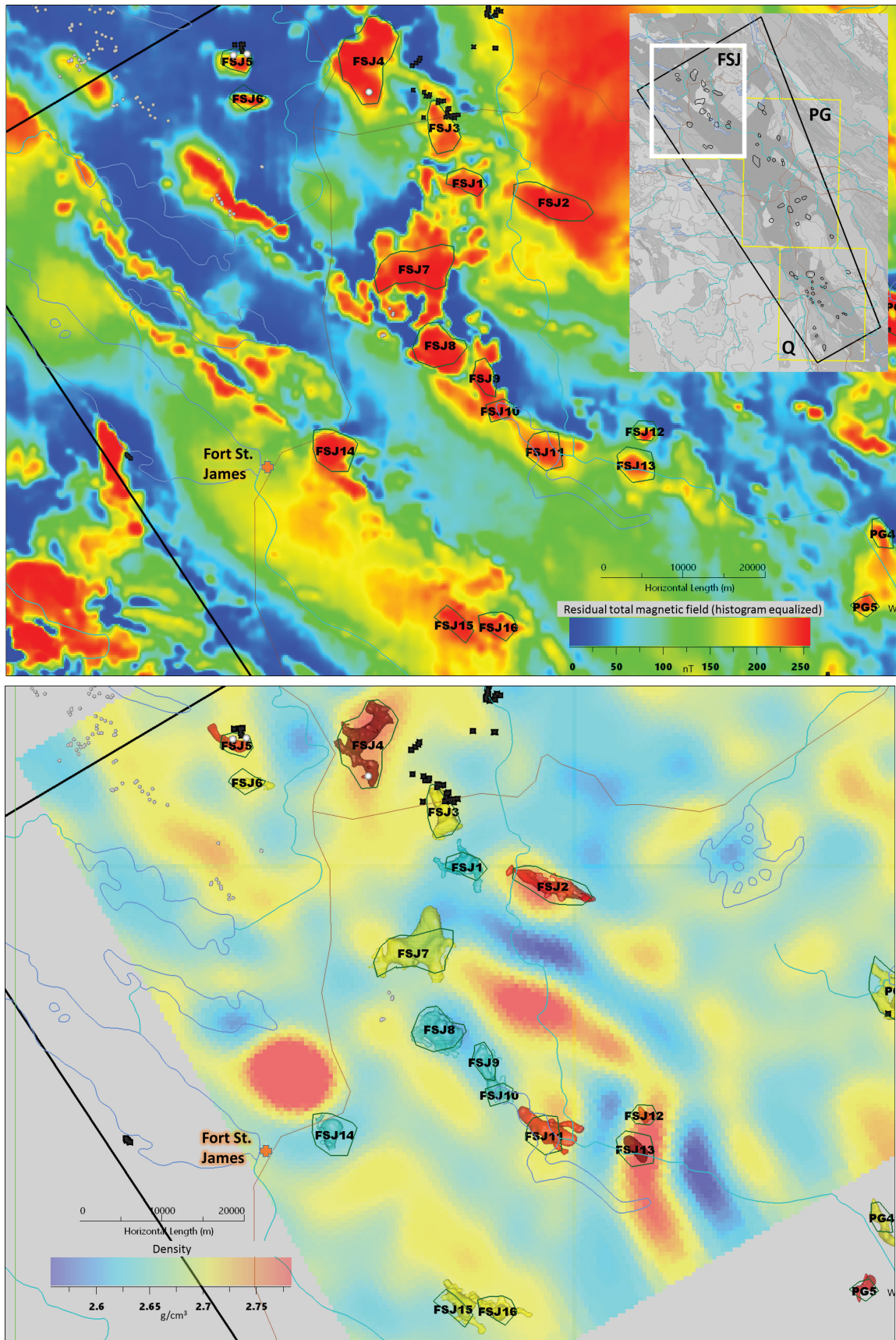


Figure 19: Targets in the Fort St. James area. Upper: magnetic map showing magnetic target locations; lower: horizontal slice through density model. Blue bodies are low density, yellow are medium density, and red are high density. Black squares are drill holes, white spheres are rock samples from this project, grey circles are rock samples recorded in the Canadian Rock Physical Property Database (Enkin, 2018).

density targets are presumed to have a greater abundance of mafic minerals reflecting dioritic rocks. High density rocks could also be localized mafic units or gabbroic intrusions. A few of the targets classed as moderate density sit on the margins between gravity lows and gravity highs (e.g., FSJ7, FSJ15, FSJ16). The densities of these magnetic bodies may not be accurately represented.

Four targets are slightly anomalous, with high magnetic susceptibilities and low to moderate densities. These are located geographically near mapped Miocene to Pleistocene Chilcotin Group basalts. Chilcotin basalts are often vesicular (Bevier, 1983), and high rock porosities tend to lead to low densities. It is possible that these magnetic targets, or parts of them, are not intrusive rocks, but are instead low density, magnetite-bearing basalt. These bodies are large deep masses, however, whereas Chilcotin Group basalts are recent flat-lying deposits, generally expected to be less than 100 m thick based on Southern Interior Plateau modelling by Andrews and Russell (2008). Another possibility is that these bodies are covered or buried serpentinized ultramafic bodies. Targets FSJ7 and FSJ14 correlate spatially with mapped ultramafic units. Serpentinization of ultramafic rocks generates magnetite and converts dense ferromagnesian minerals to low-density talc and serpentine minerals (Toft et al., 1990). The FSJ7 high magnetic susceptibility body has a large lower susceptibility pit in the center, which gives it an unusual shape. Geologically unexpected or inaccurate shapes can often develop in inversion when a source body is remanently magnetized and remanence is not fully accounted for in the inversion modelling (Li et al., 2021).

Exploration drilling (from ARIS reports) and sampling (this study) were done in the area around FSJ3, FSJ4, and FSJ5 targets. Near these medium to high density targets, syenite, monzonite, monzodiorite, diorite, gabbro, and volcanic rocks have been recorded. Specifically, at the southern end of FSJ4, two samples were collected for this project: a basaltic trachyandesite, and a syenite (Q13A and Q13B, respectively). These samples are chlorite-muscovite/sericite-altered, with no sulfides recorded, and are moderately to highly magnetically susceptible. At FSJ5, monzonite, monzodiorite, and gabbro were sampled (Q11A, Q11B, and Q12, respectively). These samples were weakly to strongly chlorite-sericite-epidote-(+/- albite)-altered. Samples Q11A and Q11B contain pyrite and chalcopyrite, and all three samples were magnetite-bearing, and have high magnetic susceptibilities.

6.2 Targets in the northern Prince George area (“PG” targets 1–10)

In this area, targets are medium to high density (Figure 20). As in the Fort St. James area, some of the medium density targets sit on the boundaries between high- and low-density zones (e.g., PG3, and PG7), and with the coarse model it is difficult to be confident in the densities of these bodies. Other medium density targets correlate clearly with a moderate density anomaly in the model.

Several exploration drillholes in this area occur proximal to targets. There is a drillhole near the edge of the PG1 target volume that did not intersect bedrock. A hole near target PG6 also did not intersect bedrock. Holes near PG7 and PG8 recorded pyroxenite and diorite, respectively.

6.3 Targets in the southern Prince George area (“PG” targets 11–18)

Except for target PG15 which is low density, the targets in this area are medium to high density (Figure 21). There is a good spatial correlation in this map area between high magnetic susceptibility and high to medium density targets. Hand samples were collected as part of this project near three of the targets (Appendix 1). Samples from near PG13 (Q1A and Q1B) include basalt and volcanic sediment. A sample of gneiss and one of schist was collected near PG16 (Q6A and Q6B). A volcanic metasediment sample was collected near PG17 (Q5). All these samples returned very low magnetic susceptibility values below 1×10^{-3} SI, and it is likely that the source of the magnetic anomalies are deeper and were not sampled at these sites.

Several of the targets immediately south of Prince George occur in populated areas with residential buildings, roads, and other infrastructure.

6.4 Targets in the Quesnel area (“Q” targets)

Two targets in the Quesnel region are low density, whereas the remaining 21 targets range from medium to high density (Figure 22).

Most of the magnetic anomalies (high magnetic susceptibility bodies) do not directly overlie density anomalies in this area, with many of the modelled medium to high magnetic susceptibility bodies sitting along the edge of density highs (e.g., targets Q1, Q2, Q5, Q7, Q13, Q14, Q15, Q16, Q20, and Q21). The aligned north-northwest and northwest density highs are correlated with mafic volcanic stratigraphy on BCGS bedrock geology maps. The magnetic bodies seem to occur along the boundaries and contacts of the volcanic stratigraphy.

Target Q3 is a large, very high magnetic susceptibility and high-density target located in the Quesnel area. The anomaly correlates with a mapped unit that is assigned to the Polaris Ultramafic Suite on BCGS maps and described as gabbroic to pyroxenitic. A number

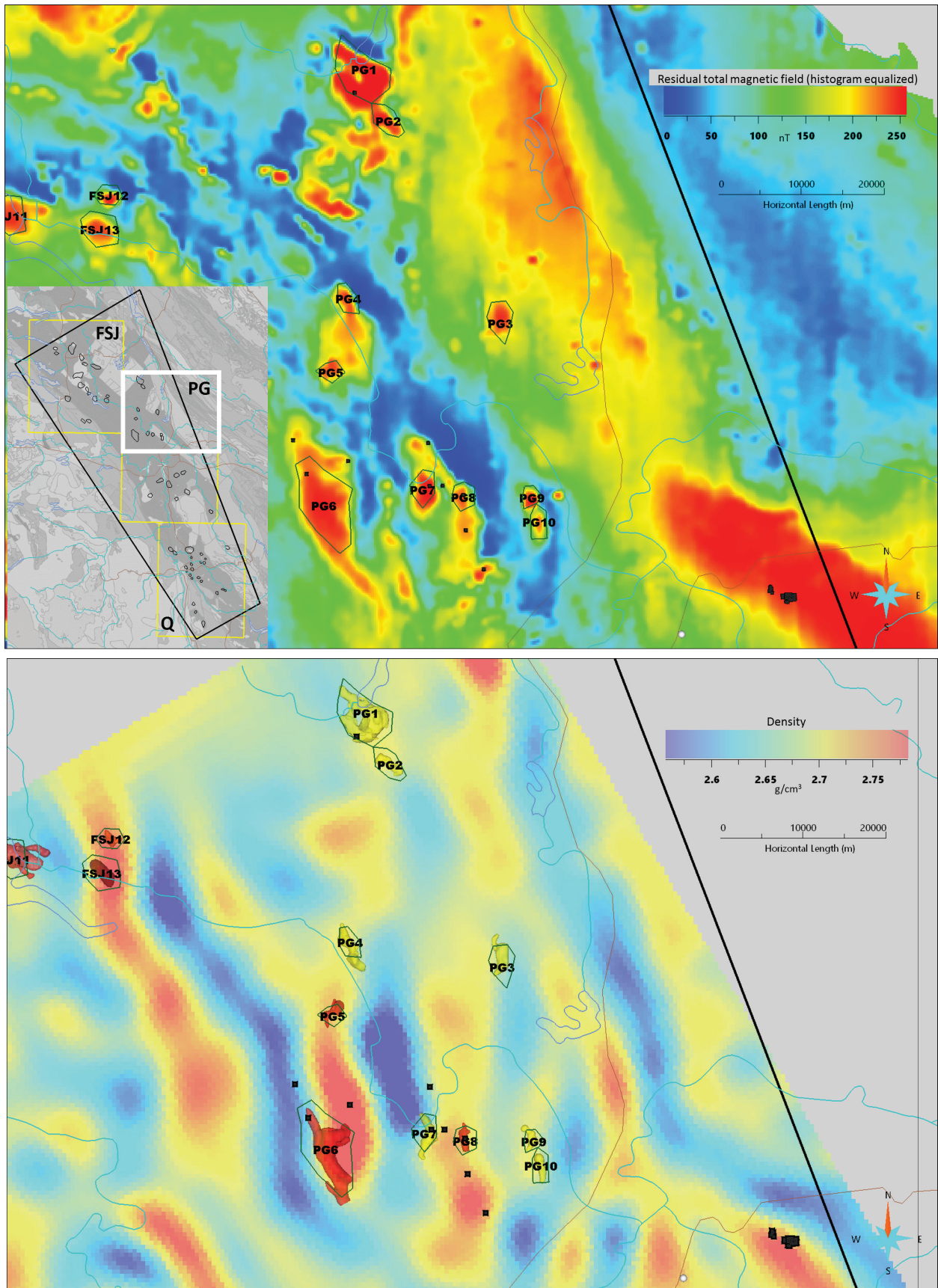


Figure 20: Targets in the northern Prince George area, upper: magnetic map showing magnetic target locations, lower: horizontal slice through density model. Blue bodies are low density, yellow are medium density, and red are high density. Black squares are drill holes.

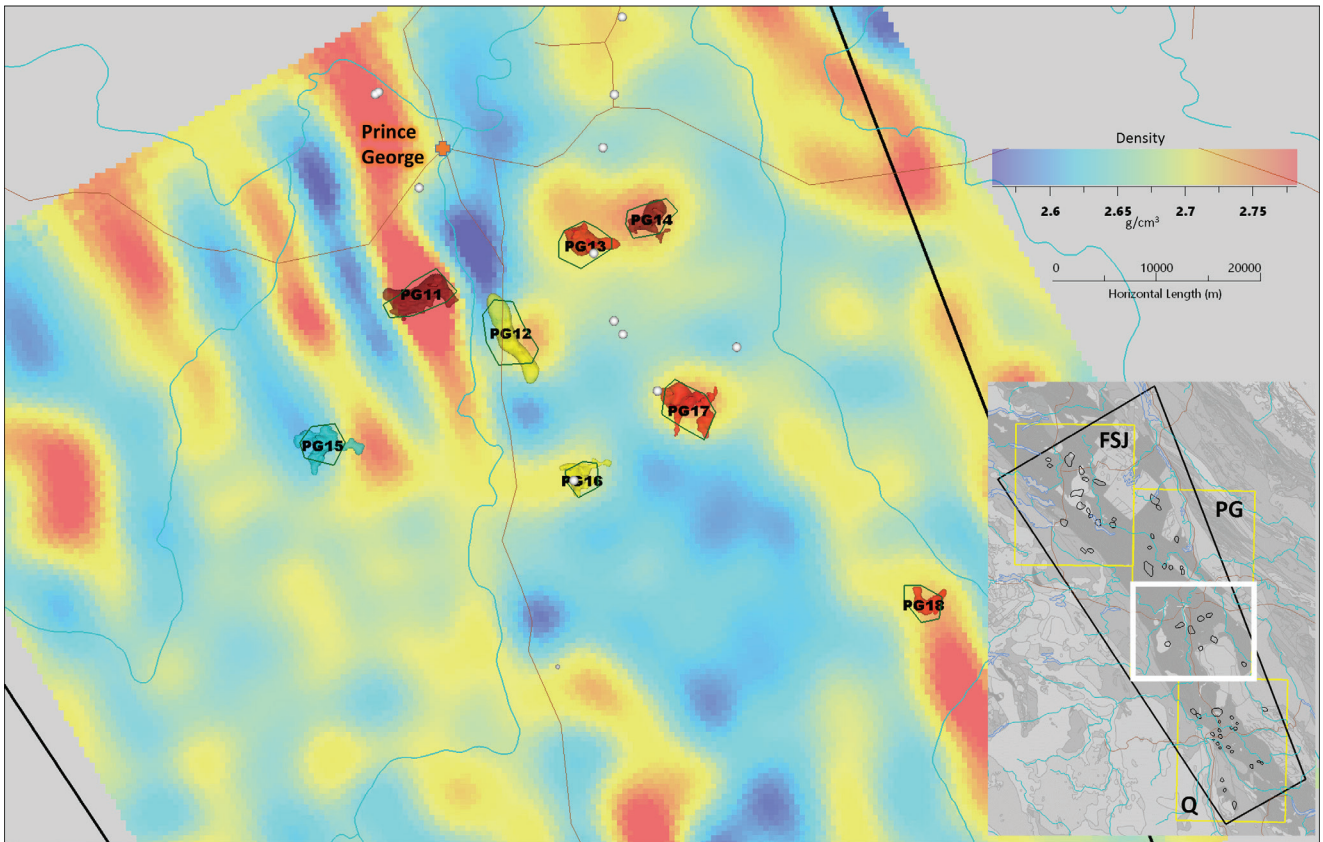
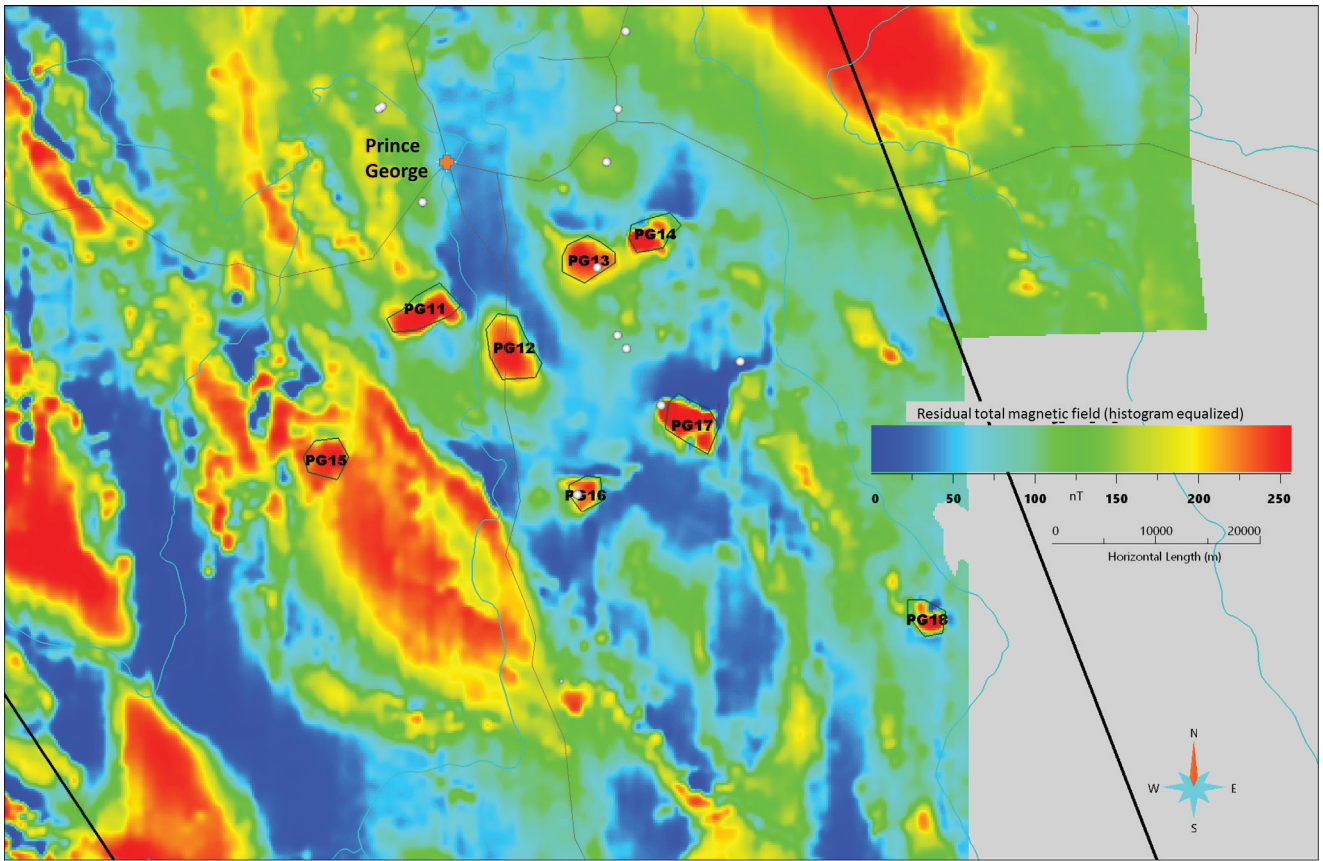


Figure 21: Targets in the southern Prince George area, upper: magnetic map showing magnetic target locations, lower: horizontal slice through density model. Blue bodies are low density, yellow are medium density, and red are high density. White spheres are rock samples from this project.

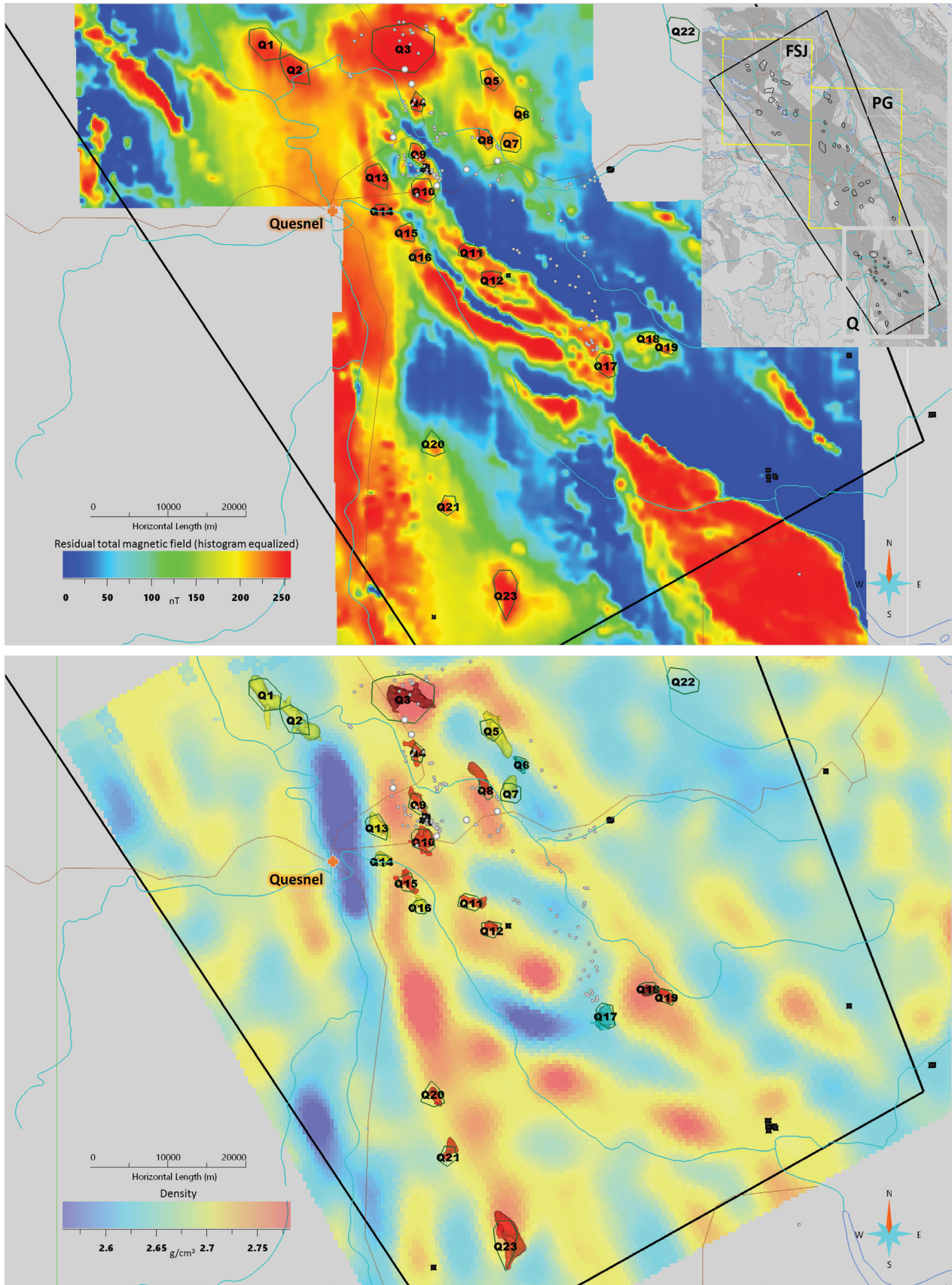


Figure 22: Targets in the Quesnel area, upper: magnetic map showing magnetic target locations, lower: horizontal slice through density model. Blue bodies are low density, yellow are medium density, and red are high density. Black squares are drill holes, white spheres are rock samples from this project, grey circles are rock samples recorded in the Canadian Rock Physical Property Database (Enkin, 2018).

of samples from the Canadian Rock Physical Property Database were collected in the vicinity of this anomaly, and include monzonite, monzodiorite, diorite and basalt.

Targets Q9 and Q10 have nearby samples and proximal drilling. The Mouse Mountain copper-gold porphyry prospect (MINFILE 093G 003) occurs between these two anomalies. Rock types identified in drillcore and listed in the Canadian Rock Physical Property Database include monzonite, diorite, volcanic rocks, and volcanic sedimentary rocks. One sample collected for this project lies just east of the Q10 target anomaly (sample Q16). This sample is a chlorite-altered monzonite that has a high susceptibility (Appendix 1).

7. TARGET PRIORITIZATION AND EXPLORATION IMPLICATIONS

In the southern Quesnel terrane, most alkalic porphyry deposit host intrusions (from the Late Triassic alkalic magmatic trend) at the regional scale are magnetic and associated with gravity highs. North of the project area, the large intrusion underlying the Mount Milligan deposit is also magnetic and high density. We therefore suggest that the highest priority alkalic porphyry targets in the central Quesnel terrane would be those with the same characteristics, i.e., targets in the moderate to high density categories. Higher density values indicate host rocks with a greater mafic mineral content, such as monzonite to diorite. The highest ('very high') density targets might indicate the presence of rocks with a large proportion of dense minerals, such as gabbro or pyroxenite.

Exceptions to the trend, indicated earlier in this report, are the Mount Polley intrusions, and the Rayfield River pluton. Alkalic-style porphyry copper-gold mineralization occurs in association with intrusive rocks in both cases, yet the intrusions are correlated with gravity lows (and are thus assumed low density). The low densities of these intrusions may be because they are, in part, syenitic (Logan and Schiarizza, 2014) with low mafic mineral content. Thus, targets with high magnetic susceptibility and low density should not be ruled out for porphyry exploration. Instead, density may provide key information for further exploration of the target. A syenitic or pyroxenitic (low or very high density, respectively) host may suggest silica-undersaturated porphyry deposit type (Lang et al., 1995b). Moderate to high density monzonite to diorite hosts may be more typical of the silica-saturated type. The mineralogy and the chemical affinity of intrusions will have an impact on alteration mineral assemblages and metallogeny. Host rock type, alteration mineral products, and metals present may all influence exploration methodologies and interpretations of data.

Tables 4–6 rank the targets based on density class and record the average thickness of surficial material above each target. Targets under the thinnest cover are most accessible to more detailed exploration. Other criteria to be considered are discussed below.

All targets generated are considered to represent regional-scale intrusions that may be the source of (or host to) a porphyry deposit, or genetically related to a porphyry deposit host intrusion. For exploration purposes, it is important to consider the small scale of alkalic porphyry deposits in British Columbia relative to the scale of the larger parent or source plutons that host them. The Mount Polley, New Afton, and Copper Mountain deposits, for example, occur within what are essentially structural traps in immediate host rocks that are confined to zones on the order of hundreds of meters to one kilometer across (Rees et al., 2020; Lipske et al., 2020; Holbek et al., 2020). Comparatively, the larger plutonic source intrusions are regularly 5-15 km across. The localized structural traps are the true target for alkalic porphyry exploration. In British Columbia and worldwide, porphyry deposits commonly occur at the edges or apices

Table 4: Magnetic targets in the Fort St. James area of B.C., sorted by density class, with average overburden thickness and features of note that overlap targets.

Target ID	Magnetic susceptibility (10^{-3} SI)	Density (g/cm^3)	Density class	Average overburden thickness (m)	Minimum overburden thickness (m)	Maximum overburden thickness (m)	Features of note
FSJ13	54.64	2.79	v. high	29	2	55	major river
FSJ4	67.59	2.75	v. high	9	0	64	
FSJ12	37.77	2.75	high	11	0	25	
FSJ2	46.68	2.72	high	98	34	127	
FSJ5	38.81	2.71	high	11	1	28	
FSJ11	37.86	2.71	high	19	5	47	First Nations reserve, residences/buildings, lake
FSJ3	54.29	2.69	med	58	22	86	
FSJ6	42.30	2.69	med	88	60	104	
FSJ16	29.23	2.69	med	20	8	31	
FSJ15	31.09	2.68	med	21	16	31	
FSJ7	77.13	2.65	med	34	4	63	
FSJ10	42.39	2.64	low	31	16	46	lake
FSJ1	43.03	2.64	low	21	1	54	
FSJ14	76.55	2.63	low	27	0	63	First Nations reserve
FSJ9	77.22	2.62	low	12	5	20	lake
FSJ8	75.75	2.62	low	17	0	68	

Table 5: Magnetic targets in the Prince George area of B.C., sorted by density class, with average overburden thickness and features of note that overlap targets.

Target ID	Magnetic susceptibility (10 ⁻³ SI)	Density (g/cm ³)	Density class	Average overburden thickness (m)	Minimum overburden thickness (m)	Maximum overburden thickness (m)	Features of note
PG11	41.56	2.85	v. high	30	1	56	
PG14	46.57	2.75	v. high	13	1	33	
PG6	46.66	2.74	high	59	9	301	residences/buildings
PG17	61.19	2.74	high	10	0	26	
PG18	36.96	2.74	high	17	1	47	
PG5	31.77	2.73	high	47	24	66	
PG8	45.38	2.73	high	107	51	160	
PG13	46.37	2.73	high	52	4	86	residences/buildings
PG16	34.46	2.70	med	39	2	84	
PG1	64.13	2.69	med	50	1	72	lake
PG2	33.16	2.69	med	10	0	37	
PG4	41.83	2.69	med	11	1	23	
PG9	44.62	2.69	med	29	22	40	residences/buildings
PG10	33.22	2.68	med	60	33	84	residences/buildings
PG12	49.16	2.68	med	97	61	132	highway, residences/buildings
PG7	48.78	2.67	med	132	4	260	major river
PG3	38.05	2.67	med	17	0	55	
PG15	29.05	2.63	low	64	6	99	residences/buildings

Table 6: Magnetic targets in the Quesnel area of B.C., sorted by density class, with average overburden thickness and features of note that overlap targets.

Target ID	Magnetic susceptibility (10 ⁻³ SI)	Density (g/cm ³)	Density class	Average overburden thickness (m)	Minimum overburden thickness (m)	Maximum overburden thickness (m)	Features of note
Q3	100.21	2.79	v. high	25	0	64	highway, residences/buildings
Q18	35.99	2.77	v. high	55	41	72	
Q19	53.77	2.74	high	85	62	104	
Q10	41.76	2.74	high	31	17	49	highway, residences/buildings
Q12	53.84	2.73	high	51	32	69	
Q15	24.16	2.73	high	4	0	12	
Q23	48.92	2.73	high	31	1	70	
Q20	30.22	2.72	high	46	6	72	
Q4	36.13	2.72	high	17	3	41	highway
Q8	35.19	2.71	high	20	8	29	major river
Q9	56.49	2.71	high	12	1	27	
Q21	50.29	2.70	high	10	0	25	
Q11	55.45	2.70	high	79	53	92	
Q13	50.60	2.70	med	44	34	50	highway, residences/buildings
Q16	26.40	2.70	med	15	1	34	
Q5	33.47	2.69	med	68	54	81	
Q14	37.82	2.69	med	64	41	109	residences/buildings, major river, powerline
Q1	41.33	2.67	med	31	11	75	
Q2	34.21	2.66	med	19	0	77	major river
Q7	29.69	2.65	med	27	6	46	
Q22	ND	ND	med?	10	0	27	
Q6	24.22	2.65	low	34	25	40	
Q17	30.96	2.64	low	73	37	93	

of intrusive bodies, presumably where magmatic-hydrothermal fluid flow is high. Structures that develop on the margins of or above intrusions are often the direct hosts to porphyry deposits. As such, intrusive margins, contacts, and related structures and breccias should be prioritized during local scale targeting.

For all targets, additional regional and local mineral exploration criteria should be sought prior to staking claims or planning follow-up exploration. Field investigation involving geological and alteration mapping, along with surficial and whole rock data collection should be completed. More detailed geophysical survey data should be sought or collected, and 3-D geophysical inversions of this data completed. Rock physical property data should be collected to guide interpretation of geophysical data and inversion models. All of these data will be most instructive when integrated and analyzed together in a spatial framework in 2-D and 3-D GIS platforms. A review of

porphyry deposits in British Columbia and their discovery history will inform explorers on typical scales of mineralization, and historically effective tools for discovery. Some excellent resources include Canadian Institute of Mining and Metallurgy's Cordilleran porphyry deposits volumes (most recent is the CIM Special Volume 57, Sharman et al., 2020), as well as Devine et al.'s (e.g., 2016) porphyry deposit atlases, along with NI 43-101 reports for porphyry mineral properties.

A subset of targets are in populated areas, near highways, or underlie lakes and rivers. Some of these land and geographic features were identified using satellite data (Bing Aerial Imagery) and are noted in Tables 4-6, though the list is not exhaustive. The targets should be closely evaluated by explorers using aerial imagery and other geographic information to inform accessibility prior to working in the area or staking mineral claims.

8. SUMMARY

The central Quesnel terrane of British Columbia is prospective for porphyry deposits, yet remains underexplored due to extensive glacial cover obscuring bedrock, which impedes mapping and bedrock sampling and makes exploration drilling decisions difficult. This project achieved two goals to aid exploration efforts in this part of British Columbia: 1) building an updated overburden thickness model for the central Quesnel terrane, and 2) identifying geophysical characteristics for selecting and prioritizing a suite of regional scale porphyry targets in the project area.

To understand regional variability in overburden thickness and aid exploration planning, an overburden thickness model was created by interpolating available outcrop, drilling, and groundwater well data in conjunction with bedrock depth constraints from interpreted electromagnetic inversion sections. The results show high variability in overburden thickness throughout the project area, with numerous windows of thinner overburden—25 m or less— where bedrock may be more accessible, and drilling less expensive.

A suite of exploration targets representing possible porphyry deposit host or source intrusive rocks were selected. The targets were chosen based on geophysical patterns associated with copper-gold porphyry deposits in the Quesnel terrane north and south of the project area, which indicate that alkalic-style porphyry deposit host intrusions are commonly magnetic. Magnetic and gravity inversions were completed to derive magnetic susceptibilities and densities for each target. Based on physical property investigations of known porphyry deposit host rocks, higher density targets were deemed most prospective in that they are most like alkalic deposit host rocks in southern Quesnel terrane. High density targets likely represent rocks with a greater abundance of dense mafic minerals. If they are intrusive rocks, they would be monzonitic to dioritic. Lower density targets are less like southern Quesnel terrane porphyry deposit host rocks, but are still interesting; deposits like those at Mount Polley and Rayfield River correlate with gravity lows. Rocks hosting these deposits might be more syenitic in composition, with fewer mafic minerals. Geology inferred from geophysical models can help prioritize targets for exploration as well as guide exploration.

A summary of overburden thickness and land features that might influence exploration decisions are noted for each magnetic target chosen for this project. It is hoped that this information will be combined with other excellent exploration datasets available and previous research from this area to encourage new porphyry mineral claim staking and enable local-scale follow-up work.

9. LIST OF PROJECT DELIVERABLES

I. Magnetic targets

- Magnetic targets (shapefile/.dxf)

II. Overburden models

- Overburden thickness point constraints (.csv)
- Surface representing top of bedrock/base of overburden (3-D .dxf)
- Overburden thickness model (2-D Geosoft .grd)
- Overburden thickness grid values (.csv)

III. Inversion models

- Magnetic inversion models (UBC-format mesh and model files)

- High magnetic susceptibility bodies (3-D .dxf)
- Gravity inversion models (UBC-format mesh and model files)
- Jupyter Notebooks with inversion code and modelling trials

IV. Geoscience Analyst projects

- Geoscience Analyst projects for each geographic AOI (Fort St. James, Prince George, and Quesnel blocks)

10. ACKNOWLEDGEMENTS

The authors are deeply grateful for funding, communications, and administrative support for this project from Geoscience BC. The report was improved by comments, suggestions, and corrections from three anonymous reviewers. Shaun Barker is also thanked for comprehensive reviews of the report. Thank you to Randy Enkin and team at the GSC Pacific Paleomagnetism and Petrophysics Laboratory for physical property measurements. The work benefited from discussions, suggestions, and hands-on help from Peter Kowalczyk, Doug Oldenburg, Johanna McWhirter, Bahram Najafian, and Dave Sacco. Thanks to all those who followed the work, asked questions, and provided feedback, especially fellow researchers at MDRU and UBC-GIF. Thank you to Sara Jenkins and Beth Spencer for copyediting and formatting of this report. We wish to acknowledge that the land we conducted this research on covers the traditional territories of many First Nations. We encourage anyone planning mineral exploration work to first contact First Nations. The Province of British Columbia's Consultative Areas Database can help with this (<https://maps.gov.bc.ca/ess/hm/cadb/>). The Association for Mineral Exploration (AME) also produces an Indigenous Engagement Guidebook.

11. REFERENCES

- Andrews, G.D.M. and Russell, J.K. (2008): Cover thickness across the southern Interior Plateau, British Columbia (NTS 0920, P; 093A, B, C, F): constraints from water-well records; *in* Geoscience BC Summary of Activities 2007, Geoscience BC, Report 2008-1, p. 11–20, URL <http://www.geosciencebc.com/i/pdf/SummaryofActivities2007/SoA2007-Andrews_original.pdf> [February 2020].
- Barr, D.A., Fox, P.E., Northcote, K.E. and Preto, V.A. (1976): The alkaline suite porphyry deposits: a summary; *in* Porphyry Deposits of the Canadian Cordillera, Sutherland Brown, A. (ed.), CIM Special Volume 15, p. 359–367.
- BC Geological Survey (2015): Copper in British Columbia information circular 2015, BC Ministry of Energy, Mines and Petroleum Resources, BC Geological Survey, URL <https://www2.gov.bc.ca/assets/gov/farming-natural-resources-and-industry/mineral-exploration-mining/documents/mineral-development-office/copper_september_2015.pdf> [October 2021].
- BC Geological Survey (2020): MINFILE BC mineral deposits database; BC Ministry of Energy, Mines and Petroleum Resources, BC Geological Survey, URL <<http://minfile.ca>> [July 2019].
- BC Ministry of Energy, Mines and Petroleum Resources (2020): Assessment Report Indexing System (ARIS); BC Ministry of Energy, Mines and Petroleum Resources, BC Geological Survey, URL <<https://www2.gov.bc.ca/gov/content/industry/mineral-exploration-mining/british-columbia-geological-survey/assessmentreports>> [May 2020].
- BC Ministry of Environment and Climate Change Strategy (2020): Groundwater wells database, URL <<https://catalogue.data.gov.bc.ca/dataset/groundwater-wells>> [October 2020].
- Bevier, M. L. (1983): Implications of chemical and isotopic composition for petrogenesis of Chilcotin Group basalts, British Columbia; *Journal of Petrology*, v. 24, p. 207–226., URL <<https://doi.org/10.1093/petrology/24.2.207>>
- Bissig, T. and Cooke, D.R. (2014): Introduction to the special issue devoted to alkalic porphyry Cu-Au and epithermal Au deposits; *Economic Geology*, v. 109, p. 819–825. DOI: 10.2113/econgeo.109.4.819
- Brown, R., Roste, G., Baron, J. and Rees, C. (2016): Mount Polley mine 2016 technical report; NI 43-101 report prepared for the Mount Polley Mining Corporation and Imperial Metals Corporation, 205 p., URL <https://www.imperialmetals.com/assets/docs/mount-polley-technical-report_may-20.2016.pdf> [October 2021].
- Chamberlain, C.M., Jackson, M., Jago, C.P., Pass, H.E., Simpson, K.A., Cooke, D.R. and Tosdal, R.M. (2007): Toward an integrated model for alkalic porphyry copper deposits in British Columbia (NTS 093A, N; 104G); *in* Geological Fieldwork 2006, British Columbia

- Ministry of Energy, Mines and Petroleum Resources, Paper 2007-1 and Geoscience BC, Report 2007-1, p. 259–274, URL <http://cmscontent.nrs.gov.bc.ca/geoscience/PublicationCatalogue/GeoscienceBC/GBCR2007-01-26_Chamberlain.pdf>
- Colpron, M. and Nelson, J.L. (2011): Yukon terranes – a digital atlas of terranes for the northern Cordillera; Yukon Geological Survey, URL <<http://data.geology.gov.yk.ca/Compilation/2>> [November 2020].
- Cooke, D.R., Wilson, A.J., House, M.J., Wolfe, R.C., Walshe, J.L., Lickfold, V. and Crawford A.J. (2007): Alkalic porphyry Au-Cu and associated mineral deposits of the Ordovician to Early Silurian Macquarie Arc, New South Wales, Australian Journal of Earth Sciences, v. 54, p. 445–463, DOI: 10.1080/08120090601146771
- Cui, Y., Miller, D., Schiarizza, P. and Diakow, L.J. (2017): British Columbia digital geology; BC Ministry of Energy, Mines and Petroleum Resources, BC Geological Survey, Open File 2017-8, 9 p., URL <http://cmscontent.nrs.gov.bc.ca/geoscience/PublicationCatalogue/OpenFile/BCGS_OF2017-08.pdf> [June 2019].
- Devine, F.A.M., Kowalczyk, P., Heberlein, D.R. and Kilby, W. (2016): A geo-exploration atlas of the Mount Polley porphyry copper-gold district, south-central British Columbia; Geoscience BC, Report 2016-10, URL <http://cdn.geosciencebc.com/project_data/GBCReport2016-10/GBCReport2016-10.pdf> [January 2022]
- Enkin, R.J. (2018): The Canadian Rock Physical Property Database: first public release; Geological Survey of Canada, Open File 8460, 1 zip file, DOI: 10.4095/313389
- Enkin, R.J., Cowan, D., Tigner, J., Severide, A., Gilmour, D., Tkachyk, A., Kilduff, M., Vidal, B. and Baker, J. (2012): Physical property measurements at the GSC Paleomagnetism and Petrophysics Laboratory, including electric impedance spectrum methodology and analysis; Geological Survey of Canada, Open File 7227, 42 p., DOI: 10.4095/291564
- Fitzgerald, J., Jago, C.P., Jankovic, S., Simonian, B., Taylor, C.A. and Borntraeger, B. (2020): Technical report on the Mount Milligan mine, north-central British Columbia; NI 43-101 report prepared for Centerra Gold Inc., 268 p., URL <<https://www.centerragold.com/cg-raw/cg/mtm-technical-report-2020.pdf>> [October 2021].
- Geotech Ltd. (2008): Report on a helicopter-borne versatile time domain electromagnetic (VTEM) geophysical survey: QUEST project, central British Columbia (NTS 93A, B, G, H, J, K, N, O and 94C, D), Geoscience BC, Report 2008-4, 35 p., URL <http://www.geosciencebc.com/i/project_data/QUESTdata/report/7042-GeoscienceBC_final.pdf> [June 2019].
- Government of British Columbia (2021): Copper production, production data archive; Government of British Columbia, URL <<https://www2.gov.bc.ca/gov/content/industry/mineral-exploration-mining/further-information/statistics/production/production-data-archive>> [October 2021].
- Granek, J. (2016): Application of machine learning algorithms to mineral prospectivity mapping; Ph.D. thesis, The University of British Columbia, 91 p.
- Hanley, J., Kerr, M., LeFort, D., Warren, M., MacKenzie, M. and Sedge, C. (2020): Enrichment of platinum-group elements (PGE) in alkalic porphyry Cu-Au deposits in the Canadian Cordillera: new insights from mineralogical and fluid inclusion studies; *in* Porphyry deposits of the northwestern cordillera of North America: a 25 year update, Sharman, E.R., Lang, J.R. and Chapman, J.B. (eds.), Canadian Institute of Mining, Metallurgy, and Petroleum, Special Volume 57, p. 88–109.
- Henkel, H. (1991): Petrophysical properties (density and magnetization) of rocks from the northern part of the Baltic Shield; *Tectonophysics*, v. 192, p. 1–19. DOI: 10.1016/0040-1951(91)90242-K
- Holbek, P.M., Joyes, R. and Cromwell, E. (2020): The Copper Mountain alkalic porphyry copper-gold deposit, southern British Columbia; *in* Porphyry deposits of the northwestern cordillera of North America: a 25 year update, Sharman, E.R., Lang, J.R. & Chapman, J.B. (eds.), Canadian Institute of Mining, Metallurgy, and Petroleum, Special Volume 57, p. 690–710.
- Jensen, E. P. and Barton, M. D. (2000): Gold deposits related to alkaline magmatism; *in* Gold in 2000, Hagemann, S.G. and Brown, P.E. (eds.), Society of Economic Geologists Reviews, v. 13, p. 279–314.
- Kowalczyk, P., Oldenburg, D., Phillips, N., Nguyen, T.N.H. and Thomson, V. (2010): Acquisition and analysis of the 2007–2009 Geoscience BC airborne data; *in* Abstracts from the ASEG-PESA Airborne Gravity 2010 Workshop, Aug. 22–26, Geoscience Australia, Canberra, Lane, R.L.L. (ed.), p. 115–124, URL <https://d28rz98at9flks.cloudfront.net/70673/Rec2010_023.pdf> [October 2020].
- Lang, J.R., Stanley, C.R. and Thompson, J.F.H. (1995a): Porphyry copper deposits related to alkalic igneous rocks in the Triassic-Jurassic

arc terranes of British Columbia; *Arizona Geological Society Digest*, v. 20, p. 219–236.

- Lang, J.R., Lueck, B., Mortensen, J.K., Russell, J.K., Stanley, C.R. and Thompson, J.F.H. (1995b): Triassic–Jurassic silica-undersaturated and silica-saturated alkalic intrusions in the Cordillera of British Columbia: implications for arc magmatism; *Geology*, v. 23, p. 451–454, DOI: 10.1130/0091-7613(1995)023<0451:TJSUAS>2.3.CO;2
- Lang, J. R., Stanley, C.R., Thompson, J. F. H. and Dunne, K. F. (1995c): Na-K-Ca magmatic-hydrothermal alteration in alkalic porphyry Cu-Au deposits, British Columbia; *in* *Magma, Fluids, and Ore Deposits*, Thompson, J.F.H. (ed.), Mineralogical Association of Canada, Short Course Volume 23, p. 339–366.
- Lee, R.G., Byrne, K. and Lesage, G. (2020): Distal alteration facies of Late Triassic to Early Jurassic porphyry copper deposits, British Columbia, Canada: a green rock perspective; *in* *Porphyry deposits of the northwestern cordillera of North America: a 25 year update*, Sharman, E.R., Lang, J.R. and Chapman, J.B. (eds.), Canadian Institute of Mining, Metallurgy, and Petroleum, Special Volume 57, p. 68–87.
- Ledoux, T.J. and Hart, C.J.R. (2021): Evolution of the southern Quesnel arc: potential to distinguish variability in magmatic porphyry fertility, south-central British Columbia (NTS 082E, L, 092H, I, P, 093A, B); *in* *Geoscience BC Summary of Activities 2020*, Minerals, Geoscience BC, Report 2021-01, p. 75–90, URL <http://www.geosciencebc.com/i/pdf/SummaryofActivities2020/Minerals/Sch_Ledoux_MineralsSOA2020.pdf> [November 2021].
- Li, Y., Sun, J., Li, S-L. and Leão-Santos, M. (2021): A paradigm shift in magnetic data interpretation: increased value through magnetization inversions; *The Leading Edge*, v. 40, p. 89–98, DOI: 10.1190/tle40020089.1
- Lipske, J.L., Wade, D., Hall, R.D. and Peterson, M.A. (2020): Geology and mineralization of the New Afton Cu-Au alkalic porphyry deposit, Kamloops, British Columbia; *in* *Porphyry deposits of the northwestern cordillera of North America: a 25 year update*, Sharman, E.R., Lang, J.R. and Chapman, J.B. (eds.), Canadian Institute of Mining, Metallurgy, and Petroleum, Special Volume 57, p. 648–667.
- Logan, J.M. and Mihalynuk, M.G. (2014): Tectonic controls on Early Mesozoic paired alkaline porphyry deposit belts (Cu-Au ± Ag-Pt-Pd-Mo) within the Canadian Cordillera; *Economic Geology*, v. 109, p. 827–858, DOI: 10.2113/econgeo.109.4.827
- Logan, J.M. and Schiarizza, P. (2014): The Rayfield River pluton, south-central British Columbia (NTS 92P/6): Geologic setting and copper mineralization; *in* *Geological Fieldwork 2013*, British Columbia Ministry of Energy, and Mines, British Columbia Geological Survey Paper 2014-1, p. 15–27.
- Logan, J.M. and Schiarizza, P. (2011): Geology of the Quesnel and Stikine terranes and associated porphyry deposits; *Exploration Undercover; a practical example using the QUEST study area*, Geoscience BC and BC Geophysical Society workshop, 2011, URL <http://www.geosciencebc.com/i/pdf/Presentations/UnderCoverWS2011/Talk_4_Schiarrizza.pdf> [January 2020].
- Logan, J.M., Schiarizza, P., Struik, L.C., Barnett, C., Nelson, J.L., Kowalczyk, P., Ferri, F., Mihalynuk, M.G., Thomas, M.D., Gammon, P., Lett, R., Jackaman, W. and Ferbey, T. (2010): Bedrock Geology of the QUEST map area, central British Columbia: British Columbia Geological Survey, Geoscience Map 2010-1, Geoscience BC report 2010-5 and Geological Survey of Canada Open File 6476, URL<<http://www.geosciencebc.com/s/2010-005.asp>> [June 2019].
- Logan, J.M. and Mihalynuk, M.G. (2005): Regional geology and setting of the Cariboo, Bell, Springer and Northeast Porphyry Cu-Au zones at Mount Polley, south-central, British Columbia; *in* *Geological Fieldwork 2004*, British Columbia Ministry of Energy, Mines and Petroleum Resources, British Columbia Geological Survey Paper 2005-01, p. 249-270, URL <http://cmscontent.nrs.gov.bc.ca/geoscience/PublicationCatalogue/Paper/BCGS_P2005-RR07_Logan.pdf> [October 2021].
- Maynard, D.E., Ward, B.C., Geertsema, M., Roberts, N. and Sacco, D. (2010): Relative drift thickness map, north-central BC, (93G, 93H/w, and 93J/s); Geoscience BC, Map 2010-14-1, scale 1:250 000, URL <http://cdn.geosciencebc.com/project_data/GBC_Report2010-14/GBC_Map_2010-14-1.pdf> [June 2019].
- Mihalynuk, M.G. and Logan, J.M. (2010): Recipe for Cu-Au-Ag ± Mo porphyry deposits: ingredients from the northern Cordilleran terranes; *in* *Cordilleran Metallogeny: Porphyry Settings 2010: Program with Abstracts, 2010*, Geological Association of Canada, Cordilleran Section, Vancouver, BC, Canada, 26 p.
- Mira Geoscience Ltd. (2009): QUEST Project: 3-D inversion modeling, integration, and visualization of airborne gravity, magnetic, and electromagnetic data, BC, Canada; Geoscience BC, Report 2009-15, 87 p., URL <http://www.geosciencebc.com/i/project_data/GBC_Report2009-15/Report/Mira_AGIC_GeoscienceBC_Quest_Geop_Modelling_Report_2009-15.pdf> [June 2019].

- Mitchinson, D.E., Enkin, R.J. and Hart, C.J.R. (2013): Linking porphyry deposit geology to geophysics via physical properties: adding value to Geoscience BC geophysical data, Geoscience BC, Report 2013-14, 116 p., URL <http://www.geosciencebc.com/i/project_data/GBC_Report2013-14/GBC_Report2013-14.pdf> [November 2019].
- Montsion, R.M., Saumur, B.M., Acosta-Gongora, P., Gadd, M.G., Tschirhart, P. and Tschirhart, V. (2019): Knowledge-driven mineral prospectivity modelling in areas with glacial overburden: porphyry Cu exploration in Quesnellia, British Columbia, Canada; *Applied Earth Science*, v. 128, p. 181–196, DOI: 10.1080/25726838.2019.1675403
- Mortensen, J.K., Ghosh, D.K. and Ferri, F. (1995): U-Pb geochronology of intrusive rocks associated with copper-gold porphyry deposits in the Canadian Cordillera; *in* *Porphyry deposits of the northwestern cordillera of North America*, Schroeter, T.G. (ed.), Canadian Institute of Mining, Metallurgy, and Petroleum, Special Volume 46, p. 142–158.
- Natural Resources Canada (1962): British Columbia - 61-1 total field magnetic data, Canadian Airborne Geophysical Data Base; Airborne Geophysics Section, Geological Survey of Canada, Lands and Minerals Sector, Natural Resources Canada, URL <<https://open.canada.ca/data/en/dataset/d8fbc222-20c3-5573-a583-aba4618dfb3>> [March 2021]; Open Government, Government of Canada. (2013, April 26). *Open Government Licence - Canada*. Retrieved from <http://open.canada.ca/en/open-government-licence-canada>
- Natural Resources Canada (1992): National Gamma Ray Spectrometry database, circa 2001, Mount Milligan, Canadian Airborne Geophysical Database; Airborne Geophysics Section, Geological Survey of Canada, Lands and Minerals Sector, Natural Resources Canada, URL <<https://open.canada.ca/data/en/dataset/8338b600-eaf8-5021-aa03-8109ccf10770>> [May 2020]; Open Government, Government of Canada. (2013, April 26). *Open Government Licence - Canada*. Retrieved from <http://open.canada.ca/en/open-government-licence-canada>
- Natural Resources Canada (2004): National Gamma Ray Spectrometry database, circa 2001, Mount Polley (Imperial Metals), Canadian Airborne Geophysical Database; Airborne Geophysics Section, Geological Survey of Canada, Lands and Minerals Sector, Natural Resources Canada, URL <<https://open.canada.ca/data/en/dataset/26098bfa-4dff-5900-9dc4-47486f730c0b>> [May 2020]; Open Government, Government of Canada. (2013, April 26). *Open Government Licence - Canada*. Retrieved from <http://open.canada.ca/en/open-government-licence-canada>
- Natural Resources Canada (2020): Canada 200 magnetic data compilation, residual total field data, Canadian Airborne Geophysical Data Base; Airborne Geophysics Section, Geological Survey of Canada, Lands and Minerals Sector, Natural Resources Canada, URL <<https://open.canada.ca/data/en/dataset/752fe3fc-d871-5ae1-9bd9-2b6f65880a8d>> [October 2019]; Open Government, Government of Canada. (2013, April 26). *Open Government Licence - Canada*. Retrieved from <http://open.canada.ca/en/open-government-licence-canada>
- Natural Resources Canada (2021): Copper facts; Natural Resources Canada, URL <<https://www.nrcan.gc.ca/our-natural-resources/minerals-mining/minerals-metals-facts/copper-facts/20506>> [October 2021].
- Nelson, J. L. and Bellefontaine, K.A. (1996): The geology and mineral deposits of north-central Quesnellia, Tezzeron Lake to Discovery Creek, central British Columbia; BC Ministry of Energy, Mines and Petroleum Resources, Bulletin 99, 112 p.
- Rees, C., Gillstrom, G., Ferreira, L., Bjornson, L. and Taylor, C. (2014): Geology of the Mount Polley Intrusive Complex; Geoscience BC Map 2014-08-1, scale 1:10 000, URL <http://www.geosciencebc.com/i/project_data/GBCReport2014-08/GBCReport2014-08_map.pdf> [October 2021].
- Rees, C., Gillstrom, G. and Riedell, K.B. (2020): The Mount Polley porphyry copper deposit, south-central British Columbia; *in* *Porphyry deposits of the northwestern cordillera of North America: a 25 year update*, Sharman, E.R., Lang, J.R. and Chapman, J.B. (eds.), Canadian Institute of Mining, Metallurgy, and Petroleum, Special Volume 57, p. 567-600.
- Sander Geophysics Ltd. (2008): Airborne gravity survey, Quesnellia region, British Columbia; Geoscience BC, Report 2008-8, 121 p., URL <http://www.geosciencebc.com/i/project_data/QUESTdata/GBCReport2008-8/Gravity_Technical_Report.pdf> [November 2019].
- Sander Geophysics Ltd. (2010): Airborne Gravity Survey QUEST South, British Columbia, 2009, Geoscience BC Report 2010-6, 97 p. URL <http://cdn.geosciencebc.com/project_data/GBC_Report2010-6/GBC_Report2010-6_Technical_Report.pdf> [November 2021].
- Sánchez, M.G., Bissig, T. and Kowalczyk, P. (2015): Toward an improved basis for beneath-cover mineral exploration in the QUEST area, central British Columbia: new structural interpretation of geophysical and geological datasets; Geoscience BC, Report 2015-15, scale 1:500 000, URL <http://cdn.geosciencebc.com/project_data/GBCReport2015-15/ExecutiveSummary_2015_015.pdf> [May 2020].

- Schipper, B. W., Lin, H.-C., Meloni, M. A., Wansleeben, K., Heijungs, R. and van der Voet, E. (2018): Estimating global copper demand until 2100 with regression and stock dynamics; *Resources, Conservation and Recycling*, v. 132, p. 28–36, URL <<https://doi.org/10.1016/j.resconrec.2018.01.004>> [October 2021].
- Schodde, R. (2019): Trends in exploration; International Mining and Resource Conference (IMARC), Melbourne, October 2019, URL <<https://minexconsulting.com/trends-in-exploration/>> [October 2021].
- Sharman, E.R., Lang, J.R. and Chapman, J.B., editors (2020): Porphyry deposits of the northwestern cordillera of North America: a 25 year update; Canadian Institute of Mining, Metallurgy, and Petroleum, Special Volume 57, 726 p.
- Sillitoe, R.H. (1972): A plate tectonic model for the origin porphyry copper deposits; *Economic Geology*, v. 67, p. 184–197, DOI: 10.2113/gsecongeo.67.2.184
- Sillitoe, R.H. (2000): Gold-rich porphyry deposits: descriptive and genetic models and their role in exploration and discovery; in *Gold in 2000*, Hagemann, S.G. and Brown, P.E. (eds.), Society of Economic Geologists Reviews, v. 13, p. 315–345.
- Sillitoe, R.H. (2010): Porphyry deposit systems; *Economic Geology*, v. 105, p. 3–41, DOI: 10.2113/gsecongeo.105.1.3
- Thomas, M.D., Pilkington, M., Anderson, R.G. and Mareschal, J.-C. (2011): Geological significance of high-resolution magnetic data in the Quesnel terrane, Central British Columbia; *Canadian Journal of Earth Sciences*, v. 48, p. 1065–1089, DOI: 10.1139/e10-109
- Thomas, M. D. (2019): Gravity and magnetic models of the Iron Mask Batholith, south-central Canadian Cordillera, British Columbia; Geological Survey of Canada, Current Research 2019-1, 24 p., DOI: 10.4095/314517
- Thompson, J.F.H., Lang, J.R. and Stanley, C.R. (2001): Platinum group elements in alkaline porphyry deposits, British Columbia; *Exploration and Mining in British Columbia 2001*, BC Ministry of Energy, Mines and Petroleum Resources, Mines Branch, p. 57–64.
- Toft, P. B., Arkani-Hamed, J. and Haggerty, S. E. (1990): The effects of serpentinization on density and magnetic susceptibility: A petrophysical model; *Physics of the Earth and Planetary Interiors*, v. 65, p. 137–157, URL <[https://doi.org/10.1016/0031-9201\(90\)90082-9](https://doi.org/10.1016/0031-9201(90)90082-9)>

LIST OF APPENDICES

Digital Appendix 1: Petrophysical data

Digital Appendix 2: Water well database

Digital Appendix 3: ARIS exploration drillhole database

Appendix 1: Petrography and Terraspec report

Appendix 2: Magnetic inversions methodology

Appendix 3: Gravity inversions methodology

APPENDIX 1: SUPPLEMENTAL PETROGRAPHY REPORT



Sample ID: Q1B
MDRU ID: GAP-QT-1019-DM-001B
Rock type: Volcanic sediment
Alteration: Chlorite-Carbonate
Sulfide: Pyrite-chalcopyrite

UTM NAD 83 Z10
UTM North: 5962485
UTM East: 530938
Lat: 53.8100
Long: -122.5302

Rock Description:
Light grey to green strongly foliated Greenschist rock with chloritization and very weak sericite alteration.



PETROGRAPHY

Preparation Thin Section Polished Thin Section Polished Slab

Scanned section images:



Billet Scan



Polished Thin Section



Crossed-Polarized Light (XPL)

Thin Section Summary:

Rock Type: Volcanic sediment
Lithochemistry notes: SiO₂ 41.9; CaO - 12.25%, LOI - 12.15%, TOT/C - 2.65%, TOT/S - 0.65%, SO₃ - 0.899%
Sulfide: Pyrite-chalcopyrite
Magnetic Susceptibility average: 0.30
SWIR Assemblage: Chlorite

Thin section description:

Fine- to medium-grained green schist with strong foliation and banding cut by narrow irregular carbonate veinlets. 30-35% chlorite forms main texture with 2-3% cubic pyrite 0.25-2mm in length occurring with the chlorite (Figs 1-2). Locally <0.25% chalcopyrite forms along the edge of pyrite grains (Figs 3-4). Sericite where present is very weak with chlorite dominant in schistosity banding. Silica, clay, iron-oxide and local remnant biotite present in banding. Carbonate veining cross-cuts foliation and are 1-2mm in width.



Sample ID: Q3A
MDRU ID: GAP-QT-1019-DM-003A
Rock type: Phyllite
Alteration: FeOx
Sulfide: Oxidized pyrite

UTM NAD 83 Z10
UTM North: 5954724
UTM East: 533725
Lat: 53.7401
Long: -122.4887

Rock Description:
Very fine-grained black to grey phyllite to mylonite rock. Strongly oxidized with remnant sulfide zones. Originally volcanic tuff(?) with remnant flattened lamelli or boudinaged grains from mylonitic texture.



PETROGRAPHY

Preparation Thin Section Polished Thin Section Polished Slab

Scanned section images:



Billet Scan



Polished Thin Section



Crossed-Polarized Light (XPL)

Thin Section Summary:

Rock Type: Phyllite
Lithochemistry notes: Not Analyzed
Sulfide: Oxidized pyrite
Magnetic Susceptibility average: 0.30
SWIR Assemblage: Spectral

Thin section description:

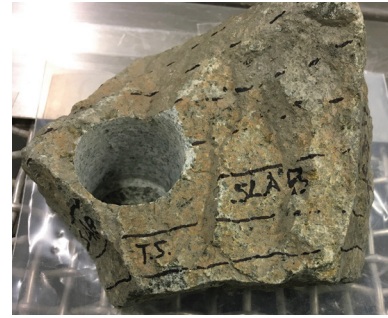
Fine-grained phyllitic to schistoic textured rock with coarse pockets of silica, carbonate, iron-oxide and remnant pyrite (Figs 1-6). Silica-Fe-Oxide form elongate boudins with sulfide in core oxidized to hematite plus or minus goethite (Figs 4, 6). Carbonate forms in open space in center of boudins (Fig. 2) or as interstitial grains with silica (Fig. 5). Groundmass made up of very-fine grained silica, feldspars, micas, and other unidentified material possibly glass, clay and oxides.



Sample ID: Q3B
MDRU ID: GAP-QT-1019-DM-003B
Rock type: Alkalic Gabbro
Alteration: Chlorite
Sulfide: Oxidized pyrite

UTM NAD 83 Z10
UTM North: 5954724
UTM East: 533725
Lat: 53.7401
Long: -122.4887

Rock Description:
Medium- to coarse-grained porphyritic alkalic gabbro with 2-4mm plag, amphibole grains and local pyroxene and biotite crystals. Strong chloritization of mafic grains.



PETROGRAPHY

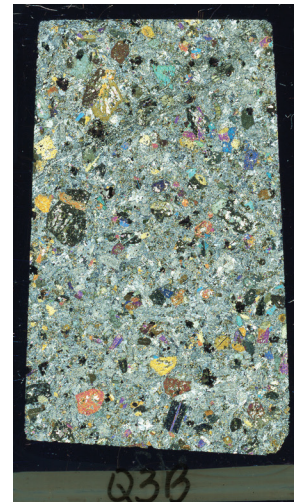
Preparation Thin Section Polished Thin Section Polished Slab
Scanned section images:



Billet Scan



Polished Thin Section



Crossed-Polarized Light (XPL)

Thin Section Summary:

Rock Type: Alkalic Gabbro

Lithochemistry notes: SiO₂ - 49.3%, CaO - 9.71%, MgO - 5.36%, Tot/S - 0.04%

Sulfide: Oxidized pyrite

Magnetic Susceptibility average: 0.57

SWIR Assemblage: Chlorite-Phengite-Hornblende

Thin section description:

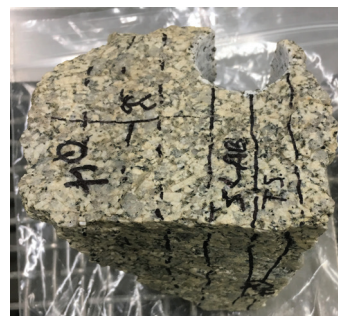
Coarse to medium-grained texture with equant feldspar and amphibole grains set in fine-grained feldspathic groundmass (Fig. 1). Strong chloritization of mafic grains with replacement along cleavage planes and fractures to complete replacement of grains with minor epidote (Figs. 2-3). Chlorite is massive to mottled and occurs in groundmass with weak sericitization of feldspars. Local rare amorphous oxidized sulfides <1mm occur throughout section primarily with chlorite alteration (Figs. 4-6). Pyrite oxidizing to hematite with little to no magnetite present in sample (Fig. 6). Carbonate also occurs with chloritization primarily as massive replacement fill in coarse chlorite zones (Fig. 4).



Sample ID: Q4
MDRU ID: GAP-QT-1019-DM-004
Rock type: Granodiorite porphyry
Alteration: Clay-chlorite
Sulfide: None

UTM NAD 83 Z10
UTM North: 5953489
UTM East: 544626
Lat: 53.7282
Long: -122.3236

Rock Description:
Light beige coarse-grained granodiorite porphyry with euhedral 3-5mm plagioclase phenocrysts (45-55%), rounded quartz eyes (25-30%), 10-15% potassium feldspar, and fine- to medium-grained mafic grains (biotite + amphibole).



PETROGRAPHY

Preparation Thin Section Polished Thin Section Polished Slab

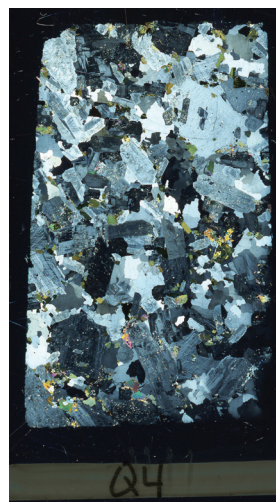
Scanned section images:



Billet Scan



Polished Thin Section



Crossed-Polarized Light (XPL)

Thin Section Summary:
Rock Type: Granodiorite porphyry
Lithochemistry notes: SiO₂ - 66.8%, CaO - 3.9%, Na₂O - 4.13%, K₂O - 3.25%
Sulfide: None
Magnetic Susceptibility average: 6.01
SWIR Assemblage: Montmorillonite-Chlorite

Thin section description:
 Coarse phenocrysts of feldspar and quartz with weak clay alteration with very weakly chloritized amphibole & biotite grains (Figs 1-3). Groundmass dominated by coarse interlocked feldspar grains. Local white mica alteration of feldspar, generally though alteration is weak.



Sample ID: Q5
MDRU ID: GAP-QT-1019-DM-005
Rock type: Metasediment
Alteration: Biotite/Chlorite
Sulfide: Trace pyrite

UTM NAD 83 Z10
UTM North: 5949291
UTM East: 537041
Lat: 53.6910
Long: -122.4391

Rock Description:
Very fine-grained black to grey metasediment. Local 0.3mm grains ~5% of rock. Oxidized fractures contain fine-grained pyrite.



PETROGRAPHY

Preparation Thin Section Polished Thin Section Polished Slab

Scanned section images:



Billet Scan



Polished Thin Section



Crossed-Polarized Light (XPL)

Thin Section Summary:

Rock Type: Metasediment
Lithochemistry notes: SiO₂ - 70.1%, Fe₂O₃ - 3.7%, Na₂O - 5.64%
Sulfide: Trace pyrite
Magnetic Susceptibility average: 0.03
SWIR Assemblage: Aspectral

Thin section description:

Fine-grained metasedimentary rock with foliation defined by biotite and porphyroblasts of cordierite and other silicates (Figs 1-2). Weak chlorite in matrix with biotite mostly fresh. Local fractures contain sulfide oxidizing to goethite and/or hematite (Figs 3-4). Silicates are <0.1mm with local porphyroblasts up to 0.5mm. Foliation not strongly defined but some biotite stretched and rotated.



Sample ID: Q7
MDRU ID: GAP-QT-1019-DM-007
Rock type: Volcanic sediment
Alteration: Epidote-Chorite-White Mica-Carbonate
Sulfide: None

UTM NAD 83 Z10
UTM North: 5985134
UTM East: 533654
Lat: 54.0134
Long: -122.4864

Rock Description:
Pale green to grey fine-grained metasediment with chlorite-carbonate and silicification.



PETROGRAPHY

Preparation Thin Section Polished Thin Section Polished Slab

Scanned section images:



Billet Scan



Polished Thin Section



Crossed-Polarized Light (XPL)

Thin Section Summary:

Rock Type: Volcanic sediment
Lithochemistry notes: SiO₂ - 49.0%, CaO - 11.61%, MgO - 7.17%, TOT/C - 0.2%, LOI - 2.91
Sulfide: None
Magnetic Susceptibility average: 0.34
SWIR Assemblage: Epidote-Hornblende-Phengite

Thin section description:

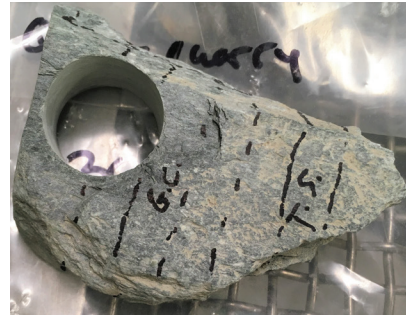
Very fine-grained mottled green-black groundmass of chlorite-oxide-clay with nodules of calcite-silica-chlorite and cut by clay alteration (Fig. 1-3). Local small epidote grains present along edge of nodules and oxidized pockets. White-mica forms acicular grains growing into nodules may be clay (pyrophyllite).



Sample ID: Q7-Quarry
MDRU ID: GAP-QT-1019-DM-007Q
Rock type: Volcanic sediment
Alteration: Chlorite-White Mica-Carbonate
Sulfide: Oxidized pyrite

UTM NAD 83 Z10
UTM North: 5985134
UTM East: 533654
Lat: 54.0134
Long: -122.4864

Rock Description:
Grey to green strongly foliated greenschist or tuff with calcite veining and chlorite-sericite alteration. Fine <5 mm oxidized black clasts. Intense alteration with high LOI, total carbon, and water.



PETROGRAPHY

Preparation Thin Section Polished Thin Section Polished Slab

Scanned section images:



Billet Scan



Polished Thin Section



Crossed-Polarized Light (XPL)

Thin Section Summary:

Rock Type: Volcanic sediment

Lithochemistry notes: SiO₂ - 41.0%, CaO - 12.05%, MgO - 7.17%, TOT/C - 2.55%, Ni - 148.6 ppm, LOI - 12.89%, H₂O+ - 5.07%

Sulfide: Oxidized pyrite

Magnetic Susceptibility average: 0.34

SWIR Assemblage: Chlorite-Phengite

Thin section description:

Intensely altered rounded to subrounded tuffaceous clasts to chlorite-carbonate in very-fine grain glassy to sericite-chlorite matrix (Figs. 1-3). Chlorite is finely crystalline grey-green makes up 60-65% of section. Cut by <1mm irregular calcite veinlets parallel and perpendicular to foliation. 3-5% opaque grains appear to be oxidized sulfides (pyrite?) (Fig. 4), elevated Ni in lithochem possibly related to these grains.



Sample ID: Q8
MDRU ID: GAP-QT-1019-DM-008
Rock type: Volcanic sediment
Alteration: Chlorite
Sulfide: rare pyrite

UTM NAD 83 Z10
UTM North: 5977690
UTM East: 532914
Lat: 53.9465
Long: -122.4985

Rock Description:
Fine-grained light grey silicified sediment or volcanic sediment. Hair-line fractures with rusty colored pyrite and carbonate. Dark to light banding.



PETROGRAPHY

Preparation Thin Section Polished Thin Section Polished Slab

Scanned section images:



Billet Scan



Polished Thin Section



Crossed-Polarized Light (XPL)

Thin Section Summary:

Rock Type: Volcanic sediment
Lithochemistry notes: SiO₂ - 58.6%, Al₂O₃ - 17.1% Fe₂O₃ - 6.35%, Na₂O - 5.0%
Sulfide: rare pyrite
Magnetic Susceptibility average: 0.31
SWIR Assemblage: Epidote-Chlorite

Thin section description:

Dark to light grey fine microclastic texture of subrounded to angular feldspar-silica clasts in chloritized cement with local ratty sulfides in dark banding along fracture planes (Figs 1-2). Strong silicification in clasts, cement and late fine quartz veinlets (Figs. 3-4). Oxidized clasts and cement make up darker banding with lighter zones more silicified. Rare epidote present along edges of clasts with chlorite. Oxidized sulfides <0.25% of section.



Sample ID: Q9
MDRU ID: GAP-QT-1019-DM-009
Rock type: Basaltic Trachyandesite
Alteration: Chlorite-biotite
Sulfide: Oxidized pyrite

UTM NAD 83 Z10
UTM North: 5972610
UTM East: 531820
Lat: 53.9010
Long: -122.5157

Rock Description:
Dark black to purple fine-grained crystalline basaltic trachyandesite with biotite-chlorite alteration. Cut by massive quartz-carbonate veins with pyrite.



PETROGRAPHY

Preparation Thin Section Polished Thin Section Polished Slab

Scanned section images:



Billet Scan



Polished Thin Section



Crossed-Polarized Light (XPL)

Thin Section Summary:

Rock Type: Basaltic Trachyandesite
Lithochemistry notes: SiO₂ - 53.7%, Al₂O₃ - 19.38% Fe₂O₃ - 5.26%, Na₂O - 4.25%, K₂O - 3.2%
Sulfide: Oxidized pyrite
Magnetic Susceptability average: 0.28
SWIR Assemblage: Chlorite-Hornblende

Thin section description:

Crowded equant plagioclase feldspar phenocrysts in biotite-chlorite altered groundmass (Figs. 1-3). Feldspar makes up 35-40% of section and form grungy weak to moderate clay altered textures. Quartz-carbonate-sulfide veins are irregular 0.5-1mm in width with sulfide rare and oxidizing to hematite (Figs. 2, 4). Biotite is dominant with local chloritization primarily adjacent to quartz veins but can occur pervasively through section.



Sample ID: Q11A
MDRU ID: GAP-QT-1019-DM-011A
Rock type: Monzonite
Alteration: Chlorite-sericite
Sulfide: Pyrite-chalcopyrite-magnetite

UTM NAD 83 Z10
UTM North: 6083594
UTM East: 414884
Lat: 54.8921
Long: -124.3271

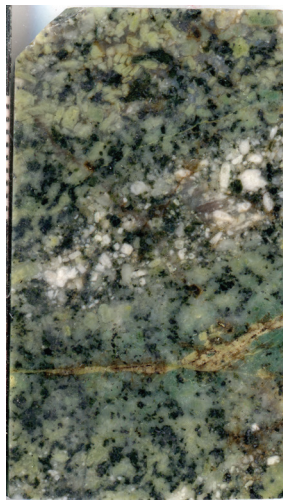
Rock Description:
Strong altered granular monzonite with chlorite-epidote-albite alteration. Fractures have sulfide as chalcopyrite+pyrite and pink mineral (Kspar? Fe-carbonate).



PETROGRAPHY

Preparation Thin Section Polished Thin Section Polished Slab

Scanned section images:



Billet Scan



Polished Thin Section



Crossed-Polarized Light (XPL)

Thin Section Summary:

Rock Type: Monzonite

Lithochemistry notes: SiO₂ - 56.0%, Al₂O₃ - 18.69% Fe₂O₃ - 5.26%, Na₂O - 4.42%, K₂O - 5.54% , Cu - 0.12%, Au - 150.3 ppb

Sulfide: Pyrite-chalcopyrite-magnetite

Magnetic Susceptibility average: 38.80

SWIR Assemblage: Chlorite-Phengite

Thin section description:

Coarse to medium-grained porphyritic texture of massive feldspar grains with amphibole and local pyroxene (Figs. 1-2). Local accessory grains of titanite present in feldspar grains (Fig. 2). Moderate to strong ratty chlorite replacement of mafic grains with magnetite and fine-grained sulfides of chalcopyrite and pyrite (Figs. 3-6). Feldspars altering to clay and sericite with local albitization along edges of grains. Hematite present with magnetite and sulfides (Fig. 3, 5). Sulfides <0.1mm 0.25%, and chlorite up to 15% with epidote present locally.



Sample ID: Q11B
MDRU ID: GAP-QT-1019-DM-011B
Rock type: Monzodiorite
Alteration: Chlorite-sericite
Sulfide: Pyrite-chalcopyrite-magnetite

UTM NAD 83 Z10
UTM North: 6083594
UTM East: 414884
Lat: 54.8921
Long: -124.3271

Rock Description:
Granular porphyritic monzodiorite with plagioclase, amphibole-pyroxene (5%), and pyrite-chalcopyrite veining. Local chlorite-epidote alteration.



PETROGRAPHY

Preparation Thin Section Polished Thin Section Polished Slab

Scanned section images:



Billet Scan



Polished Thin Section



Crossed-Polarized Light (XPL)

Thin Section Summary:

Rock Type: Monzodiorite

Lithochemistry notes: SiO₂ - 51.4%, Al₂O₃ - 18.49% Fe₂O₃ - 8.5%, CaO - 8.64, Cu - 683.7 ppm, Au - 121 ppb

Sulfide: Pyrite-chalcopyrite-magnetite

Magnetic Susceptibility average: 69.50

SWIR Assemblage: Chlorite-Phengite

Thin section description:

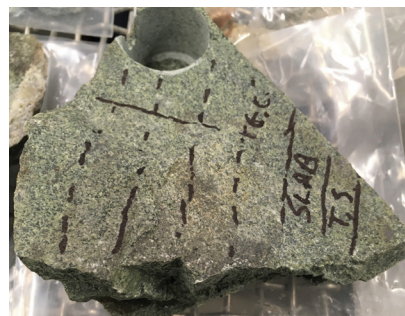
Coarse to medium grained porphyritic texture of feldspar with medium grained pyroxene and amphibole in fine-grained feldspathic groundmass and abundant opaques (Figs. 1-4). Epidote alteration with chlorite is weak with local carbonate replacement pods. Feldspars altering to clay and weak white mica. Veins and fracture fill of sulfide pyrite>>chalcopyrite occurs with chlorite-sericite (Figs. 4-5). Magnetite is common 4-5% and present throughout groundmass (Fig. 6).



Sample ID: Q12
MDRU ID: GAP-QT-1019-DM-012
Rock type: Metamorphic? Gabbro/Amphibolite?
Alteration: Chlorite-sericite
Sulfide: rare pyrite

UTM NAD 83 Z10
UTM North: 6083730
UTM East: 416532
Lat: 54.8936
Long: -124.3014

Rock Description:
Strongly altered amphibolite to gabbro, crystalline (1-2mm) with pervasive chlorite-epidote alteration.



PETROGRAPHY

Preparation Thin Section Polished Thin Section Polished Slab

Scanned section images:



Billet Scan



Polished Thin Section



Crossed-Polarized Light (XPL)

Thin Section Summary:

Rock Type: Metamorphic? Gabbro/Amphibolite?
Lithochemistry notes: SiO₂ - 44.4%, Al₂O₃ - 18.44% Fe₂O₃ - 12.09%, CaO - 10.49,
Sulfide: rare pyrite
Magnetic Susceptibility average: 43.80
SWIR Assemblage: Chlorite-Phengite

Thin section description:

Intensely altered (chlorite>epidote) medium grained amphibole and sericitized feldspar grains with 3-4% magnetite and <0.25% pyrite with hematite alteration (Figs. 1-4). Strong clay and oxidation of groundmass with 6-8% altered amphibole and pyroxene(?). Magnetite occurs as amorphous <0.5mm grains throughout groundmass 2-3% (Fig. 3). Pyrite is strongly oxidized and generally rare (Fig. 4).



Sample ID: Q13A
MDRU ID: GAP-QT-1019-DM-013A
Rock type: Basaltic Trachyandesite
Alteration: Chlorite-sericite
Sulfide: None

UTM NAD 83 Z10
UTM North: 6079115
UTM East: 431309
Lat: 54.8544
Long: -124.0700

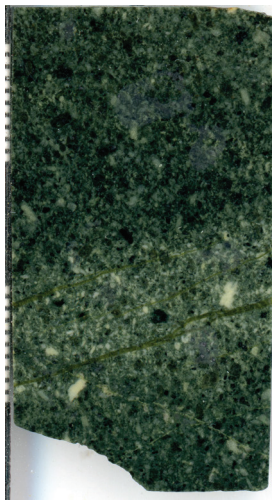
Rock Description:
Grey to green very finely-grained crystalline volcanic rock with fine fractures filled with chlorite-sericite. Rare <1mm pyroxene and slightly coarser feldspar.



PETROGRAPHY

Preparation Thin Section Polished Thin Section Polished Slab

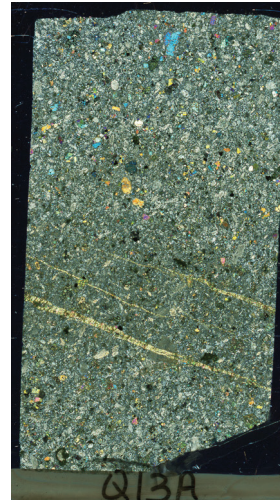
Scanned section images:



Billet Scan



Polished Thin Section



Crossed-Polarized Light (XPL)

Thin Section Summary:

Rock Type: Basaltic Trachyandesite

Lithochemistry notes: SiO₂ - 50.7%, Al₂O₃ - 16.58% Fe₂O₃ - 9.53%, CaO - 7.97, MgO - 5.03

Sulfide: None

Magnetic Susceptibility average: 20.50

SWIR Assemblage: Chlorite-Phengite

Thin section description:

Fine-grained mottled groundmass and moderately porphyritic basaltic trachyandesite with sericitized feldspar and chloritized pyroxene and amphibole phenocrysts. Cut by veins and fracture fill of yellow-green-brown chlorite veins with sericite veinlets (Figs. 1-5). Veins are 0.5mm to 2mm in width, planar with minor irregularity with local gangue of opaque oxides that appear to be magnetite (Fig. 4). 1-2% opaques throughout section that have resorption textures and oxidized rims of FeOx.



Sample ID: Q13B
MDRU ID: GAP-QT-1019-DM-013B
Rock type: Syenite
Alteration: Intense chlorite-muscovite
Sulfide:

UTM NAD 83 Z10
UTM North: 6079115
UTM East: 431309
Lat: 54.8544
Long: -124.0700

Rock Description:
Massive, medium-grained crystalline syenite with 2-3mm crystals and phenocrysts of plagioclase, quartz, and amphibole.



PETROGRAPHY

Preparation Thin Section Polished Thin Section Polished Slab

Scanned section images:



Billet Scan



Polished Thin Section



Crossed-Polarized Light (XPL)

Thin Section Summary:

Rock Type: Syenite

Lithochemistry notes: SiO₂ - 59.7%, Al₂O₃ - 19.53% Fe₂O₃ - 3.87%, CaO - 2.93, MgO - 0.46, K₂O - 6.81

Sulfide:

Magnetic Susceptibility average: 6.40

SWIR Assemblage: Chlorite-Muscovite

Thin section description:

Medium- to coarse-grained equigranular texture of strongly altered feldspar grains with 3-5% strongly to intensely chlorite altered amphibole phenocrysts (Figs. 1-4). Section cut by parallel <0.5 to 1mm planar muscovite veinlets. Chlorite and FeOx common along edge of muscovite veinlets. Amphiboles completely altered to chlorite with internal texture destruction but outline of amphibole grains remain.



Sample ID: Q14
MDRU ID: GAP-QT-1019-DM-014
Rock type: Volcanic mudstone
Alteration: Chlorite
Sulfide: pyrite veins

UTM NAD 83 Z10
UTM North: 5890076
UTM East: 542375
Lat: 53.1584
Long: -122.3663

Rock Description:
Very fine-grained black to dark brown volcanic mudstone.



PETROGRAPHY

Preparation Thin Section Polished Thin Section Polished Slab

Scanned section images:



Billet Scan



Polished Thin Section



Crossed-Polarized Light (XPL)

Thin Section Summary:

Rock Type: Volcanic mudstone
Lithochemistry notes: SiO₂ - 63.0%, Fe₂O₃ - 6.28%, CaO - 3.25, MgO - 3.59,
Sulfide: pyrite veins
Magnetic Susceptibility average: 0.32
SWIR Assemblage: Chlorite

Thin section description:

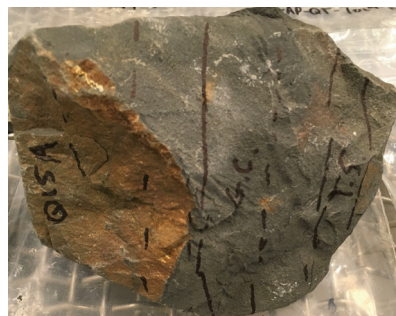
Very fine-grained banded dark brown to light grey granular texture with grains of feldspar, quartz, glass, and fine clasts locally chlorite altered (Figs 1-3). Fine irregular sulfide veinlets cut banding and are dominantly pyrite (Figs 1, 3-4), with very rare very-fine grained disseminated sulfide, opaques in groundmass primarily magnetite and FeOx. Fracture fill of silica also present in section (Fig. 2).



Sample ID: Q15A
MDRU ID: GAP-QT-1019-DM-015
Rock type: Volcanic sediment
Alteration: Chlorite
Sulfide: rare pyrite

UTM NAD 83 Z10
UTM North: 5888194
UTM East: 543250
Lat: 53.1414
Long: -122.3534

Rock Description:
Very-fine grained dark black sedimentary rock, thinly bedded.



PETROGRAPHY

Preparation Thin Section Polished Thin Section Polished Slab

Scanned section images:



Billet Scan



Polished Thin Section



Crossed-Polarized Light (XPL)

Thin Section Summary:

Rock Type: Volcanic sediment
Lithochemistry notes: SiO₂ - 56.1%, Fe₂O₃ - 6.86%, TOT/S - 0.23%
Sulfide: rare pyrite
Magnetic Susceptibility average: 0.41
SWIR Assemblage: Chlorite

Thin section description:

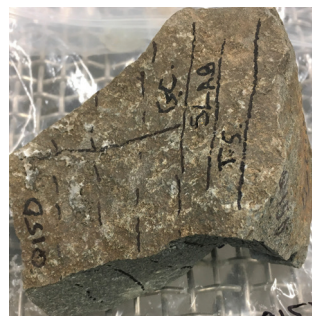
Very fine-grained granular texture of quartz, feldspar, chlorite and FeOx (Fig. 1). 10-12% chlorite, 25-30% oxides. Local micro-fractures of sulfide only presence of pyrite in section (Figs. 2-3).



Sample ID: Q15D
MDRU ID: GAP-QT-1019-DM-015D
Rock type: Monzonite
Alteration: Chlorite-muscovite
Sulfide: Pyrite Chalcopyrite

UTM NAD 83 Z10
UTM North: 5888194
UTM East: 543250
Lat: 53.1414
Long: -122.3534

Rock Description:
Massive dark grey crystalline monzonite with 1mm grains of plagioclase, amphibole, quartz, and rare pyroxene phenocrysts. 2-3mm long amphibole (5%).



PETROGRAPHY

Preparation Thin Section Polished Thin Section Polished Slab

Scanned section images:



Billet Scan



Polished Thin Section



Crossed-Polarized Light (XPL)

Thin Section Summary:

Rock Type: Monzonite
Lithochemistry notes: SiO₂ - 56.6%, Al₂O₃ - 17.75% Fe₂O₃ - 5.69%, CaO - 6.03, TOT/S - 0.26%, SO₃ - 0.357
Sulfide: Pyrite Chalcopyrite
Magnetic Susceptibility average: 0.58
SWIR Assemblage: Chlorite-Prehnite-Paragonite

Thin section description:

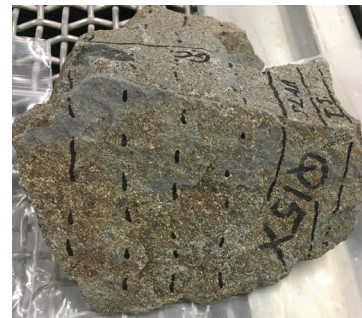
Medium-grained equigranular texture with local porphyritic coarser amphibole and biotite phenocrysts (Figs. 1-2). Feldspar groundmass altered to white-mica/clay with weak chlorite-hematite alteration of mafic phenocrysts. Accessory grains of apatite-titanite and other silicates are common (Fig. 3-4). 1-2% disseminated sulfide occurs as <1mm amorphous to blocky grains of pyrite with finer-grained chalcopyrite (Figs 5-6). Cu does not show up in lithochem.



Sample ID: Q15X
MDRU ID: GAP-QT-1019-DM-015X
Rock type: Monzonite
Alteration: Chlorite-sericite
Sulfide: rare pyrite

UTM NAD 83 Z10
UTM North: 5888194
UTM East: 543250
Lat: 53.1414
Long: -122.3534

Rock Description:
Massive medium-grained crystalline monzonite with plagioclase, amphibole, biotite, and quartz phenocrysts <1mm.



PETROGRAPHY

Preparation Thin Section Polished Thin Section Polished Slab

Scanned section images:



Billet Scan



Polished Thin Section



Crossed-Polarized Light (XPL)

Thin Section Summary:

Rock Type: Monzonite
Lithochemistry notes: SiO₂ - 57.9%, Al₂O₃ - 18.12% Fe₂O₃ - 5.32%, CaO - 5.5,
Sulfide: rare pyrite
Magnetic Susceptibility average: 0.23
SWIR Assemblage: Prehnite-Chlorite-Paragonite

Thin section description:

Medium-grained porphyritic texture of strongly altered feldspar and weak to moderately chloritized mafic phenocrysts in very fine-grained quartzofeldspathic groundmass (Fig. 1). Veins and fractures of muscovite-white mica are planar to moderately irregular <1mm in width and may contain clay and prehnite (Fig. 2-3). Iron oxidation (5-8%) is common and occurs primarily as hematite grains and rims along mafic grains and in clotty zones of silicates and chlorite (Figs. 3-6). Feldspar texture mainly destroyed but mafic grains still prominent.



Sample ID: Q16
MDRU ID: GAP-QT-1019-DM-016
Rock type: Monzonite
Alteration: Chlorite
Sulfide: None

UTM NAD 83 Z10
UTM North: 5875164
UTM East: 546469
Lat: 53.0240
Long: -122.3072

Rock Description:
Crystalline monzonite with plagioclase and amphibole phenocrysts 2-3mm. Chloritization of mafic phe-nocrysts.



PETROGRAPHY

Preparation Thin Section Polished Thin Section Polished Slab

Scanned section images:



Billet Scan



Polished Thin Section



Crossed-Polarized Light (XPL)

Thin Section Summary:

Rock Type: Monzonite
Lithochemistry notes: SiO₂ - 55.9%, Al₂O₃ - 18.0% Fe₂O₃ - 7.39%, CaO - 5.48, Na₂O - 5.96,
Sulfide: None
Magnetic Susceptibility average: 35.50
SWIR Assemblage: Prehnite-Chlorite

Thin section description:

Medium- to coarse-grained equigranular texture with weak to moderate chlorite alteration of mafic phenocrysts and strong chloritization in groundmass (Figs. 1, 3-4). Feldspars retain texture locally with weak to moderate seritization. Magnetite-ilmenite occur as disseminated grains (2-4%) with weak oxidation a (Figs. 2, 5). Primary biotite present <1% as fine grains with weak to moderate chlorite alteration.



Sample ID: Q18
MDRU ID: GAP-QT-1019-DM-018
Rock type: Volcanic sediment
Alteration: Quartz-carbonate-chlorite
Sulfide: None

UTM NAD 83 Z10
UTM North: 5878335
UTM East: 554247
Lat: 53.0518
Long: -122.1907

Rock Description:
Very fine-grained massive dark black volcanic sediment with fractures of carbonate and silica fill.



PETROGRAPHY

Preparation Thin Section Polished Thin Section Polished Slab

Scanned section images:



Billet Scan



Polished Thin Section



Crossed-Polarized Light (XPL)

Thin Section Summary:
Rock Type: Volcanic sediment
Lithochemistry notes: SiO₂ - 64.8%, Fe₂O₃ - 3.56%, CaO - 7.72, TOT/C - 0.51%
Sulfide: None
Magnetic Susceptibility average: 0.16
SWIR Assemblage: Chlorite

Thin section description:
Very fine-grained clastic groundmass with fracture and vein fill of carbonate (Fig. 1) and silica-white mica (Fig. 2). Groundmass is mottled with chlorite and white mica alteration of original material and local clotty zones of FeOx (Fig. 3-4). White-mica, clay, and other silicates occur as gangue in quartz veins with FeOx-white mica occurring along vein selvages of <1mm (Figs. 5-6). Carbonate appears to be late and fills open space in silicate veins and small vugs.



Sample ID: Q19A
MDRU ID: GAP-QT-1019-DM-019A
Rock type: Syenite
Alteration: Chlorite-White Mica
Sulfide: rare pyrite

UTM NAD 83 Z10
UTM North: 5877230
UTM East: 550290
Lat: 53.0422
Long: -122.2499

Rock Description:
Grey fine-grained syenite with quartz-rich matrix and 1-4mm amphibole phenocrysts.



PETROGRAPHY

Preparation Thin Section Polished Thin Section Polished Slab

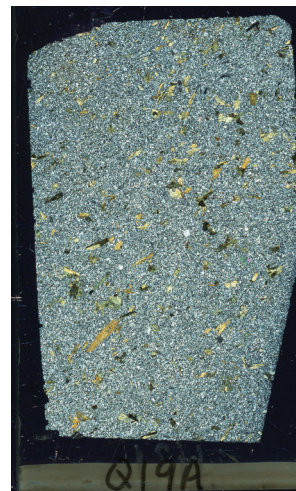
Scanned section images:



Billet Scan



Polished Thin Section



Crossed-Polarized Light (XPL)

Thin Section Summary:

Rock Type: Syenite
Lithochemistry notes: SiO₂ - 59.7%, Al₂O₃ - 17.99% Fe₂O₃ - 5.36%, CaO - 2.18, Na₂O - 7.43,
Sulfide: rare pyrite
Magnetic Susceptibility average: 0.21
SWIR Assemblage: Chlorite-Illite

Thin section description:

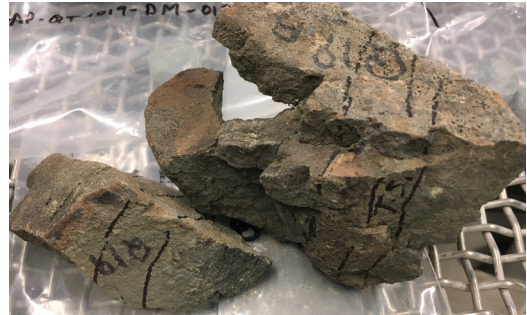
Fine-grained equigranular quartz-feldspar-amphibole groundmass with 3-5% porphyritic amphibole phenocrysts (Figs. 1-3). Very weak to weak chlorite-white mica alteration of mafic phenocrysts with hematite oxidation along cleavage planes and disseminated sulfide (Figs. 3-6). Accessory grains of apatite present.



Sample ID: Q19B
MDRU ID: GAP-QT-1019-DM-019B
Rock type: Andalucite Hornfels?
Alteration: Biotite-chlorite-carbonate
Sulfide: None

UTM NAD 83 Z10
UTM North: 5877230
UTM East: 550290
Lat: 53.0422
Long: -122.2499

Rock Description:
Very dark black to green massive very fine-grained crystalline rock. Dense with <0.5mm crystals and fractures of carbonate.



PETROGRAPHY

Preparation Thin Section Polished Thin Section Polished Slab

Scanned section images:



Billet Scan



Polished Thin Section



Crossed-Polarized Light (XPL)

Thin Section Summary:

Rock Type: Andalucite Hornfels?
Lithochemistry notes: Not Analyzed
Sulfide: None
Magnetic Susceptibility average: 0.94
SWIR Assemblage: N/A

Thin section description:

Fine- to medium-grained clast supported hornfels texture with biotite-chlorite matrix (Fig. 1). Grains of andalusite are hexagonal and are 0.25 to 1mm in width (Figs. 1-5). Biotite is dominant in groundmass with clay-FeOx and weak chlorite replacement, biotite is amorphous and infills between silicate clasts. Carbonate occurs as vug fill and coarse fracture fill (Figs. 1-3).



Sample ID: Q20
MDRU ID: GAP-QT-1019-DM-020
Rock type: Monzogabbro
Alteration: Biotite-sericite
Sulfide: Pyrite

UTM NAD 83 Z10
UTM North: 5881353
UTM East: 540905
Lat: 53.0801
Long: -122.3894

Rock Description:
Green to brown strongly weathered crystalline monzogabbro with phenocrysts of feldspar, olivine and pyroxene.



PETROGRAPHY

Preparation Thin Section Polished Thin Section Polished Slab

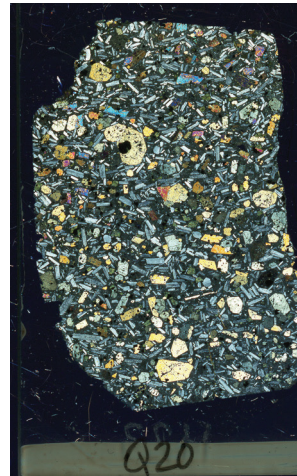
Scanned section images:



Billet Scan



Polished Thin Section



Crossed-Polarized Light (XPL)

Thin Section Summary:

Rock Type: Monzogabbro
Lithochemistry notes: SiO₂ - 48.9%, Fe₂O₃ - 13.24%, CaO - 6.3, MgO - 5.22, Na₂O - 4.56,
Sulfide: Pyrite
Magnetic Susceptibility average: 94.40
SWIR Assemblage: Spectral

Thin section description:

Porphyritic olivine monzogabbro with coarse phenocrysts of feldspar (35-40%), olivine (15-20%) and pyroxene (3-5%) in an aphanitic dark grey to brown biotite groundmass (Figs. 1-2). Local pockets of completely biotitized phenocrysts occur with biotite growing into fracture planes of olivine and clinopyroxene phenocrysts. Feldspars moderately to strongly sericitized. Sulfide (pyrite) occur as disseminated <3mm rounded grains in groundmass and with olivine/pyroxene phenocrysts (Fig. 2-3).



Sample ID: Q21
MDRU ID: GAP-QT-1019-DM-021
Rock type: Volcanic sediment
Alteration: White mica-epidote
Sulfide: rare pyrite

UTM NAD 83 Z10
UTM North: 5968765
UTM East: 514216
Lat: 53.8672
Long: -122.7838

Rock Description:
Very fine-grained dark grey to black volcanic sediment with thin bedding. Local epidote along fracture surfaces.



PETROGRAPHY

Preparation Thin Section Polished Thin Section Polished Slab

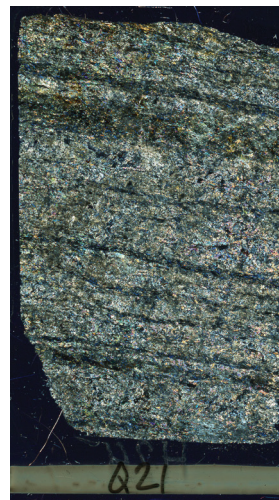
Scanned section images:



Billet Scan



Polished Thin Section



Crossed-Polarized Light (XPL)

Thin Section Summary:

Rock Type: Volcanic sediment

Lithochemistry notes: SiO₂ - 48.8%, Fe₂O₃ - 4.66%, CaO - 15.92, MgO - 4.7, LOI - 6.67%, TOT/C - 3.47%, H₂O - 4.96%

Sulfide: rare pyrite

Magnetic Susceptibility average: 0.10

SWIR Assemblage: Spectral

Thin section description:

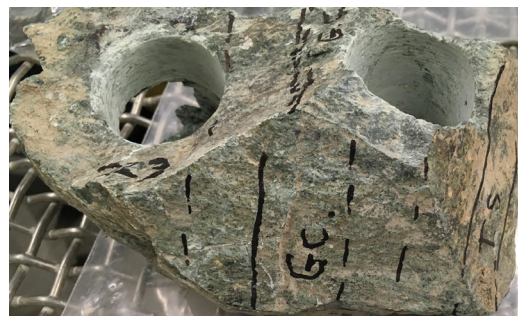
Strongly sheared, oxidized and altered rock with light to dark fine grained texture of biotite, epidote, white mica, clay and iron oxides (Figs. 1-4). Carbonate common as cement in matrix with biotite and oxides (Fig. 4). Sulfide occurs as rare blocky grains with FeOx, hematite/jarosite dominant over goethite (Fig. 4-5). Remnant sulfide <0.5%. High LOI and H₂O in lithochem suggests intense alteration of original sediment.



Sample ID: Q23
MDRU ID: GAP-QT-1019-DM-023
Rock type: Volcanic sediment
Alteration: Chlorite
Sulfide: None

UTM NAD 83 Z10
UTM North: 5977725
UTM East: 510018
Lat: 53.9478
Long: -122.8474

Rock Description:
Moderately to strongly foliated greenschist with strong chlorite-sericite alteration. Originally a tuff(?) with dark, chlorite-altered, flattened clasts.



PETROGRAPHY

Preparation Thin Section Polished Thin Section Polished Slab

Scanned section images:



Billet Scan



Polished Thin Section



Crossed-Polarized Light (XPL)

Thin Section Summary:

Rock Type: Volcanic sediment
Lithochemistry notes: SiO₂ - 49.2%, Fe₂O₃ - 9.96%, CaO - 8.55, MgO - 12.68,
Sulfide: None
Magnetic Susceptibility average: 0.45
SWIR Assemblage: Hornblende-Chlorite

Thin section description:

Strong to intense chlorite altered schistoic rock with elongate to rounded clay-chlorite altered clasts in very-fine grained dark brown foliated matrix (Figs. 1-6). Chlorite massive to fibrous in clasts with clay and locally epidote ± titanite forming within elongate clasts. Brown FeOx occurs within matrix and along edges of clasts. Clasts are rotated and resorbed along edges with fibrous to acicular clay and white mica forming large internal crystals radiating from centralized points. Clasts make up 35-40% of section with local coarser white mica/feldspar zones within darker foliated matrix.

APPENDIX 2: MAGNETIC INVERSION METHODOLOGY

Devin C. Cowan

The University of British Columbia

July 26, 2021

1. Data Compilation for Magnetic Inversion

The data compiled for this project included:

- Topography with a spacing of 100 m;
- Natural Resources Canada (NRCan) 200 m grid Residual Total Field (RTF) magnetic data (Natural Resources Canada, 2020);
- British Columbia 61-1 Total Magnetic Intensity (TMI) magnetic data (Natural Resources Canada, 1962); original survey data that makes up a component of the above compilation, with a line spacing of ~800 m and a slight direction along the Northing;
- Overburden thickness inferred from the interpretation of stitched 1D inversion of airborne VTEM data (detailed in main report). The overburden thickness is defined at all sites in this study.

The inducing field parameters used were appropriate for the center of the survey area (longitude 123°13'30" W and latitude 54°17'39" N), with data having been processed assuming a uniform field on the date 15th of September 2007. The inducing field does not vary more than one degree within the survey area, therefore a single direction for the inducing field was a reasonable assumption.

2. Upward Continuation for Basement Inversion

A basement model was first recovered from upward continued magnetic data to guide local-scale magnetic inversion models. The goal was to upward continue the data such that it would contain only regional-scale features. We began with Natural Resources Canada 200 m magnetic data grid (Figure 1, Natural Resources Canada, 2020). In this step, we:

- Extracted the NRCan RTF data and topography lying within an extended area of interest (20 km outside the original region of interest);
- Rotated the NRCan magnetic data and topography into a local coordinate system;
- Re-gridded the NRCan magnetic data to a uniform spacing of 200 m;
- Upward continued the data to 4000 m and 8000 m (Figure 2), with an assumed uniform flight height of 305 m;
- Down-sampled the upward continued data to a minimum distance of 2500 m; and
- Extracted the upward continued data within the true area of interest and used the topography to assign elevations to the data with an assumed flight height of 8000 m.

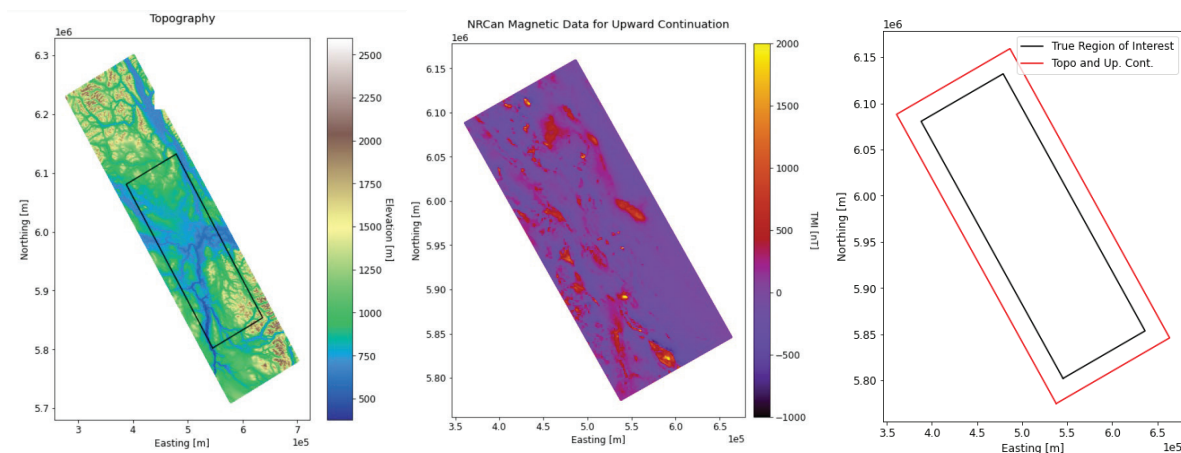


Figure 1. Topography with area of interest marked (left). Processed NRCan 200 m magnetic data (Natural Resources Canada, 2020, middle). Region of interest and extended region used to crop topography and NRCan data (right).

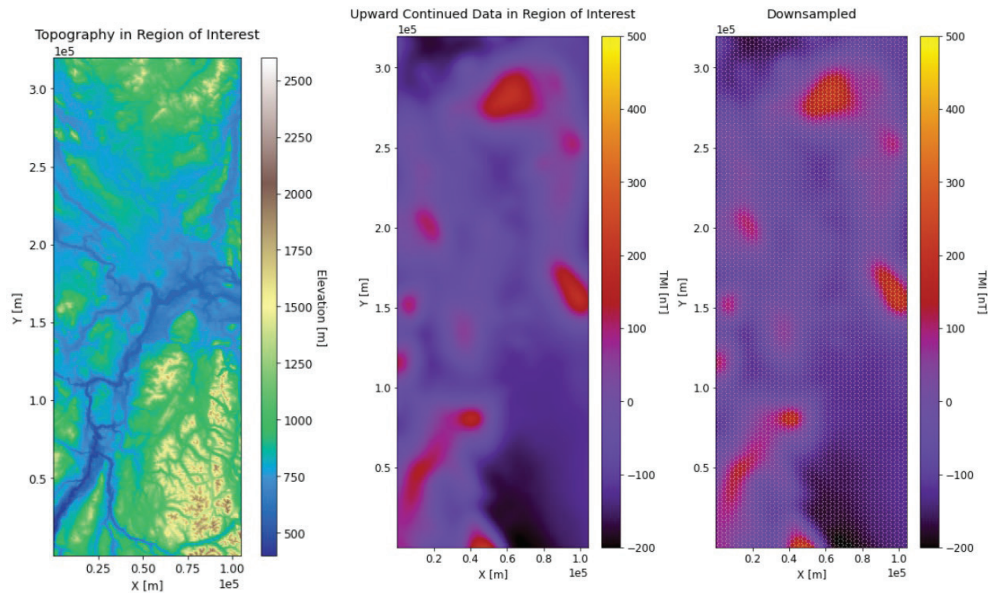


Figure 2. Topography in region of interest (left). Upward continued NRCan 200 m grid magnetic data, upward continued to 8000 m height (middle). Upward continued data down-sampled to 2500 m (right).

3. Basement Models

For basement model inversions (Figure 3), we used the upward continued data at 4000 m and 8000 m gridded uniformly with a spacing of 200 m. Inversion codes from SimPEG (Cockett et al., 2015) were used for modelling. Different objective functions, or regularization functions, which control the character of the model, were applied to explore model outcomes (Figure 3).

- The choice in regularization (L0, L1, L2) used to recover the basement model had little to no impact on the shape and magnitude of the predicted data at the actual receiver locations.
- Upward continued data at 4000 m still contained some frequency content on the scale of local magnetic anomalies for some sites. Upward continuing to 8000 m ensured a true basement model containing only large-scale regional trends.
- Ultimately, we chose the L1 basement model from data upward continued to 8000 m.

4. Data Preparation for Local Site Inversions

TMI data, topography, and overburden thickness data were extracted and prepared for site inversions (Figure 4).

For the magnetic data, we:

- Extracted the observed B.C. 61-1 TMI magnetic data (Natural Resources Canada, 1962) within the local target site (example in Figure 5);
- Down-sampled the magnetic data to a minimum distance of 200 m;
- From the site geometry, determined the boundaries of the local OcTree mesh that would be used for inversion (this is discussed in the local site inversion section), “scooped” this portion out of the basement model and forward modelled at the corresponding data to determine the ‘external’ contribution; and
- Subtracted the background (“external”) contribution from the original data (Figure 6).

For the topography and overburden thickness, we:

- Extracted the topography and overburden thickness within an extended area (extended 1500 m outside the area of interest); and

- Interpolated the overburden thickness data to the locations defining local topography, then subtracted those values to obtain a surface layer defining the bottom of the overburden.

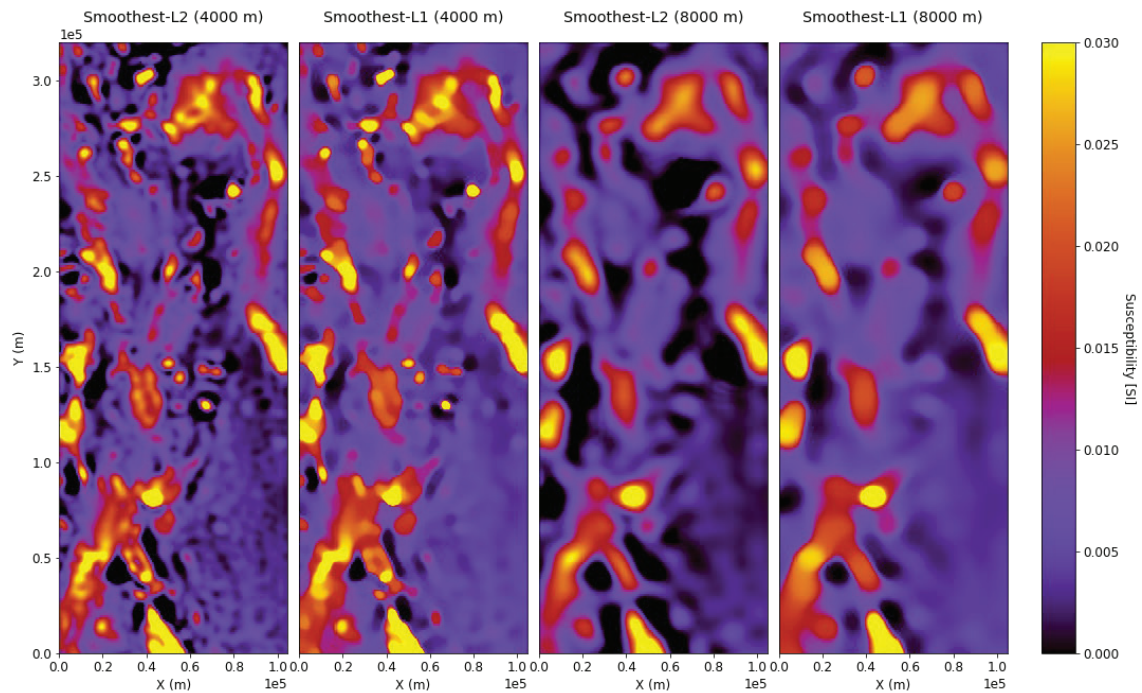


Figure 3. Basement models in the area of interest for different regularizations and upward continuation heights in the rotated coordinate system.

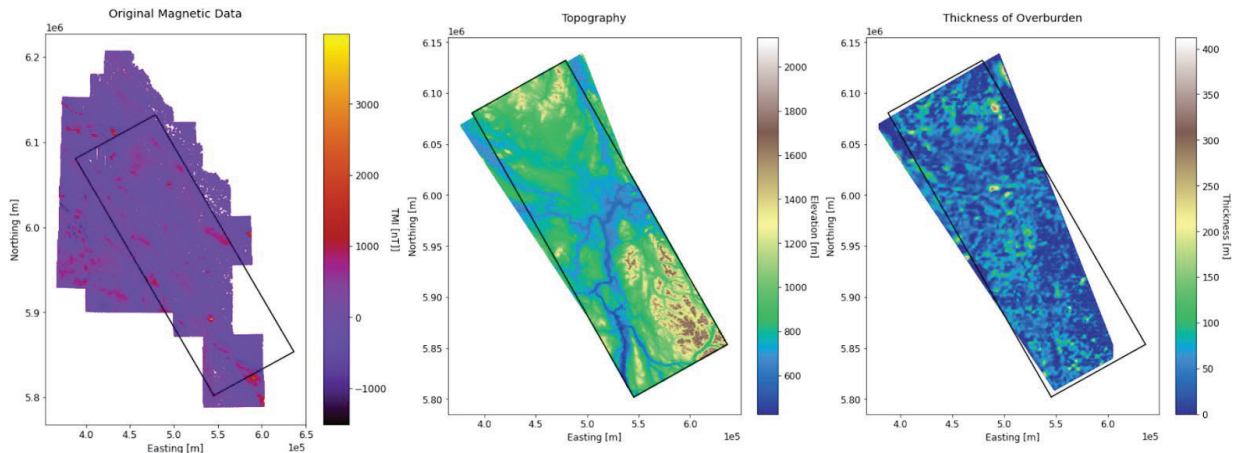


Figure 4. Total Magnetic Intensity (TMI) magnetic data (left, Natural Resources Canada, 1962), topography (middle) and overburden thickness inferred from stitched 1D TEM inversion (right).

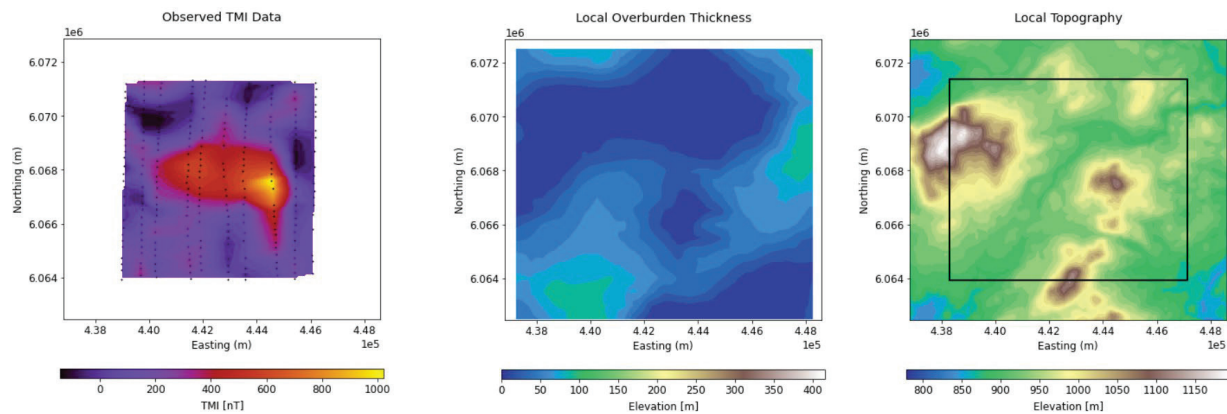


Figure 5. Down-sampled magnetic data within example local site (left); extracted overburden thickness used for local inversion (middle); and topography used for local inversion (right).

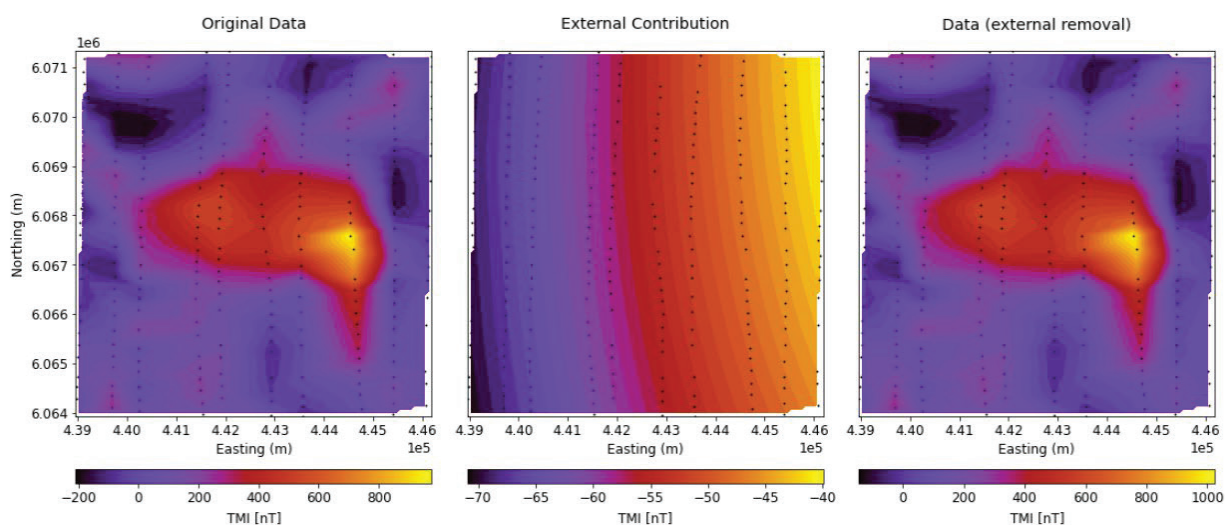


Figure 6. Original magnetic data at example local site (left); external contribution from regional basement model (middle); and local magnetic data used for local site inversion (right).

5. Local Site Inversions

To avoid the cumbersome task of manually setting up and running inversions at each local target site, we created an automated process. The automated process was responsible for constructing an OcTree mesh based on the local survey geometry, assigning uncertainties to the data, and inverting the data with various regularizations in order to explore the model space.

Uncertainties of 2 nT were assigned to the data for all local site inversions. This value was obtained by manually inverting the data at several sites before creating the automation process. By assigning a floor, as opposed to a percent, we avoided fitting the background at the expense of fitting magnetic anomalies.

For each local OcTree mesh, the smallest horizontal cell size was obtained by dividing the width of the local site by 100, with a minimum and maximum allowable size of 40 m and 100 m, respectively. The smallest vertical cell size was fixed at 40 m. With padding, every OcTree mesh extended to a minimum of 10 km in all directions from the region of interest.

For both the reference and recovered models, we assume the susceptibility of overburden is 0 SI. As a result, only the cells below the surface defining the bottom of the overburden (obtained in section 4) are active in the inversion. The reference model was created by interpolating the L1 basement model (see section 3) to all active inversion cells in the local OcTree mesh.

Data were inverted for 5 different regularizations. The regularization can be defined by the following model objective function:

Eq1.

$$\phi(\mathbf{m}) = \alpha_s \left\| \mathbf{W}_s(\mathbf{m} - \mathbf{m}_{\text{ref}}) \right\|^p + \alpha_x \left\| \mathbf{W}_x \mathbf{m} \right\|^{q_x} + \alpha_y \left\| \mathbf{W}_y \mathbf{m} \right\|^{q_y} + \alpha_z \left\| \mathbf{W}_z \mathbf{m} \right\|^{q_z}$$

where p , q_x , q_y and q_z define the norm of the smallness and smoothness terms, and the α parameters define the relative impact of the smallness and smoothness terms on the recovered model. Note that in SimPEG, the \mathbf{W} matrices have been normalized such that the impact of the smallness and smoothness terms is equal when all α parameters are set to 1.

The regularizations used at every local target site are tabulated in Table 1. Preliminary inversions performed manually showed that a 1-norm on the smoothness terms recovered structures that were ideal for interpretation; using an L2-norm recovered structures that were excessively smooth and difficult to interpret.

Table 1. Regularizations for target sites

Name	$\alpha_s, \alpha_x, \alpha_y, \alpha_z$	p, q_x, q_y, q_z
Unconstrained_Smooth_L1	1e-10, 1, 1, 1	1, 1, 1, 1
Modestly_Constrained_L2_L1_L1_L1	0.1, 1, 1, 1	2, 1, 1, 1
Modestly_Constrained_L1_L1_L1_L1	0.1, 1, 1, 1	1, 1, 1, 1
Equally_Constrained_L2_L1_L1_L1	1, 1, 1, 1	2, 1, 1, 1
Equally_Constrained_L1_L1_L1_L1	1, 1, 1, 1	1, 1, 1, 1

In the *Unconstrained_Smooth_L1* inversion, the smallness term is negligible and the inversion is purely driven by the data; i.e. not constrained by the reference model. For the *Modestly_Constrained* inversions, we wanted to include the reference model. However we are not sure how well the reference model characterizes the background at this scale. We do not want to aggressively constrain the inversion with the reference model in this case. As a result, we set $\alpha_s = 0.1$, effectively setting the impact of the smallness term to be one 10th of the impact of each of the smoothness terms. For the *Equally_Constrained* inversions, we set all alpha parameters to 1, effectively setting the smallness and smoothness terms to have equal impact on the inversion. For inversions constrained by the reference model, we inverted using both an L1 and an L2-norm on the smallness. This was done in order to recover models with both smooth and more compact structures.

6. Evaluation of Automated Inversion Results and Manually Reruns of Target Site Locations

At each site, the convergence curves (examples in figures 7 and 8) and misfit maps were used to evaluate the uncertainties applied to the data for automated inversion. If the data were globally overfit/underfit, or if certain regions of the misfit maps were significantly overfit/underfit compared other regions, the inversion was re-run with a manually specified set of uncertainties.

The locations and dimensions of structures in the recovered models at each site were also evaluated (example in figures 9 and 10). If recovered structures clearly extended into the padding cells, the inversion was re-run using a manually constructed OcTree mesh with a deeper core mesh region. And if recovered structures were clustered near the surface, the inversion was re-run with an OcTree mesh with finer discretization near the surface.

For each local target site, we have tabulated a simple assessment of the quality of the automated inversion results (Tables 2, 3, and 4). And in the final column, we state the parameters in the script that were altered to produce the manual inversion results that will be used for interpretation. In no instances were the regularization parameters of the inversion changed.

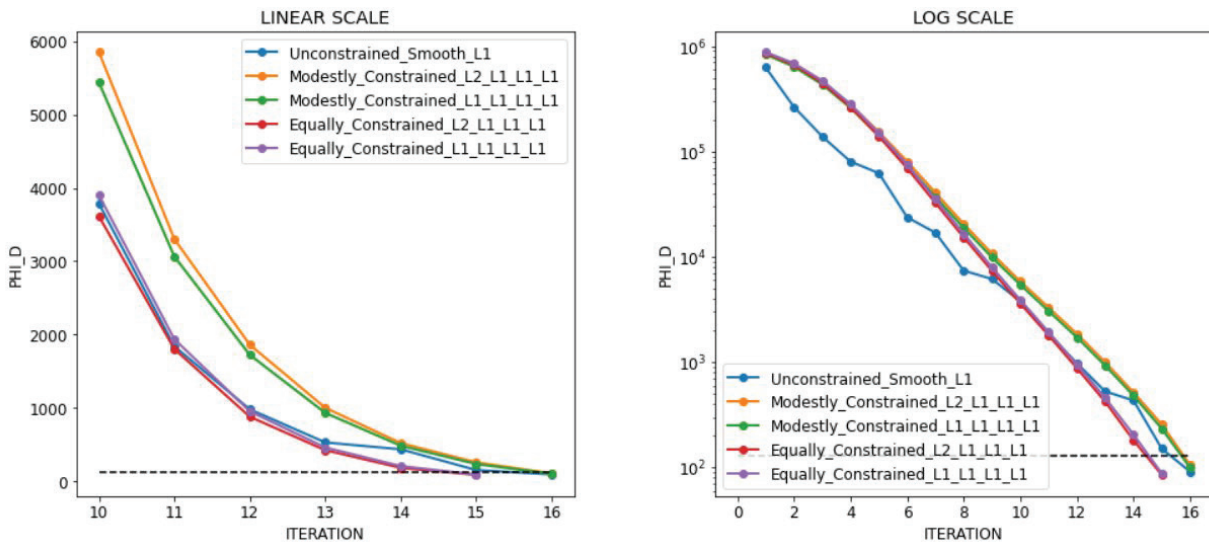


Figure 7. Linear convergence during L2 as we approach target misfit (left). Log-scale convergence during L2 (right).

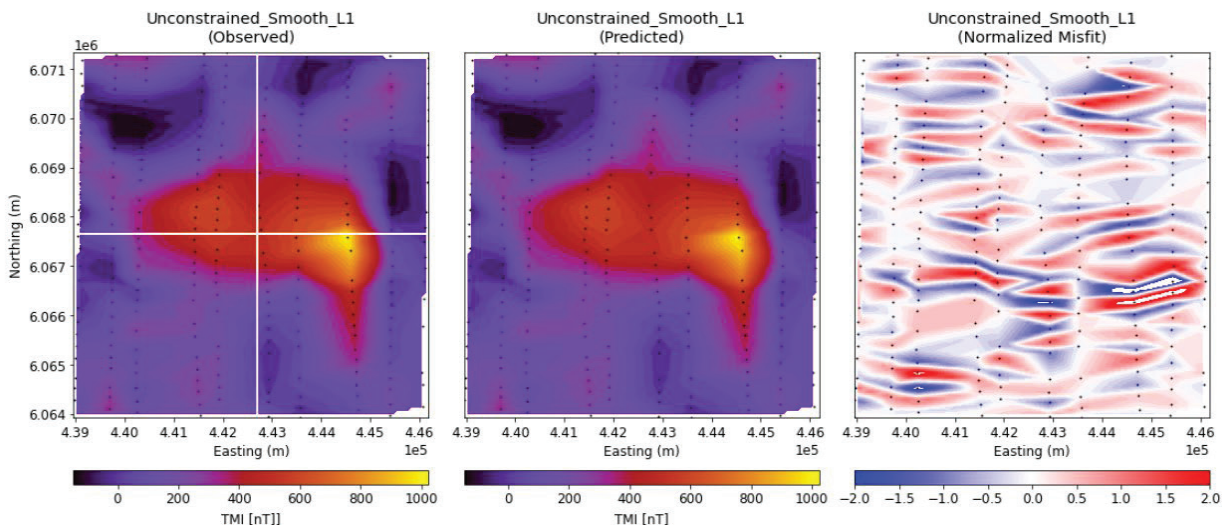


Figure 8. Observed (left), predicted (middle) and normalized misfit (right) for unconstrained inversion at example local site.

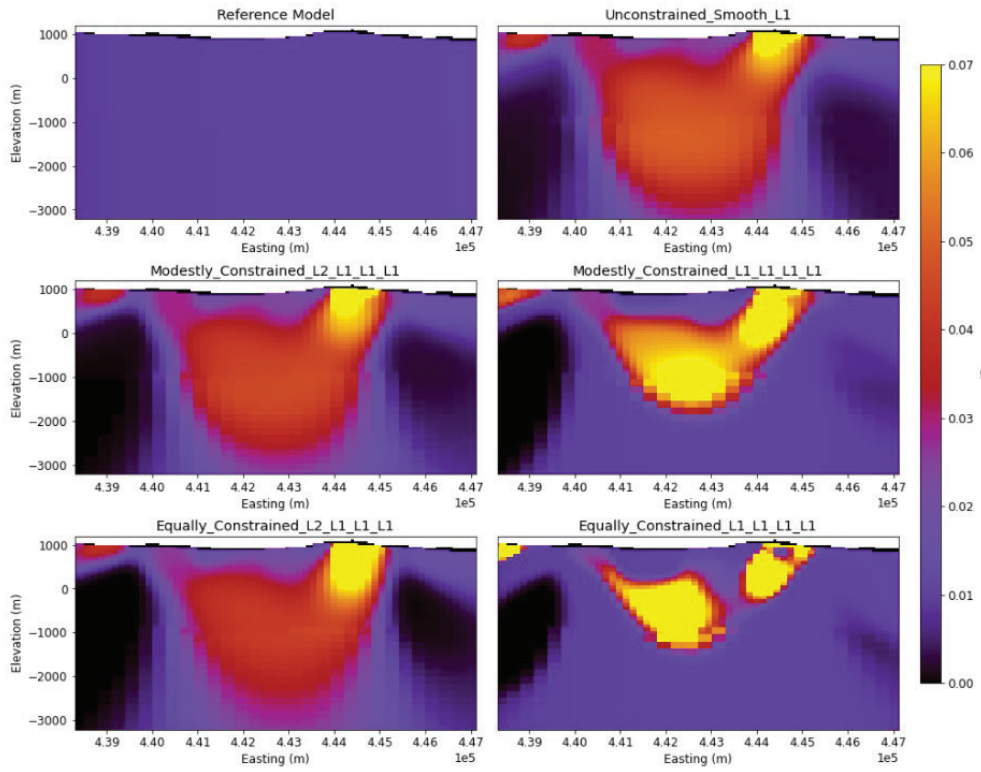


Figure 9. Local magnetic inversion sections along the Easting for example site in Figure 8.

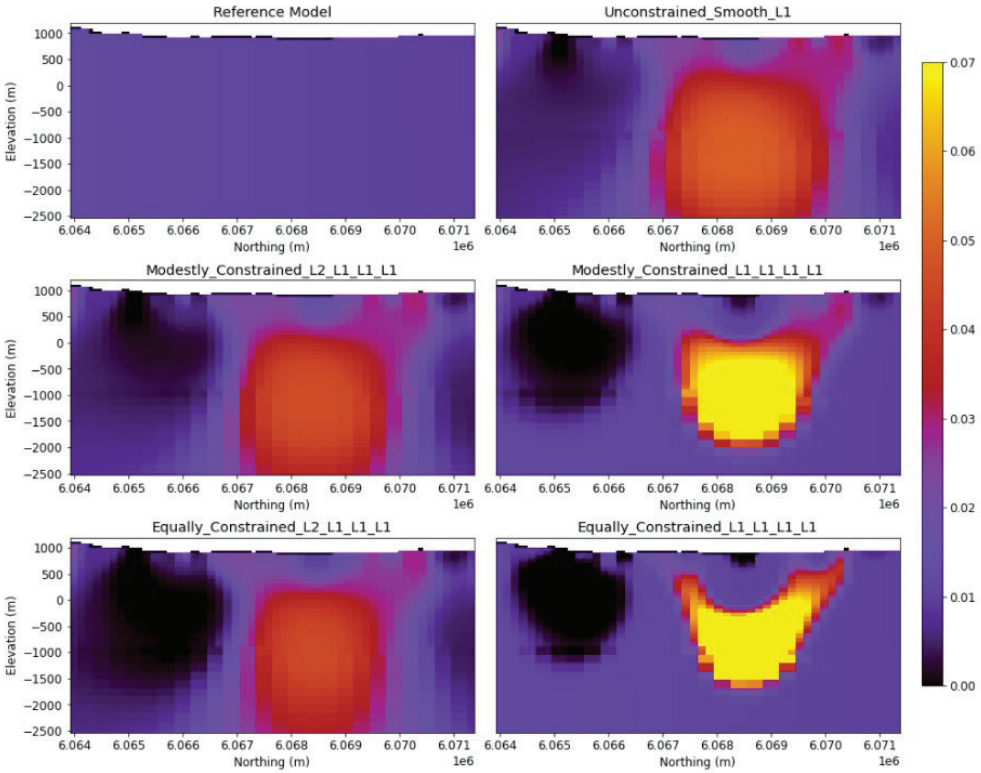


Figure 10. Local magnetic inversion sections along the Northing for example site in Figure 8.

Table 2. Inversion Summary, Fort St. James Block

Site	Convergence	Data Misfit	Recovered Models	Rerun?
FSJ-1	Convergence does not flatten out	Good		
FSJ-2	Flattens out before target misfit. Overfit?	Some higher misfits correlated with anomaly. Overfitting background slightly	Mild artifacts at cell size increase. Compact near surface structure	Re-run with: n_cells_topo=8 n_cells_core=[0, 12, 12] floor_unc_0 = 5 nT floor_unc_1 = 2.5 nT
FSJ-3	Hits target misfit at the 'elbow'	Good		
FSJ-4	Takes a while to reach target misfit Also flattens out before target. Overfit? Remanence?	Some regions of higher misfit. Not necessarily correlated with the anomaly	At first glance it had higher susceptibility ~0.1 but still looked quite plausible.	
FSJ-5	Convergence does not flatten out	Good (sparse data coverage)	Data coverage for this site is sparse. Probably not well-constrained by data	
FSJ-6	Most convergences look good, but imperfect for some regularizations	Good (sparse data coverage)	Data coverage for this site is sparse. Probably not well-constrained by data	
FSJ-7	Reaches target misfit as curve is flattening out but possibly slightly overfit	Good but slightly overfitting background		
FSJ-8	Takes a while to reach target misfit, doesn't really flatten	Not completely unstructured	At first glance it had higher susceptibility ~0.1 but still looked quite plausible.	
FSJ-9	Flattens out just before reaches target	Some highly localized areas of high misfit. Clear lower misfits in background region	Mild artifacts at cell size increase. Significant near surface structures	Re-run with: n_cells_topo=8 n_cells_core=[0, 12, 12] Specialize uncertainties
FSJ-10	Convergence does not flatten out	Good	Not an isolated anomaly so not sure how constrained by data	
FSJ-11	Good	Good		

Site	Convergence	Data Misfit	Recovered Models	Rerun?
FSJ-12	Convergence does not flatten out	Clear higher misfits over a very compact anomaly	Very isolated, near surface structure.	Re-run with: n_cells_topo=8 n_cells_core=[0,12,12] floor_unc_0=2 floor_unc_1=0.25
FSJ-13	Convergence does not flatten out	Good		
FSJ-14	Convergence does not flatten out	Good but slightly overfit background		Re-run with: n_cells_topo=8 n_cells_core=[0,12,12] floor_unc_0=3 floor_unc_1=1.5
FSJ-15	Convergence does not flatten out	Good but slightly overfit background	Minimal artifacts at cell size increase	
FSJ-16	Convergence does not flatten out	Good but slightly overfit background		

Table 3. Inversion Summary, Prince George Block

Site	Convergence	Data Misfit	Recovered Models	Rerun?
PG-1	Moderately good	Overfit background	Good	Re-run with: n_cells_topo=8 n_cells_core=[0,12,12] floor_unc_0=2.5 floor_unc_1=1
PG-2	Flattens out slightly before target misfit	Good	Good but structures more shallow than default discretization	
PG-3	Good	Barely overfitting background but not concerning	Good	
PG-4	Good	Good	Good	
PG-5	Good	A line of high misfits due to flight lines that are close together	Small artifact associated with overfitting. Dominant feature seems to be shallow.	Re-run with: n_cells_topo=8 n_cells_core=[0,12,12] floor_unc_0=4.5 floor_unc_1=1.5
PG-6	Good	Overfitting background slightly but it's not excessive	Good	
PG-7	Good	Overfitting where data coverage is sparse and underfitting anomaly slightly	Good	
PG-8	Good	Alright	Not isolated anomaly. Unsure if improved by rerunning	
PG-9	Pretty good	Obviously underfitting the small compact anomaly	Recovered body shallower than default discretization.	Re-run with: n_cells_topo=8 n_cells_core=[0,12,12] floor_unc_0=3 floor_unc_1=1
PG-10	Good, except for unconstrained	Clear underfit region near North end		Re-run with: n_cells_topo=8 n_cells_core=[0,12,12] floor_unc_0=2.5 floor_unc_1=1

Site	Convergence	Data Misfit	Recovered Models	Rerun?
PG-11	Possibly overfit	Overfitting background	Shallower than default discretization. Mild artifacts from overfitting	Re-run with: n_cells_topo=8 n_cells_core=[0,12,12] floor_unc_0=3 floor_unc_1=1
PG-12	Good	Moderately underfitting around anomaly for some regularizations	Good	
PG-13	Good	Clearly overfit background		Re-run with: n_cells_topo=8 n_cells_core=[0,12,12] floor_unc_0=4 floor_unc_1=1
PG-14	Good	Overfit region	Major structure extending to surface	Re-run with: n_cells_topo=8 n_cells_core=[0,12,12] floor_unc_0=2 floor_unc_1=1
PG-15	Good	A slightly overfit region where data coverage is sparse. Not overly concerning	Good	
PG-16	Good	Slightly overfit at edges of AOI	Good	
PG-17	Overfit; flattens out before target	Regions of high misfit. Overfit where data coverage is sparse	Some artifacts due to overfitting. Anomaly extending to surface	Re-run with: n_cells_topo=8 n_cells_core=[0,12,12] floor_unc_0=6 floor_unc_1=2
PG-18	Good	Underfit near anomaly	Near surface structure that extends to surface	Re-run with: n_cells_topo=8 n_cells_core=[0,12,12] Custom uncertainties

Table 4. Inversion Summary, Quesnel Block

Site	Convergence	Data Misfit	Recovered Models	Rerun?
Q-1	Good	Good	Anomaly not fully covered by data. Not sure how well constrained structure is	
Q-2	Good	Satisfactory	Good	
Q-3	Good	Notable region of higher misfits	Big structure that extends to surface	Re-run with: n_cells_topo=8 n_cells_core=[0,12,12] floor_unc_0=3 floor_unc_1=1
Q-4	Good	Good	Extends to surface but good shape	
Q-5	Good	Good	Good	
Q-6	Good except unconstrained	Good	Good	
Q-7	Good	Good	Deep and low amplitude.	
Q-8	Good	Isolated higher misfits right over peak anomaly but it's not that bad	Structure extends to from depth all the way to surface	Re-run with: n_cells_topo=8 n_cells_core=[0,12,12] floor_unc_0=2.5 floor_unc_1=1
Q-9	Good	Good	Good	
Q-10	Good	Acceptable	Good	
Q-11	Pretty good	Obvious regions of higher misfit near anomaly	Structure does extend to surface	Re-run with: n_cells_topo=8 n_cells_core=[0,12,12] floor_unc_0=3 floor_unc_1=1
Q-12	Good	Good	Slightest overfit artifact in compact norm results	
Q-13	Good	Highest misfits toward the easting	Good	
Q-14	Good	Clear isolated high misfits over peak anomaly	Compact near-surface structure extending to surface	Re-run with: n_cells_topo=8 n_cells_core=[0,12,12] floor_unc_0=3 floor_unc_1=1

Site	Convergence	Data Misfit	Recovered Models	Rerun?
Q-15	Possibly starting to flatten out slightly	Good	No major overfitting artifacts	
Q-16	Good	Not bad	Good	
Q-17	Starts to flatten out but not smoothly before hitting target	Good	No major overfitting artifacts.	
Q-18	Good	Isolated higher misfits right over peak anomaly	Compact structure at surface with possible deeper structure	Re-run with: n_cells_topo=8 n_cells_core=[0,12,12] floor_unc_0=3 floor_unc_1=1
Q-19	Good	1 uncorrelated data point with a higher misfit.	Good	
Q-20	Good	Not bad	Not a high amplitude structure compared to background	Re-run with: n_cells_topo=8 n_cells_core=[0,12,12] floor_unc_0=3 floor_unc_1=1
Q-21	Good	Higher misfits over a compact anomaly	Likely at surface. Not a lot of data for this site	
Q-22	N/A	N/A	N/A	N/A
Q-23	Good	Possibly some regions of higher misfit but not too bad	Interesting anomaly	Re-run with: n_cells_topo=4 n_cells_core=[0,8,12] floor_unc_0=3 floor_unc_1=1

7. References

- Cockett, R., Kang, S., Heagy, L. J., Pidlisecky, A., and Oldenburg, D. W. (2015): SimPEG: An open source framework for simulation and gradient based parameter estimation in geophysical applications. *Computers & Geosciences*, 85, 142-154. DOI: [10.1016/j.cageo.2015.09.015](https://doi.org/10.1016/j.cageo.2015.09.015)
- Natural Resources Canada (2020): Canada 200 magnetic data compilation, residual total field data, Canadian Airborne Geophysical Data Base; Airborne Geophysics Section, Geological Survey of Canada, Lands and Minerals Sector, Natural Resources Canada, URL <<http://gdr.agg.nrcan.gc.ca/gdrdap/dap/search-eng.php>> [October 2019].
- Natural Resources Canada (1962): British Columbia - 61-1 total field magnetic data, Canadian Airborne Geophysical Data Base; Airborne Geophysics Section, Geological Survey of Canada, Lands and Minerals Sector, Natural Resources Canada, URL <<http://gdr.agg.nrcan.gc.ca/gdrdap/dap/search-eng.php>> [March 2021].

APPENDIX 3: GRAVITY INVERSION METHODOLOGY

Thibaut Astic, Ph.D.

The University of British Columbia

August 5, 2021

1. Summary

We performed Tikhonov (least-squares) and Sparse inversions of the QUEST airborne gravity survey at various scales for the area of interest. Regional equivalent layer inversions were run, with coverage over most of the surveyed area. Smaller-scale (on the order of several km) sites corresponding with the suite of magnetic targets were investigated, but the resolution of the Bouguer data was not suitable to resolve near-surface features at this scale. Instead, a regional scale inversion was supplemented with 3-D information through completion of intermediate-scale inversions. The survey was divided into four blocks with lengths ~ 100 km, and inverted in 3-D.

2. Data

This report focuses on the process used to invert the gravity data acquired during an airborne gravity survey collected as part of the Geoscience BC QUEST program in British Columbia. The data were acquired in 2008 by Sander Geophysics Limited (2008) using their AIRGrav system.

The line spacing of this survey is 2,000 m with a nominal flight height of 200 m (but an average flight height of 300 m). We have focused our effort on a subsection, delimited by the black outline in Figure 1.

In all the following inversions, we chose to work with the isostatically corrected and filtered Bouguer anomaly (named "ISOBGL3.5" in the original database; see the original survey report for more details on data corrections; Sander Geophysics Ltd., 2008).

For the regional- and intermediate-scale inversions (sections 3 and 6, respectively), the rectangular area of interest outlined in black in Figure 1 was used to define the local coordinates system along its axis.

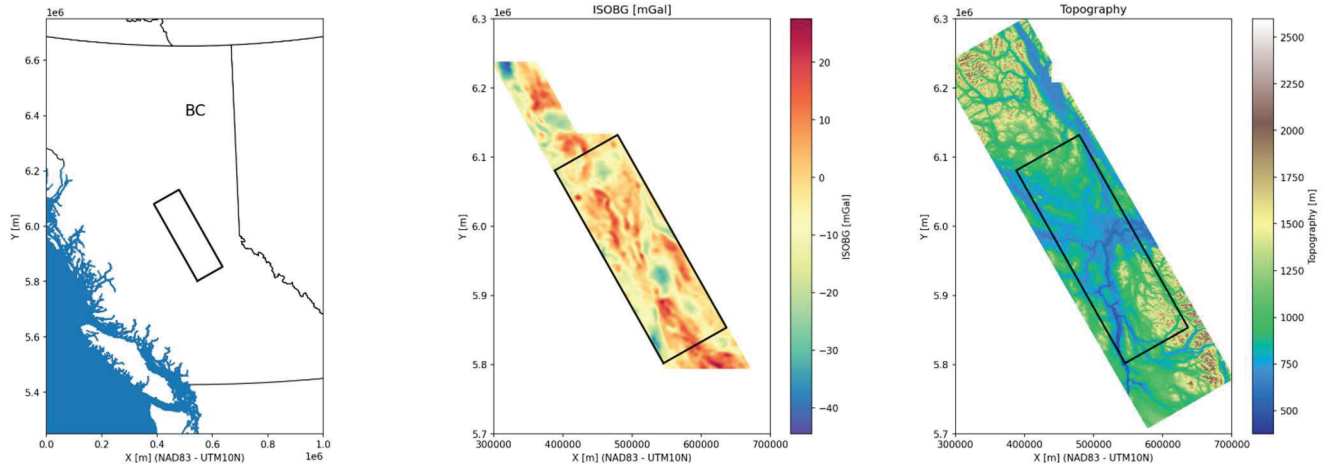


Figure 1. Area of Interest (black outline) (left); gravity data (middle); and topography within the AOI (right).

3. Regional Inversions

We performed equivalent layer inversions of the full gravity dataset using inversion code from SimPEG (Cockett et al., 2015). This type of inversion can be used to estimate the regional background density contrast and gravity signal.

3.1 Equivalent layer inversion

The regional inversions were performed using a flat, horizontal, Octree mesh draped over the topography. Two meshes were tested for the regional equivalent source: the first one with cells extending from the topographic surface to 0 m elevation (mean sea level; altitude = 0 m), and the second with cells extending down to -100 km elevation (approximately to the base of the crust). The equivalent layer inversions assume that the Earth is vertically homogeneous; the idea is similar to an equivalent source inversion.

The core of the Octree mesh is composed of square cells with a side length of 500 m. For the regularization, we ran multiple inversions spanning several combinations of norms for the smallness and smoothness terms (Fournier & Oldenburg, 2019; Oldenburg & Li, 2005).

We attempted a Free Air Anomaly inversion to recover “true” densities instead of density contrasts using the first mesh that extended from topography down to 0 m (sea level). This, unfortunately, was not successful. We assume the results were not successful because: (1) the Free Air Anomaly data is subject to a constant shift of value; (2) data processing did not allow recovery of this information (raw channels are too noisy to be exploitable, and processed channels have altered the data); and (3) we failed to take into account density variations within the geoid (elevations below 0 m).

We proceeded to complete the regional inversion using equivalent layer inversion and using the isostatically-corrected Bouguer anomaly data. Both meshes were tried, but ultimately the second was used where cells extend from topography down to -100 km (approximate base of crust).

3.2. Data preparation

To prepare for the regional inversion, the gravity data were rotated in a local coordinates system to obtain a rectangular area of interest aligned with the X and Y axes; this alignment improves our ability to grid and upward continue. We upward continued the data to an elevation of 2,000 m for visualization, and 8,000 m for regional removal purposes, and down sampled every 2,000 m. An elevation of 8,000 m preserves only the longest data wavelengths, which are important for regional signal removal. In Figure 2, we show inversion results for the gravity data with an upward continuation of 2,000 m, with inversion parameters described below. We assumed a uniform noise level of 0.1 mGal for the upward continued data. Associated misfit maps are shown in Figure 3.

3.3. Inversion parameters

In Figure 2, we show the outcomes of the regional inversions for several sets of parameters. All inversions share the following parameters:

- mesh: 500 m cells
- 2000 m data spacing
- 2000 m upward continuation
- inverting Bouguer anomaly, isostatically corrected
- assumed noise: 0.1 mGal
- local coordinate system
- total gradient regularization (Fournier and Oldenburg, 2019)
- $m_{ref} = m_{init} = 0$. g/cc (density contrast)
- lower and upper bounds: -1.5 and 1.5 g/cc

The differences between the various inversions are explained below:

- **LpLq- / Lq-** — Sparse regularization with both smallness with norm p and smoothness with norm q (as=ax=ay=1, auto-scaling) / Sparse regularization with smoothness only with norm q (as=0; ax=ay=1)
- **SensW / NoSensW** — with / without sensitivity weights

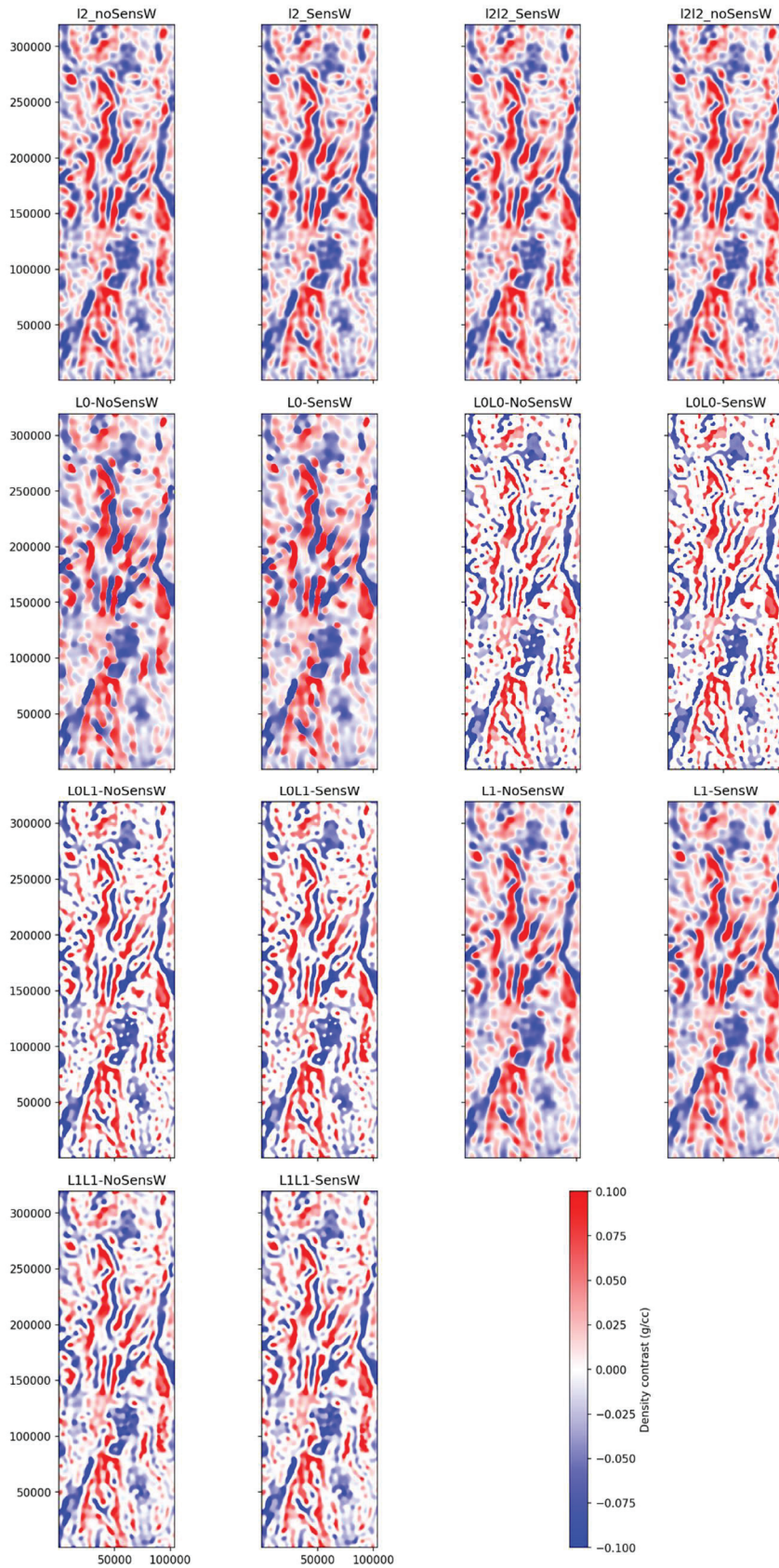


Figure 2. Results in local coordinates (see Fig. 1) from the gravity equivalent layer inversions with data upward continued at a height of 2,000 m and a mesh extending to -100 km elevation.

3.4. Results and discussion

The regional inversions were an efficient way to extract large density-contrast structures. The choice of regularization, mesh thickness, noise levels all impact the outcome, as described below:

- With a mesh extension down to 0 or –100 km depth, the models imaged the same structures; only the amplitude of the density-contrast values changed;
- We chose to use a noise level 0.1 mGal, which is below the instrument floor (0.5 mGal); the reasons are (1) upward continuation filters out the higher frequencies; and (2) data processing by the acquisition company had previously smoothed the data, but lower noise levels were required to constrain the final solution;
- Results weighted or not weighted by sensitivity do not differ significantly; as such, we recommend using the weighted models;
- With a goal of determining background, we prefer using a smoothness only model, like “L1-SensW”; the L0 regularizations are too influential on the model. Nevertheless, we judged it necessary to run inversions with smallness terms to assess its impact;
- In those inversions, the data misfit maps of the Sparse (LpLq) inversions are preferred, as they have fewer correlated signals than the Tikhonov (L2) inversions

Ultimately, we recommend using the model “L1-SensW” for this exercise.

3.5. Regional removal

In subsequent inversions, when a regional signal was removed at a “local” site, the process was:

1. take the observation locations of the local survey from which the regional signal is to be removed as well as remove its associated local mesh;
2. rotate this survey and local mesh in the local coordinates system;
3. remove the volume occupied by the mesh from the equivalent layer mesh; this is done by draping the top of the regional mesh to the bottom of the local mesh instead of to the topography;
4. forward the response of the regional density model with this modified regional mesh onto the rotated local survey locations;
5. remove this newly computed regional signal from the observations of the local survey; and finally
6. rotate back the local survey and mesh.

4. Local inversion investigations at FSJ sites 1 to 3

We now look at inversions in areas of a few km in length (local magnetic target sites) that are of interest for porphyry exploration (Fig. 4).

4.1. Data preparation

Data within the core areas of interest were selected and down sampled along lines to every 200 m.

At each site, the Octree mesh smallest cell size is $100 \times 100 \times 25$ m, which is reasonable for mapping topography and overburden. To minimize the size of the mesh, the cell size was gradually increased stepwise with depth.

Cells within the overburden were fixed at a density-contrast value of -0.27 g/cc, based on an assumed background density value of 2.67 g/cc (the value used to process the gravity data into a Bouguer anomaly), and an estimated density of 2.4 g/cc for the overburden material.

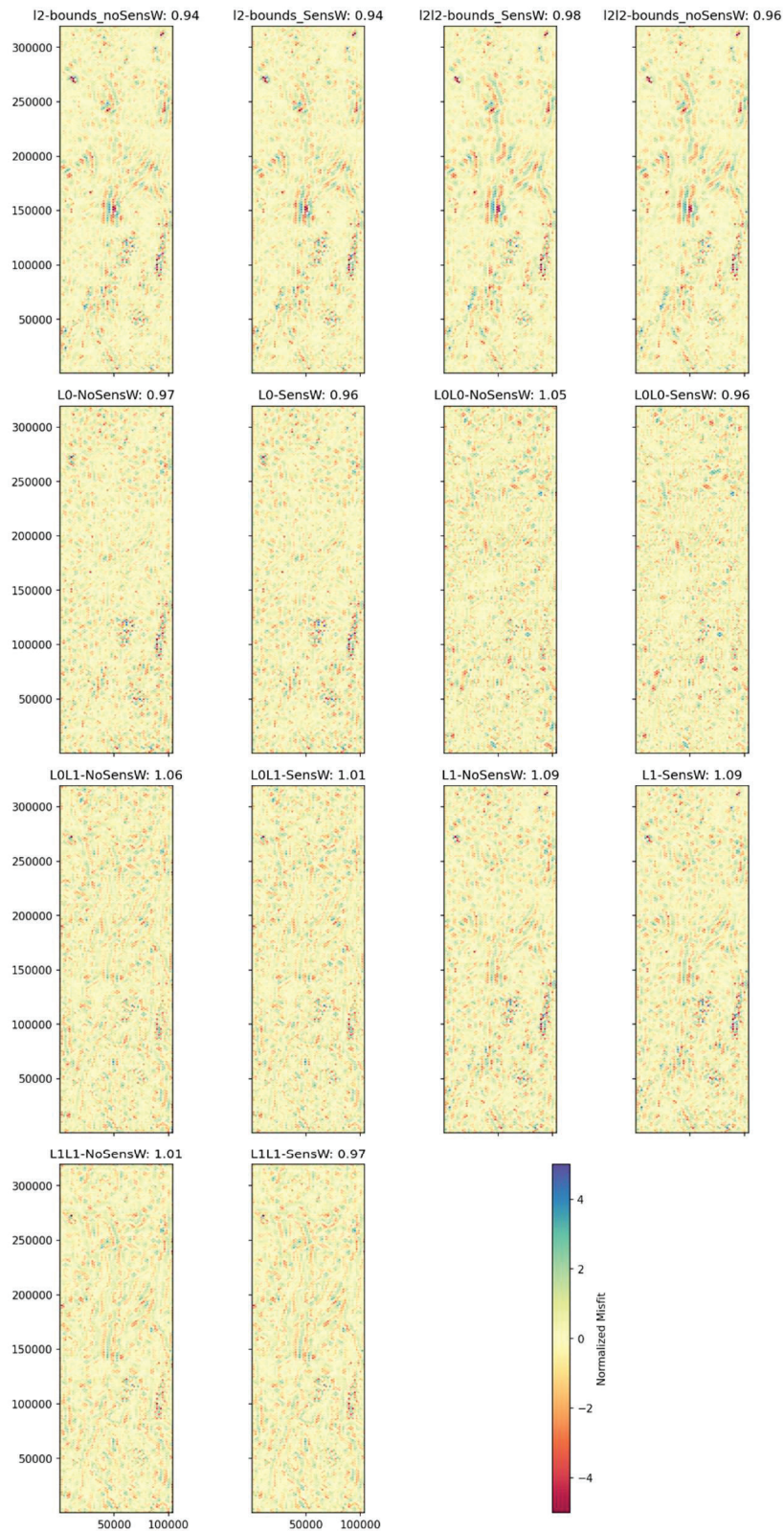


Figure 3. Normalized misfit maps in local coordinates (see Fig. 1) from the gravity equivalent layer inversions with data upward continued at a height of 2,000 m and a mesh extending to -100 km elevation. The number in the title indicates the global misfit (target of 1).

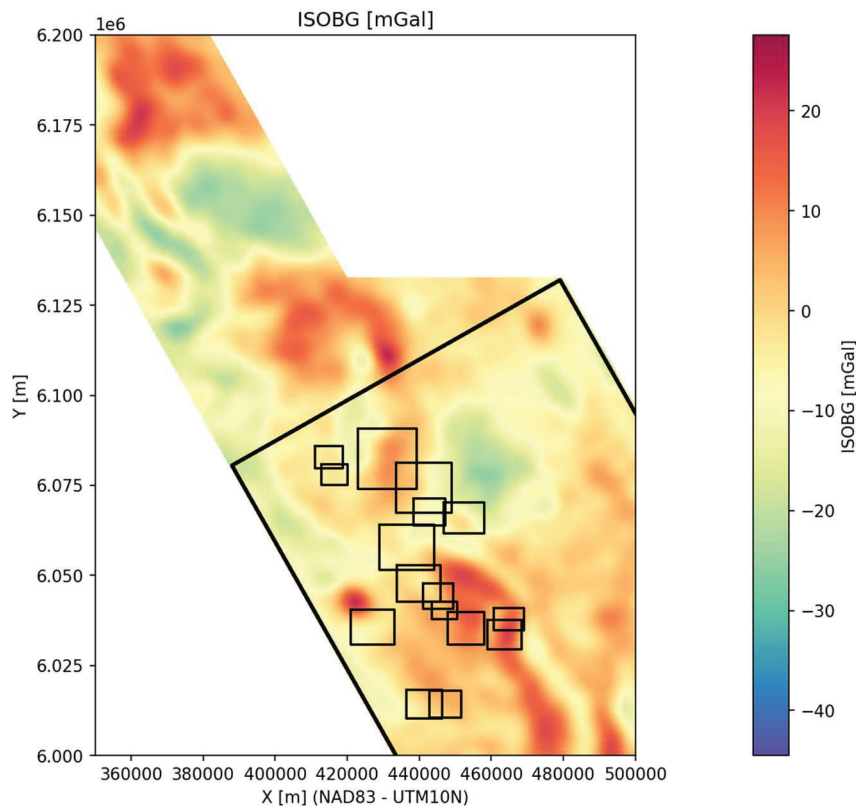


Figure 4. Fort St. James (FSJ) area sites locations.

4.2. Results

Despite multiple approaches, initial results could not extract meaningful 3-D information at the scale of the local targets, FSJ sites 1 to 3 (Figures 5 and 6). We tried inverting both the raw and residual (after regional removal) data, as well as inverting for various norms of regularizations and values of α s (from 0 to 1: 0 deactivates the term; 1 means it is as important as the smoothness terms).

Our assumption based on these early-stage inversions is that the high noise level of the instrument (0.5 mGal), along with the heavy processing inherent to airborne gravity data, have likely smoothed low-amplitude, high-frequency signals that would have been informative. To test that assessment, we evaluated site FSJ4, which shows a clear correlation with a positive gravity anomaly, and tried a systematic range of inversions. These results are reviewed in section 5 of this report.

Based on the conclusions at site FSJ4, we did not further investigate or revisit sites FSJ 1 to 3 in an attempt to try to extract higher resolution local-scale results; materials for these sites should still be considered at an early stage within the shared ZIP archive (section 8).

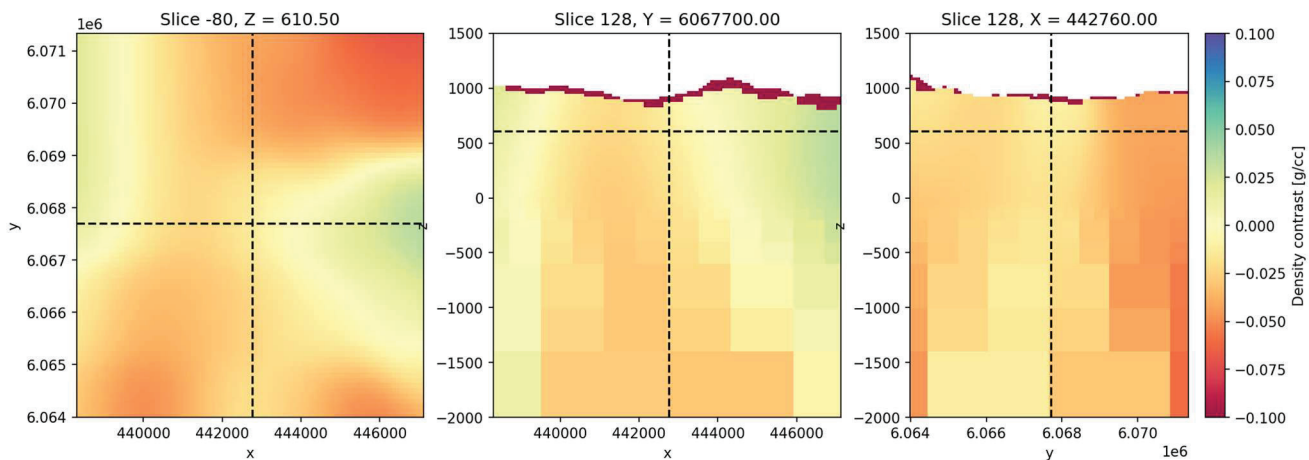


Figure 5. Smoothest inversion result at FSJ1 with L1 gradients, directly inverting for the raw Bouguer data without regional removal.

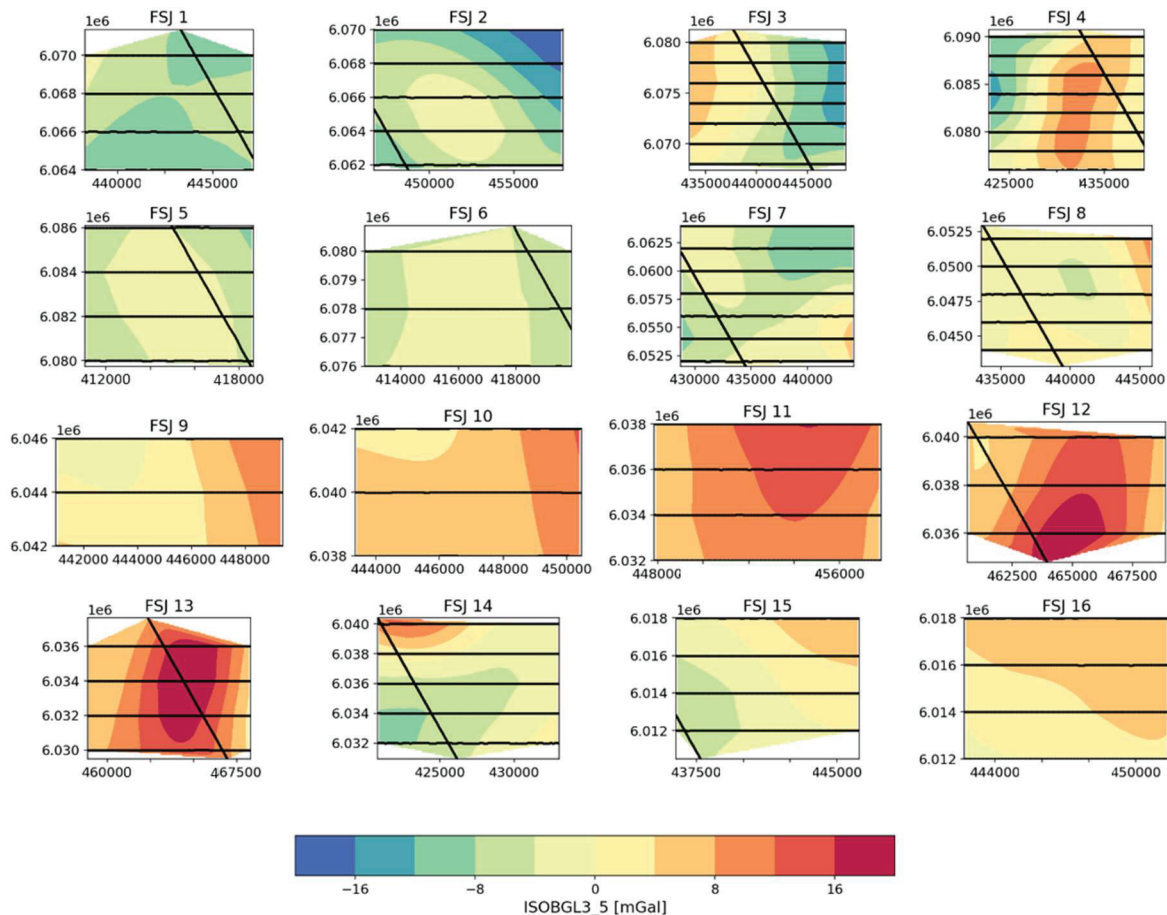


Figure 6. Bouguer anomalies at the various FSJ sites. All coordinates are in UTM 10N - NAD83.

5. Local inversion investigation at FSJ site 4

Since we were unable to model interpretable features at sites FSJ 1 to 3, we shifted our focus to site FSJ4, where gravity data exhibited a clear anomaly and had the smallest wavelength signals (Fig. 6).

5.1. Data preparation and mesh design

As previously conducted, data within the area of interest were selected and down sampled along lines to every 200 m. The noise level for the inversion was set at 0.5 mGal, the limit of the instrument. The Octree mesh smallest cell size was set to $200 \times 200 \times 25$ m, to reasonably map the topography and the overburden. To minimize the size of the mesh, the cell size gradually increases stepwise with depth.

Cells within the overburden were fixed as in the FSJ 1 to 3 sites inversions (section 4.1).

5.2. Inversion parameters

Each combination of the following parameters was run and is available through an interactive jupyter notebook under GravityInversions/FSJ4 inversions, file: *range jupyter/3 FSJ4 visualize all inversions.ipynb* (see Figure 7):

- various importances for the smallness term in the regularization α : 0, $1e-6$, and 1 (equal to the smoothness)
- inversion of: (1) the original down sampled data; or (2) the residual data, after removal of a background signal determined from the regional inversions (see section 3.5);
- reference model: (1) a uniform null half-space, or (2) the density model “L1-SensW” from regional inversion;
- For the smallness term norm: 2-norm, 1-norm, or 0-norm; and
- For the smooth term norm: 2-norm or 1-norm was used.

5.3. Results

These inversions confirmed that the information content of the gravity data did not permit recovery of interpretable results at the scale of the local target sites. The high noise threshold of the instruments (0.5 mGal) can mask signals from near-surface targets that are within a range of one to a few mGals or lower. Moreover, it is likely that the processing of the airborne gravity data removed all short wavelengths from the data; indeed, the gravity data at all sites are very smooth (Fig. 6).

6. Intermediate-scale inversions

In an attempt to recover 3-D information from the gravity survey after inversions were completed for the local target sites, we decomposed the full survey into four blocks of appropriate sizes for 3D inversion (Fig. 8). The blocks were defined based on the rotated local coordinates system, which facilitated rectangular blocks and simplified the design of the mesh. These inversions were not tiled inversions; instead, each block overlaps its neighboring blocks by 5,000 m.

6.1. Data preparation

The inversions were performed in the rotated local coordinates system, similar to the regional inversions (section 3). Data within each block were down sampled to 2,000 m. No regional signal was removed. The noise level was set to the instrument’s noise, 0.5 mGal, which is low, but previous investigation indicated that the data were smoothed significantly.

In [11]: plot_model_app()

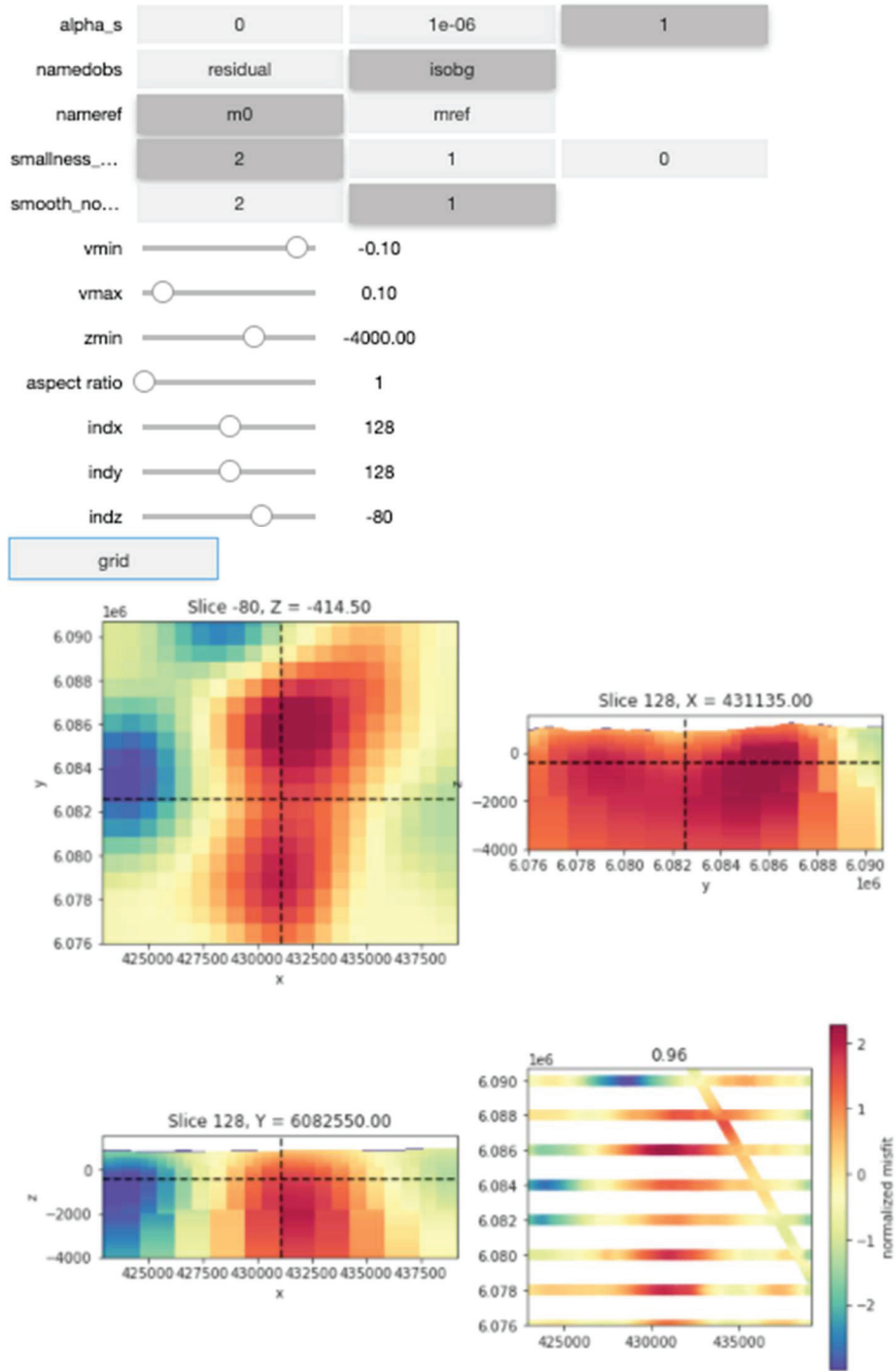


Figure 7. Interactive visualization tools depicting all inversions at FSJ4.

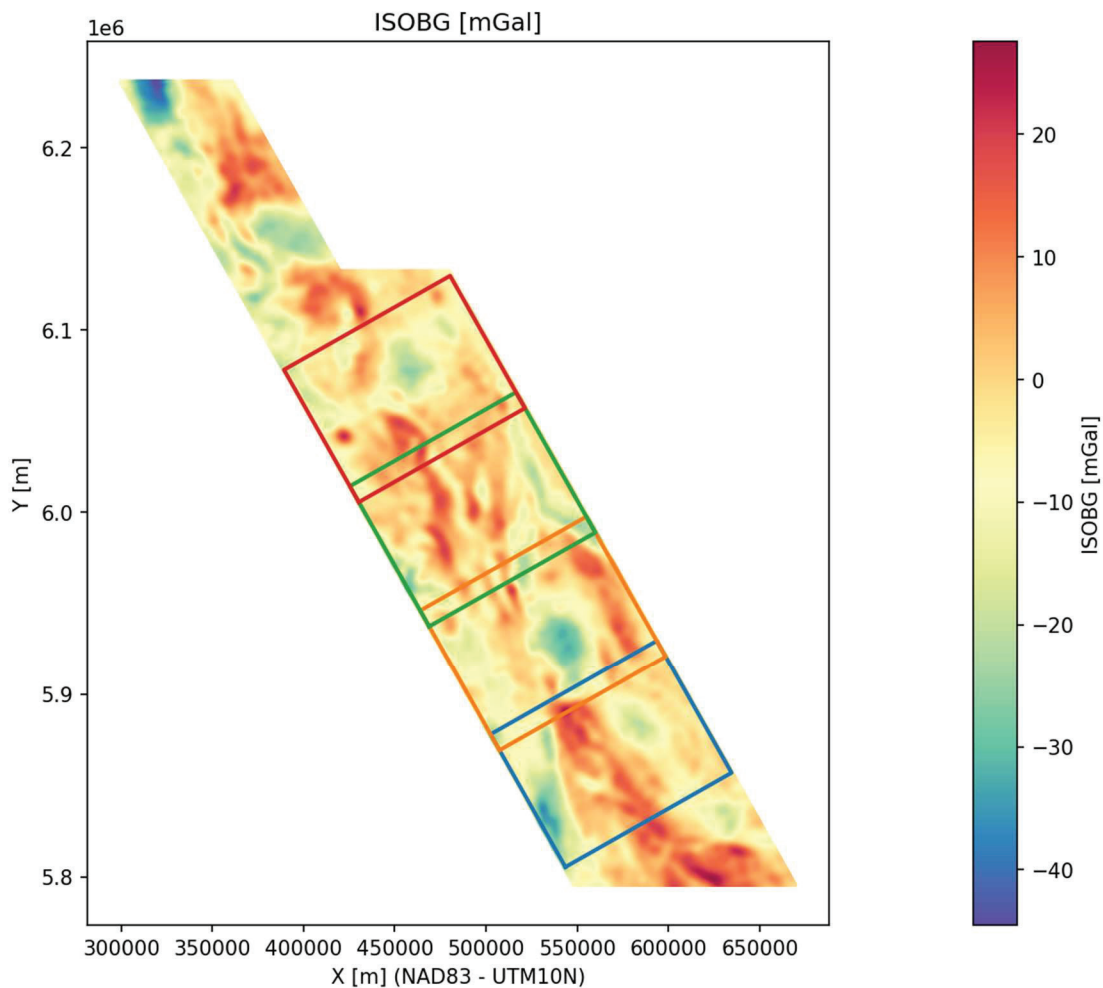


Figure 8. Locations of the intermediate-scale inversion blocks, showing overlap.

The Octree mesh smallest cells were $500 \times 500 \times 100$ m. The cell sizes increased stepwise with depth to minimize the size of the mesh. Cells within the overburden were fixed at -0.27 g/cc. Padding distance was equal to or greater than the core area length.

6.2. Inversion parameters

Based on the results of the equivalent layer inversions (section 3) and the inversions at FSJ4 (section 5), we chose to invert for the smoothest model (no smallness term), using both 2-norm and 1-norm for the smoothness norms.

6.3. Results

Each inversion is available for visualization through an interactive jupyter notebook under *GravityInversions/intermediate blocks inversion jupyter/2 intermediateBlocks visualize all inversions.ipynb* (Fig. 9). These inversions offer improved 3-D insights into the area, and align well with the regional layer inversions.

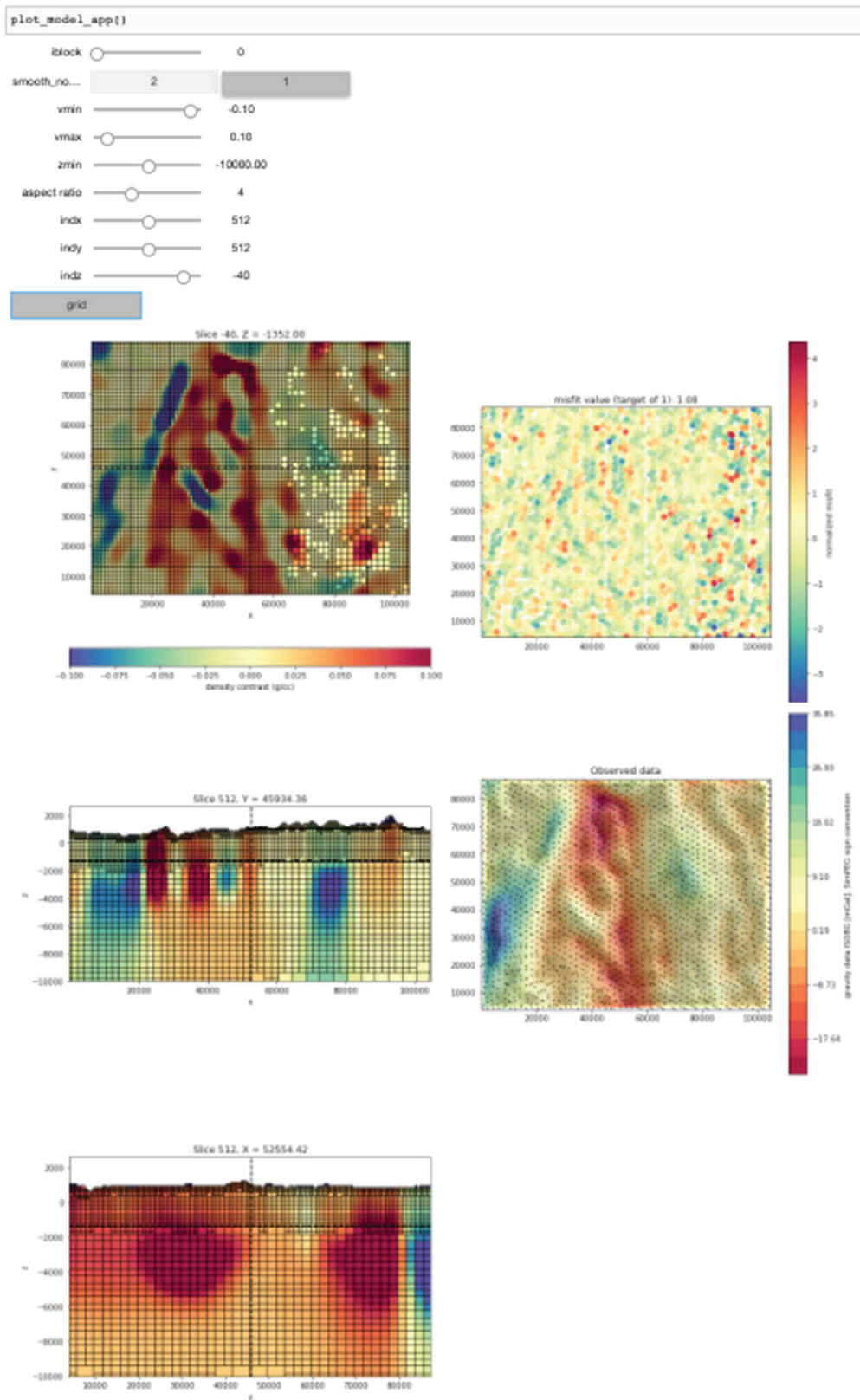


Figure 9. Interactive notebook to visualize the results of the intermediate scale inversions.

7. Conclusions

We performed Tikhonov and Sparse regional to local inversions of the QUEST airborne gravity datasets. We encountered challenges that are inherent to the survey, especially regarding the lack of high-frequency (less than 10 km) and low amplitude (less than a few mGal) signals. As such, localized targets in the study area (e.g. target areas FSJ1–3), chosen based on higher resolution magnetic surveys to support porphyry exploration, were not well-resolved from the gravity data. We instead focused on regional and intermediate-scale inversions, both equivalent layer and 3-D. The results showed coherent geologic structures, some of which match magnetic features of interest for porphyry exploration, albeit at a much lower resolution.

8. Deliverables

- Regional- and intermediate-scale inversions were imported into a Geoscience ANALYST project that is included in the deliverables package for this report (Fig. 10).
- The entirety of the work done for this project is shared in a ZIP archive named “*GravityInversions*”. This archive contains the results in various formats, including in UBC-GIF (Geophysical Inversion Facility)’s format for all observed and predicted data, recovered density contrast models, and meshes.

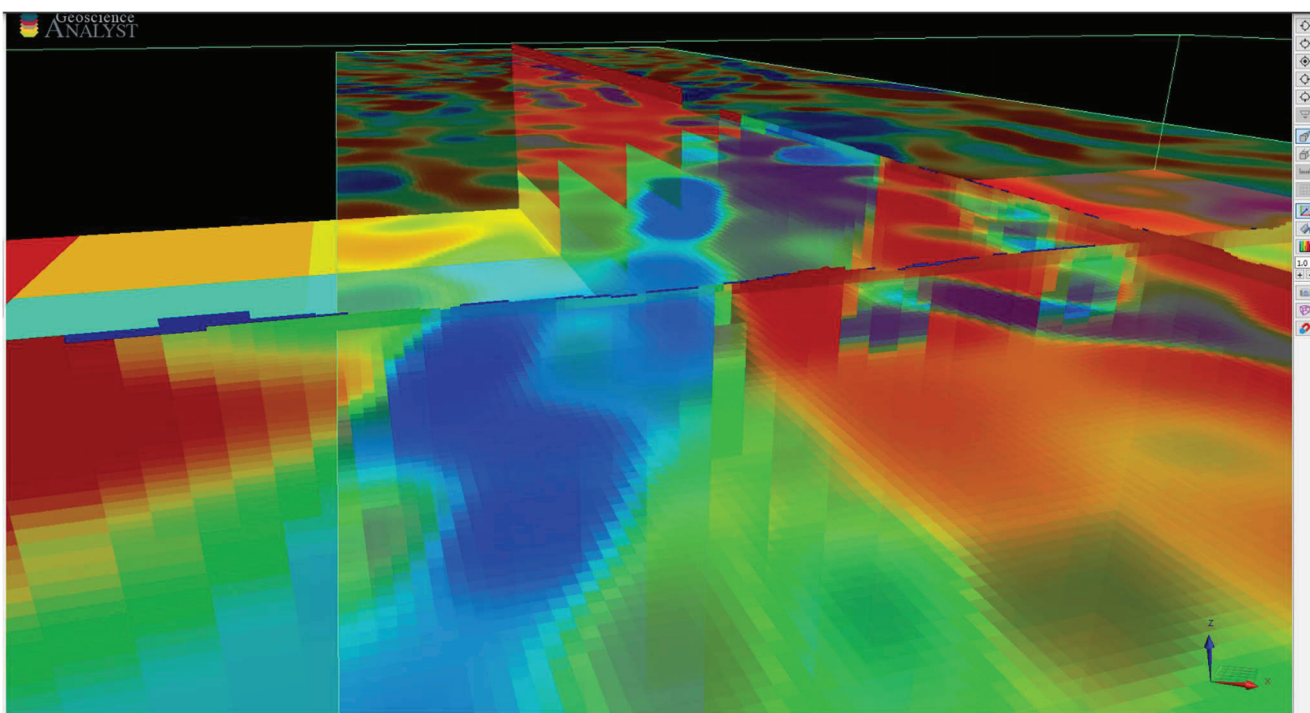


Figure 10. Geoscience ANALYST 3-D project.

10. References

- Cockett, R., Kang, S., Heagy, L. J., Pidlisecky, A., and Oldenburg, D. W. (2015): SimPEG: An open source framework for simulation and gradient based parameter estimation in geophysical applications. *Computers & Geosciences*, 85, 142-154. DOI: 10.1016/j.cageo.2015.09.015
- Fournier, D. and Oldenburg, D. W. (2019): Inversion using spatially variable mixed ℓ_p norms, *Geophysical Journal International*, 218, 268–282.
- Oldenburg, D. W. and Li, Y. (2005): Inversion for Applied Geophysics: A Tutorial, in *Near-Surface Geophysics*, Chapter. 5, p. 89–150, *in* Butler, D. K. (ed.), Society of Exploration Geophysicists.
- Sander Geophysics Ltd. (2008): Airborne gravity survey, Quesnellia region, British Columbia; Geoscience BC, Report 2008-8, 121 p., URL <http://www.geosciencebc.com/i/project_data/QUESTdata/GBCReport2008-8/Gravity_Technical_Report.pdf> [November 2019].

